Auditory-Somatosensory Integration in Dorsal Cochlear Nucleus Mediates
Normal and Phantom Sound Perception

by

Seth D. Koehler

A dissertation submitted in partial fulfillment
of the requirements for the degree of
Doctor of Philosophy
(Biomedical Engineering)
in the University of Michigan
2013

Doctoral Committee:

Research Professor Susan E. Shore, Chair
Professor J. Wayne Aldridge
Professor Douglas C. Noll
Professor Emeritus Kensall D. Wise
Associate Professor Michal R. Zochowski

Dedication

This work is dedicated to the giants upon whose shoulders I stand—most especially Theresa and our miniature

giants, Chelsea and Clara.

Acknowledgements

As I reflect for a few moments while checking the final details of this dissertation, I am incredibly grateful for the support and encouragement of so many people throughout this process. Most importantly, I thank Theresa for her love, constant support, and for working incredibly hard to make this endeavor possible for me and our family. Chelsea and Clara, I hope one day you realize that it took just moments with you to bring me great joy and keep me motivated. I thank my parents, Ellen and Paul, for their support and encouragement and the years they spent homeschooling us, their kids, providing an incredible educational foundation. My advisor, Dr. Shore took a risk on an engineer and provided me an incredible opportunity to engage in fascinating research in an incredible lab at a great university with incredible scientists, and constantly taught, motivated, and challenged me to ask good scientific questions and present clean, simple, well thought out arguments. I will always be grateful.

To my committee members, Dr. Aldridge, Dr. Noll, Dr. Wise, and Dr. Zochowski, I am grateful for your insight and feedback on these projects. To Dr. Noll, as chair of the BME department, thank you for your support over the years; I would not have had this opportunity without it. Dr. Bledsoe, thank you for your thoughtful questions and encouraging ideas over many years; your advice and mentorship has been invaluable. Dr. Duncan, thank you for your perspective and constant willingness to engage with personal and professional advice. To Dr. Manis, thank you for your insights and feedback. To Dr. Basura, collaborating with you was personally and professionally refreshing; running these experiments with you made them less daunting and I look forward to continued collaboration.

Without the incredible support and contributions of current and former members of the Shore lab, especially Dr. Chris Sumner, Dr. Susanne Dehmel, Chunhua Zeng, Beth Hand, and Gary Dootz, this dissertation would not have

Table of Contents

List of Figures

List of Abbreviations

ABR – Auditory brainstem response
BBN – Broad band noise
BF – Best frequency
BI – Bimodal interval
CN – Cochlear nucleus
CV – Coefficient of variation
DCN – Dorsal cochlear nucleus
ENT – Exposed with no tinnitus evidence
ET – Exposed with tinnitus evidence
FSL – Mean first spike latency
FISI – Mean first inter-spike interval
GPIAS – Gap Prepulse Inhibiton of Acoustic Startle
LTD – Long-term depression
LTP – Long term potentiation
NMDAR – N-Methyl-D-Aspartate receptor
PKC – Protein kinase C
PSTH – Post-stimulus time histogram
Sp5 – Spinal trigeminal nucleus
STDP – Stimulus-timing dependent plasticity
TTS – Temporary threshold shift

Abstract

The dorsal cochlear nucleus (DCN) is the first auditory brainstem nucleus that processes and relays sensory information from multiple sensory modalities to higher auditory brain structures. Converging somatosensory and auditory inputs are integrated by bimodal DCN fusiform neurons, which use somatosensory context for improved auditory coding. Furthermore, phantom sound perception, or tinnitus, can be modulated or induced by somatosensory stimuli including facial pressure and has been linked to somatosensory-auditory processing in DCN. I present three *in vivo* neurophysiology studies in guinea pigs investigating the role of multisensory mechanisms in normal and tinnitus models.

1) DCN fusiform cells respond to sound with characteristic spike-timing patterns that are controlled by rapidly inactivating potassium conductances. I demonstrated here that somatosensory stimulation alters sound-evoked firing rates and temporal representations of sound for tens of milliseconds through synaptic modulation of intrinsic excitability.

2) Bimodal plasticity consists of alterations of sound-evoked responses for up to two hours after paired somatosensory-auditory stimulation. By varying the interval and order between sound and somatosensory stimuli, I demonstrated stimulus-timing dependent bimodal plasticity that implicates spike-timing dependent synaptic plasticity (STDP) as the underlying mechanism. The timing rules and time course of stimulus-timing dependent plasticity closely mimic those of STDP at synapses conveying somatosensory information to the DCN. These results suggest the DCN performs STDP-dependent adaptive processing such as suppression of body-generated sounds.

3) Finally, I assessed stimulus-timing dependence of bimodal plasticity in a tinnitus model. Guinea pigs were exposed to a narrowband noise that produced temporary shifts in auditory brainstem response thresholds and is known to produce tinnitus. Sixty percent of guinea pigs developed tinnitus according to behavioral testing by gap-induced prepulse inhibition of the acoustic startle response. Bimodal plasticity timing rules in animals with verified tinnitus were broader and more likely to be anti-Hebbian than those in sham animals or noise-exposed animals that did not develop tinnitus. Furthermore, exposed animals with tinnitus had weaker suppressive responses than either sham animals or exposed animals without tinnitus. These results suggest tinnitus development is linked to STDP, presenting a potential target for pharmacological or neuromodulatory tinnitus therapies.

Chapter 1: Introduction

The dorsal cochlear nucleus (DCN) is a multi-layered structure containing heterogenous cell types (Hackney, 1990) and complex micro-circuitry (Young and Davis, 2002). It is innervated by the auditory nerve, descending projections from auditory cortex, and projections from non-auditory structures including somatosensory brainstem nuclei and vestibular nuclei. Often called a cerebellar-like structure for its resemblance to the circuitry of the cerebellum, the DCN has been hypothesized to adaptively process auditory information by using multisensory information to suppress self-generated sounds or perform complex sound localization tasks (Oertel and Young, 2004). Principal cells project to the inferior colliculus (refs:) and directly to regions of the auditory thalamus that encode multisensory information (refs:), thus conveying multisensory information processed in the DCN to higher auditory structures.

The studies described in this dissertation expand our understanding of ion channel mechanisms underlying multisensory integration, and synaptic mechanisms underlying multisensory plasticity, as well as their contribution to tinnitus, a central auditory system disorder characterized by phantom auditory perception in the absence of sound. Understanding these mechanisms provides a foundation for improved understanding of DCN function. Here I briefly review auditory, multisensory, and plasticity principles and literature that provide context for understanding the implications of the results presented here.

Multisensory convergence and integration in dorsal cochlear nucleus

Multisensory information converges and is integrated throughout the brain (Meredith, 2002) and improves performance on behavioral tasks (Calvert and Thesen, 2004), such as detection near-threshold stimuli when sound and tactile stimuli are synchronous and spatially congruent (Tajadura-Jimenez et al., 2009). The DCN is one site of multisensory convergence, receiving projections from a variety of non-auditory sources, including somatosensory brainstem nuclei and ganglia (Kirzinger and Jurgens, 1991; Wright and Ryugo, 1996; Luthe et al., 2000; Shore et al., 2000; Zhou and Shore, 2004; Haenggeli et al., 2005b) and vestibular nuclei, along with descending projections from auditory cortex (Schofield and Coomes, 2006), noradrenergic projections from locus coeruleus (Ebert, 1996), and cholinergic projections from superior olivary complex and tegmental nucleus (Shore et al., 1991; Sherriff and Henderson, 1994; Mellott et al., 2011).

Auditory and non-auditory inputs arrive in the DCN through segregated pathways in the deep (III/IV) and surface (I) layers, respectively (Fig. 1.1). Fusiform cells, one of two principal cell types, have their somata in layer II with distinct sets of basal and apical dendrites in layers III/IV and I, respectively. Auditory nerve fibers terminate on the basal dendrites (Manis and Brownell, 1983; Stabler et al., 1996b), while parallel fibers, the axons of granule cells, terminate on the apical dendrites. Giant cells, the other principal cell type, have their somata and a single dendritic arbor in the deep DCN (III/IV) and receive few parallel fiber terminals, but may receive feed forward excitatory input from fusiform cells (Smith and Rhode, 1985). Somatosensory projections to DCN target primarily granule cells, thus leading to direct excitation through parallel fibers and indirect inhibition, through cartwheel cells, of fusiform cells and limited excitation of giant cells.

Stimulation of parallel fibers and somatosensory brainstem nuclei and ganglia elicits excitatory and inhibitory responses in fusiform cells (Saade et al., 1989; Davis et al., 1996; Kanold and Young, 2001; Shore et al., 2003). Fusiform cells not only respond to somatosensory stimulation, but also perform non-linear integration of

2

somatosensory and auditory inputs (Shore, 2005; Shore et al., 2008). Multisensory integration is usually measured by comparing the average firing rates of responses to bimodal stimuli with unimodal responses to each component of the bimodal stimulus presented independently (Stein and Meredith, 1990; Stein and Meredith, 1993; Populin and Yin, 2002; Meredith et al., 2006). For example, neurons integrate multisensory stimuli when the bimodal response is larger than the sum of the unimodal responses. In addition to firing rate, characteristics of spatio-temporal spiking patterns, in particular spike latencies, are important for encoding auditory information (Chase and Young, 2006). Understanding somatosensory influence on DCN spike-timing is important here because membrane potential history controls the spiking patterns of fusiform cells through de-inactivating potassium channel conductances (Manis, 1990; Kanold and Manis, 1999).

The first study described in this dissertation (Chapter 2) explores multisensory integration in temporal spiking patterns by comparing latency and regularity of auditory response with and without preceding somatosensory stimulation (Koehler et al., 2011). This study shows somatosensory influence on two temporal properties of DCN responses to sound, latency and regularity, that have the potential to encode loudness (Heil, 2004) and pitch (Wiegrebe and Meddis, 2004), respectively.

Spike-timing dependent plasticity in cerebellar-like circuits

Spike-timing dependent plasticity (STDP), a form of synaptic plasticity first postulated by Hebb (Hebb, 2002) is found at synapses throughout the brain and has been proposed as a fundamental mechanism for the development and maintenance of cortical and subcortical computational circuitry in the brain (for a detailed history and review, see (Markram et al., 2012). Precise temporal correlations between synaptic input and post-synaptic spikes produce STDP, with the order determining the resulting long-term potentiation or long-term depression. Two forms of STDP, Hebbian and anti-Hebbian, have been identified in the DCN(Tzounopoulos et al., 2004). Hebbian synapses are

3

characterized by long-term potentiation when synaptic input precedes spikes and long-term depression when synaptic activity follows spikes while anti-Hebbian synapses are characterized by the reverse timing rule.

In the DCN, Hebbian STDP, dependent on N-Methyl-D-Aspartate receptors (NMDAR), has been demonstrated at parallel fiber synapses on fusiform cell dendrites while endocannabinoid-dependent anti-Hebbian STDP is found at parallel fiber synapses on cartwheel cells (Tzounopoulos et al., 2007). The STDP observed at parallel fiber synapses has been proposed as a mechanism for adaptive processing, using non-auditory synaptic input from parallel fibers to predict relevant or irrelevant sounds (Roberts and Leen, 2010; Sawtell, 2010). There are relatively few studies that have assessed the influence of STDP *in vivo* (for a list of 18 published before 2010 see (Shulz and Jacob, 2010), none of which studied the DCN. However, temporally associated bimodal stimuli do induce long-lasting changes in DCN sound-evoked firing rates (Dehmel et al., 2012c) that have a time course consistent with the action of STDP.

The second study described in this thesis (Chapter 3) pairs somatosensory stimuli that provide presynaptic input and sound stimuli that generate post-synaptic spiking activity to assess the contribution of STDP to *in vivo* DCN responses. By measuring the change in firing rate while varying the interval and order between paired sensory stimulation, we show stimulus-timing dependent bimodal plasticity. The presence of stimulus-timing dependent bimodal plasticity implicates STDP as a key plasticity mechanism by which multisensory inputs influence responses to sound in DCN.

Somatic tinnitus and the dorsal cochlear nucleus

Tinnitus is the phantom perception of sound in silence, usually caused by noise exposure and hearing damage, or somatic insults such as craniomandibular disorders (Rubinstein et al., 1990). While at least one third of adults have experienced tinnitus, the incidence rate for chronic bothersome tinnitus is between 10 and 15% (Heller, 2003). Interestingly, there is a strong somatosensory component to tinnitus, as tactile and proprioceptive stimuli (Pinchoff et al., 1998; Sanchez et al., 2007), such as pressure on the face or a jaw thrust, can modulate the pitch and loudness of

tinnitus. Not only can up to 80% of tinnitus patients modulate their tinnitus by somatosensory maneuvers, but 20% of human subjects with no history of tinnitus can elicit a phantom sound perception with these maneuvers (Levine et al., 2003).

Many studies have confirmed tonotopically-restricted spontaneous hyperactivity that resembles tone-evoked activity (Kaltenbach and Afman, 2000) in DCN neurons following sound exposure (Kaltenbach and McCaslin, 1996; Kaltenbach et al., 2004) and in behaviorally-confirmed tinnitus models (Brozoski et al., 2002; Dehmel et al., 2012c). With strong short and long-lasting influence on firing rates and spike timing that encode sound, somatosensory inputs present a putative pathway to mediate the somatosensory influence on tinnitus. After hearing damage, the somatosensory influence on DCN is enhanced, with new innervation (Zeng et al., 2009a) and lower threshold for excitatory response to trigeminal nucleus (Sp5) stimulation in neurons with elevated spontaneous rates (Shore et al., 2008). Most importantly, bimodal plasticity, a long-lasting change in sound-evoked firing rates following bimodal stimulation, is significantly enhanced in a noise-exposure induced tinnitus model (Dehmel et al., 2012c). This raises the question of how changes in bimodal plasticity are involved in tinnitus generation.

As we show in Chapter 3, bimodal plasticity is stimulus-timing dependent, reflecting STDP at parallel fiber synapse conveying somatosensory information. In Chapter 4, the contrast is revealed between stimulus-timing dependent bimodal plasticity in sham guinea pigs, noise-exposed guinea pigs without tinnitus, and noise-exposed guinea pigs with tinnitus. We discover evidence that STDP timing rules broaden and shift towards anti-Hebbian and away from bimodal suppression and propose a process by which these changes could contribute to tinnitus associated spontaneous hyperactivity.

5
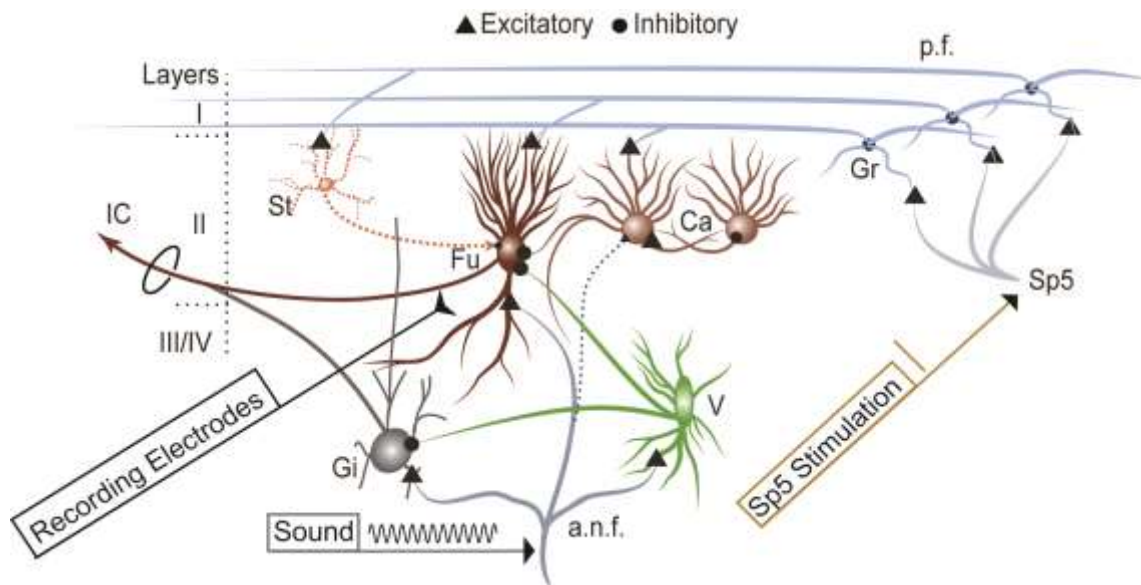
Figures

Figure 1.1 - Cartoon illustration of relevant cell types and micro-circuitry in the DCN. Auditory nerve fibers terminate in excitatory synapses on Fusiform (Fu), Giant (Gi), and Vertical (V) cell dendrites in layer III/IV. Giant cell and fusiform cell axons project to Inferior Colliculus (IC). Vertical cells provide feed forward inhibition to Fu and Gi cells. Trigeminal nucleus fibers (Sp5) excite granule (Gr) cells. Parallel fibers (p.f.), the axons of granule cells excite Fusiform cells and Cartwheel cells (Ca) which in turn inhibit fusiform cells. These studies use mutli-channel recording electrodes to record spiking activity primarily from Fusiform and Giant cells, along with some Vertical cells. Sound is used to elicit auditory nerve activity and drive spiking activity. Electrical stimulation of Sp5 is used to stimulate the somatosensory inputs to granule cells, and thus elicit synaptic events at parallel fiber synapses in DCN.

Chapter 2: Somatosensory Inputs Alter Auditory Spike Timing

The study presented here in Chapter 2 has been published in the European Journal of Neuroscience (Koehler et al., 2011).

The principal output cells of the dorsal cochlear nucleus (DCN), the pyramidal cells, are activated by sound through auditory nerve inputs onto their basal dendrites (Manis and Brownell, 1983; Stabler et al., 1996b). However, these cells also receive somatosensory input from dorsal column and trigeminal brainstem nuclei (Kirzinger and Jurgens, 1991; Wright and Ryugo, 1996; Luthe et al., 2000; Zhou and Shore, 2004; Haenggeli et al., 2005b). These excitatory projections terminate initially on CN granule cells (Zhou et al., 2007) whose axons then activate the apical dendrites of the pyramidal cells (Fig. 1.1). The first studies to demonstrate responses of pyramidal cells to the somatosensory system (Saade et al., 1989; Davis et al., 1996; Kanold and Young, 2001) showed that these cells could be excited or inhibited by stimulating brainstem somatosensory nuclei. Later studies showed that bimodal stimulation with sound and somatosensory stimulation could enhance or suppress the firing rates of pyramidal cells to the sound stimulus (Shore, 2005; Shore et al., 2008) demonstrating that these cells are capable of multiplicative multisensory integration (Stein and Meredith, 1990; Stein and Meredith, 1993; Populin and Yin, 2002; Meredith et al., 2006). While multisensory integration is usually analyzed using average spike rate, more recent

reports show that multisensory integration can also be represented by alterations of spike timing (Zahar et al., 2009).

The spike timing of pyramidal cells is influenced by the membrane potential prior to depolarization (Manis, 1990; Kanold and Manis, 1999). *In vitro* studies show that prior hyperpolarization can delay first spike latencies (FSLs)

and increase the first interspike intervals (FISI) (Manis, 1990; Kanold and Manis, 2005), as well as alter firing precision (Street and Manis, 2007), suggesting that brief perturbations across sensory domains, through multisensory integration, could influence spike timing. Altering spike-timing of pyramidal cells by somatosensory inputs could change the way these cells encode sound and influence the representation of sound-location information (Young et al., 1992; May, 2000; Oertel and Young, 2004), as well as filtering self-generated sounds (Bell et al., 1997a; Oertel and Young, 2004). These tasks can utilize contextual somatosensory information regarding face or vocal muscle movement, pinnae and/or head position time-locked to an auditory stimulus. Consequently, we investigated the effects of auditory-somatosensory integration on spike-timing of responses to sound in pyramidal cells. We predicted that *in vivo* activation of granule cell inputs to pyramidal cells by trigeminal nucleus (Sp5) stimulation would change pyramidal cell characteristic temporal responses by delaying FSLs and FISIs and changing firing regularity and precision.

Materials and Methods

Surgical Preparation

Experiments were performed on 7 mature, female, pigmented guinea pigs (250-350 g, Elm Hill). All procedures were approved by the University of Michigan Committee on the Use and Care of Animals (UCUCA). Animals were anesthetized with ketamine (40 mg/kg) and xylazine (10 mg/kg) and held in a stereotaxic device (Kopf) with hollow ear bars for the delivery of sounds. Rectal temperature was monitored and maintained at 38 ± 0.5°C with a thermostatically- controlled heating pad. Supplemental anesthesia (0.25-0.5X initial dose) was given approximately hourly, after performing a digital pinch test to elicit paw withdrawal. Unit thresholds to broadband noise were monitored throughout the experiment to assess the physiological condition of the animals. The bone overlying the cerebellum and posterior occipital cortex was removed and a small amount of cerebellum was aspirated to reveal the surface of DCN.

Acoustic Stimulation

Acoustic stimuli were 100 ms broadband noise or 50 ms tone bursts (1.5 ms rise/fall times) presented at different levels to assess neural thresholds, BFs, latencies and rate-level functions. Stimuli were delivered to the ears with Beyer dynamic earphones (DT-48) coupled to the hollow ear bars using TDT system III hardware for digital-to-analog conversion and analog attenuation. Digital signals were generated and delivered to the TDT hardware by a Pentium PC using a custom MATLAB software package. Stimuli were generated using a sampling rate of 50 kHz with 16-bit resolution. Tones were calibrated using a ¼ inch condenser microphone (Bruel & Kjaer, Mic:4136, Preamp:2619, Power Supply:2804) coupled to the ear bar with a 0.2 ml tube. The microphone output was measured using custom MATLAB software. Noise was calibrated with the ¼ inch microphone and coupler attached to a sound level meter set to measure the bandwidth of interest (200 Hz-20 kHz for broad band noise). Equalization to correct for the system response was performed in the frequency domain using digital filters implemented in TDT hardware. The stimulus variable sequences were generated in pseudorandom order from within MATLAB. The maximum output of the system was 80 db SPL.

Sp5 Stimulation

Sp5 neurons were activated by passing current through a bipolar concentric stimulating electrode (Frederick Haer and Co.) directed towards the left Sp5 using stereotaxic coordinates (0.28 cm left of midline, 0.2-0.3 cm caudal to the transverse sinus, 0.9 cm below surface of cerebellum). Current (4 pulses, 3/sec) amplitudes ranged from 10 to 90 ꭐA.

In 5/7 experiments, the tip of the stimulating electrode was dipped in fluorogold before insertion to enable post mortem reconstruction of the electrode placements (see below). To assist in determining the correct locations while performing the experiment, a receptive field was recorded using the stimulating electrode as the active

recording electrode. Regions of the face and head were stimulated using a custom-built mechanical stimulator that was driven by the TDT system.

Bimodal Stimulation

Bimodal stimuli consisted of a short burst of electrical stimulation in the Sp5 followed 10 ms later by a short BF tone burst (50 ms, 20 dB SL). For assessment of bimodal integration, responses to bimodal stimuli were compared to responses to acoustic stimuli (50 ms, BF tonebursts at 20 dB SL). Unimodal acoustic and bimodal trials were either performed as test-retest blocks (300 acoustic – 300 bimodal – 300 acoustic) or were randomly interleaved.

Data Acquisition

Recordings were made in a sound-attenuating single-walled booth. A four-shank, 16-channel silicon substrate electrode (100 microns between sites, 250 microns between shanks, 177 micron^2 site area, Neuronexus, Inc, Michigan) (Fig. 2.1A,B) was used to record activity from many units simultaneously. Figure 2.1 shows the location of recording sites on the electrode array (Fig. 2.1A) and their relative positions in the DCN (Fig. 2.1B). We were able to sample from 16 locations within a small BF range without moving the probe. The electrode was inclined to an angle of 35-45° from vertical and positioned on the DCN surface 0.5-0.75 mm medial to the paraflocular recess. The tip of the electrode array was advanced 600 μm below the surface of the DCN in a ventro-rostral direction. If necessary, the electrode was repositioned until robust responses to ipsilateral acoustic stimulation were obtained.

The 16-channel electrode was connected by a 16-channel pre-amplifier and digitizer to a Tucker-Davis Technologies (TDT) data-acquisition system. The signals were filtered from 300–7500 Hz prior to analog-to-digital conversion. Analog-to-digital conversion was performed by simultaneous-sampling 12-bit converters at 25 kHz per channel. A spike detection threshold was set independently for each recording channel to four standard deviations (SDs) above the mean background noise voltage. Timestamps and associated waveforms were recorded at each threshold crossing.

Offline sorting

Spike waveforms exceeding 4 SDs above the RMS noise floor were detected at approximately 80% of the recording sites. The unit waveforms on each channel were sorted using the Plexon Offline Sorter program (Plexon, Inc., Dallas, TX) with an automated cluster analysis of principal component amplitudes (Fig. 2.1E). Units with more than 2% of spikes within a refractory window of 1 ms were excluded. Following sorting, unit waveforms were manually verified in terms of their amplitude consistency across trials and inter-spike intervals. In some cases, it was possible to sort waveforms from a single recording site into more than one unit that met statistical criteria ($p<0.05$) for independence, thus increasing our yield of individually isolated units.

Data analysis

On-line and post-experiment data analysis was performed in MATLAB. Peri-stimulus time histograms (PSTHs), response maps, rate-level functions, and thresholds were generated. A response threshold was taken to be the linearly interpolated sound level at which the difference in the mean spike rate between the driven response and the spontaneous activity satisfied a Student's t-test for statistical significance at a level of $p < 0.01$. This algorithm gave thresholds that agreed closely with visual inspection of PSTHs and rate-level functions. Threshold was also verified visually by comparing the response to the next higher level at which a strong response around the same latency was observed. Latency of the response to Sp5 stimulation was the point in time at which the firing rate was suppressed below the average firing rate or exceeded 2 SDs above the average firing rate preceding stimulation. Mean first spike latencies and first inter-spike intervals were computed for responses to BF tones (with or without Sp5 stimulation). The latency of the first spike and the interval between the first and second spikes after the onset of the tone stimulus were averaged across all trials for each stimulus condition. To assess regularity of firing to BF tones, inter-spike interval histograms and coefficients of variation (CVs) were calculated (Young et al., 1988; Parham and Kim, 1992) using Neuroexplorer software (Nex Technologies, Littleton, MA). Both the transient CV (tCV, 0-10 ms post-acoustic

11

onset) and the steady state CV (sCV, 15-45 ms post-acoustic onset) were computed. The effect of Sp5 stimulation on the firing rate of the response to BF tones was assessed using the degree of integration measure used in preceding work (Shore, 2005) to allow for comparison. Bimodal enhancement (BE) was calculated as follows: BE= [Bi-T-A)/(T+A)] x 100 where Bi is the number of spikes occurring during the bimodal response, T is the number of spikes occurring during the trigeminal response, and A is the number of spikes occurring during the acoustic response. Bimodal suppression was calculated as follows: BS = [(Bi- Uni_{max})/Uni_{max}] x100 where Uni_{max} is the maximum of T and A.

Response type classification

Units were classified based on the PSTH shape of their response to BF tones at 20 dB SL. As shown previously in the guinea pig (Stabler et al., 1996b), pyramidal cell responses typically fall into one of three temporal firing patterns: chopper units with highly regular, short latency spikes in response to BF tones can be classified as sustained or transient based on the duration of chopping (Hewitt and Meddis, 1993). For the purposes of this study, transient and sustained choppers were combined into one class of chopper units. Buildup units fired irregular spikes with a longer latency. Pauser units were similar to buildup units, but had an additional short latency response.

Histology

The locations of the recording electrodes in the DCN and the stimulating electrode in the SP5 were verified post mortem. To mark the electrode tracks, the recording and stimulating electrodes were dipped in fluorogold (2%) before being inserted into the brain. At the end of each experiment, the animal was perfused transcardially with saline followed by 4% paraformaldehyde. The brain was removed from the skull and immersed in 20% sucrose solution (Zhou and Shore, 2006). The following day, the brain was cryosectioned at 40–60 μm, placed on slides and examined under epifluorescence to document recording and stimulating locations.

Results

Recordings were obtained from 115 isolated single units with sufficient data for response-type classification (see Methods) in the pyramidal cell layer (layer II, 200-500 m from DCN surface) in response to BF tones preceded by Sp5 stimulation and to BF tones alone. The locations of the stimulating electrodes in Sp5 are shown in Figure 2.1C along with a multiunit receptive field recording obtained from the stimulating electrode while mechanically stimulating regions of the face and head (Fig. 2.1D). The largest responses were obtained when the somatic surfaces of the face (skin and muscle) were stimulated. Movement of the jaw and tongue also elicited sizable responses.

Regularity of firing as measured by CV for responses to BF tones

Of the total number of classified units, 35 were chopper units (Fig. 2.2A, D), 18 were buildup units (Fig. 2.2B, D), and 33 were pauser units (Fig. 2.2C, D). Twenty-nine units falling in between these categories are termed 'unusual' (Fig. 2.2D). Of these 115 units, it was possible to compute the transient and steady state CV for a subset of units that responded to BF tones preceded by Sp5 stimulation and BF tones alone. The mean transient CV for BF tones was 0.77 +/- 0.11 (n=50), while the mean steady state CV was 0.65 +/- 0.07 (n=48). The distribution of transient CVs (Fig. 2.2E) is broader than the distribution of steady state CVs (Fig. 2.2F), although steady-state CVs tend to be lower (indicating more regularity). In the population of units recorded in this study, CVs were similarly distributed between 0.6 and 0.95 for all groups classified by PSTH of the BF response.

Unimodal responses to Sp5 stimulation are primarily excitatory

Unimodal responses to Sp5 stimulation were recorded from 94 of the 115 single units. The majority (52.1%) of measured responses were purely excitatory, while in 9.6% of the responses, the initial excitation was followed by inhibition. A few (7.4%) cells exhibited only inhibition. Approximately one-third (30.9%) of units did not exhibit a change in firing rate to Sp5 stimulation alone. However, 18/25 of these unimodally unresponsive units did show bimodal integration (see below), and are thus considered to have occult Sp5 inputs. The mean Sp5 stimulation

13

thresholds (45µA +/- 16 s.d., n=53) were not significantly different between response types. However, the latencies of

inhibitory responses (17.3 ms +/- 6.1 s.d., n=7) to Sp5 stimulation were significantly longer than for excitatory

responses (11.5 ms +/- 4.2 s.d., n=47, unpaired t-test, t(52) = -3.217, p=.002) but no different than for complex

responses (13.7 ms +/- 5.2 s.d., n=9; unpaired t-test, t(54) = -1.376, p=0.175). Response durations were longer for

complex responses (34.3 ms +/- 17.8 s.d., n=9) than for excitatory (25.4 ms +/- 17.8 s.d., n=47) or inhibitory (24.1 ms

+/- 10.1 s.d., n=9) responses, but did not reach significance.

Sp5 stimulation can decrease regularity in response to BF tones

In units classified as chopper, pauser or buildup (and thus likely to be pyramidal cells), the temporal firing

patterns in response to BF tones were altered when the tone was preceded by Sp5 stimulation. The chopper unit

shown in Figure 2.3A responded consistently to BF tones for six hundred trials over several minutes (Fig. 2.3A1-A2),

firing in a regular manner with an average spike rate of 260 spikes/sec. When Sp5 stimulation preceded the tone by

10 ms (Fig. 2.3A3), the chopping pattern at the onset of the response was abolished and the average spike rate

decreased to 120 spikes/sec. When unimodal BF tone stimulation was retested without Sp5 stimulation, the neuron

resumed its original firing pattern, and the firing rate partially recovered to 201 spikes per second (Fig. 2.3A4–A5). The

raster plots reveal that the firing in response to BF tones was regular (Fig. 2.3B, Top, transient CV = 0.67, measured

during the first 10 ms of the response) and became less regular (Fig. 2.3B, Bottom, tCV = 0.88) when Sp5 was

stimulated, consistent with the disappearance of chopping from the PSTH. The rate suppression induced by Sp5

stimulation was similar to the reduction in noise-evoked firing rate induced by trigeminal ganglion stimulation (Shore,

2005; Shore et al., 2008). Figure 2.3C shows the effect of Sp5 stimulation on a pauser unit. In this case, prior Sp5

stimulation decreased the average firing rate from 75 spikes/sec to 56 spikes/sec and induced a more consistent

interval between the first and second spike, which is reflected in the decrease in tCV. Figure 2.3D shows another

chopper unit in which there was a decrease in regularity with little change in the steady state firing rate of the neuron

14

but an increase in the onset firing rate. Regularity changes can thus occur independently of rate changes after Sp5 stimulation (see Figure 2.5C for more detail on the relationship between regularity and firing rate). The changes in regularity appear to increase as the bimodal pairing continues from the first trial (bottom row of the raster) to the last trial (top row of the raster) in Figures 2.3C and 2.3D.

Changes in regularity by prior Sp5 stimulation depend on unimodal response regularity.

Across the population of units with measurable CVs, the distribution after Sp5 stimulation of transient (Fig. 2.4A) and steady-state (Fig. 2.4C) CVs is broader and has a higher mean than the distribution of transient and steady-state CVs of acoustic responses (Fig. 2.2D and 2.2F). Mean steady state CVs increased significantly from 0.64 +/- 0.06 s.d. to 0.67 +/- 0.09 s.d. with Sp5 stimulation (paired t-test, $t(45)=-2.090$, $p=0.042$) while mean transient CVs increased from 0.77 +/- 0.11 s.d. to 0.81 +/- 0.13 s.d. (paired t-test, $t(47)=-1.794$, $p=0.079$). Out of 46 units, 19 showed decreased transient CVs (increased regularity) and 27 showed increased transient CVs (decreased regularity) following Sp5 stimulation. Units that showed increased regularity had an average decrease in the transient CV of 16.3% while those that showed a decrease in regularity had an average increase in the transient CV of 13.8 %. Of the units with a change in regularity, 13/46 did not respond to unimodal Sp5 stimulation, indicating that timing changes can be independent of supra-threshold somatosensory responses.

The change in transient regularity with Sp5 stimulation was dependent on the initial regularity prior to Sp5 stimulation (Fig. 2.4B, $r^2=0.28$, $F(1,46) = 17.869$, $p<0.001$). When the transient acoustic response was more regular (left side of graph), the response tended to be less regular with Sp5 stimulation, i.e. its CV increased (points above the horizontal line). When the acoustic response was less regular (right side of graph) the acoustic response became more regular (i.e., its transient CV decreased) with Sp5 stimulation. Although this observation is clearest for the transient regularity measurements (Fig. 2.4B), it is also apparent for the steady-state portion of the response (sCV, Fig. 2.4D, $R^2=0.156$, $F(1,44) = 8.130$, $p=.007$).

Prior Sp5 stimulation enhances or suppresses firing rate of the acoustically evoked response

Bimodal integration was quantified in 69 units using the "degree of integration" index (see Methods), which measures how much the firing rate of the bimodal response surpasses the linear summation of the responses to sound and Sp5 stimulation alone . Thirty eight percent of units showed bimodal enhancement while 40.6% of units showed bimodal suppression. The remaining 21.7% did not show bimodal integration. There was a mean increase in firing rate of 35.3% in units showing enhancement, while there was a mean reduction in firing rate of 24.3% in units showing suppression. Interestingly, unit type was an important factor in whether bimodal integration was enhancing or suppressive, as described below.

Chopper units show bimodal enhancement and buildup units show bimodal suppression

Figure 2.5A shows that chopper unit responses were typically enhanced, while buildup unit responses were mostly suppressed by Sp5 stimulation. Pauser and unusual units showed both suppressive and enhancing bimodal integration.

The temporal changes in bimodal responses do not depend on the change in firing rate

The increase in regularity was not significantly correlated with the degree of bimodal integration (R^2=.014, $F(1,28) = 0.387$, $p = 0.539$; Fig. 2.5B). However, suppression of the firing rate by bimodal stimulation (left half of Figure 2.5B) was more often (7 vs. 3 units) accompanied by an increase in regularity of the response (i.e., a decrease in the CV). Enhancement of the firing rate (right half of Figure 2.5B) was more often (10 vs. 7 units) accompanied by a decrease in the regularity of the response (i.e., an increase in the CV).

Additionally, the change in CV in units that did show rate integration is similar to the change in CV in units that did **not** show rate integration (data not shown). As the CV measure itself is not independent of spike rate, we examined the relationship between change in CV and change in spike rate in Figure 2.5C. The transient CV shows a weak but significant correlation (r^2=0.111, $F(1,45) = 5.596$, $p = 0.022$) with firing rate measured in the same time

window indicating that the variation in firing rate explains 10 % of the variation in tCV. However, the effect that is shown in Figure 2.5C is the opposite of what would be expected from rate-dependent effects for which, at higher rates, the effects of the refractory period should lead to lower CV values (i.e., more "regularity" because the spike interval distribution is compressed by the effects of the refractory period). In addition, at lower rates, the effect of the refractory period would become less (as a function of rate), and so the correlation should decrease, and the CV should become (relatively) larger instead of smaller, as observed. Thus, factors other than firing rate contribute to the changes in regularity.

Prior Sp5 stimulation increases the acoustic response latency

The mean first spike latency (FSL) of the response to BF tones was calculated for 74 single units responding to BF tones alone and to BF tones preceded by Sp5 stimulation. Figure 2.6A shows one example of a FSL shift, in which Sp5 stimulation increased the FSL averaged over 200 trials from 25.5 ms to 27.8 ms. Sp5 stimulation shortened the FSL in 24.3% of units by an average of 3.64 ms and lengthened the FSL in 75.7% of units by an average of 5.62 ms. Sixty nine percent of the units had a shorter FISI (average decrease of 4.31 ms +/- 2.83 s.d.) and 32% of the units had a longer FISI (average increase of 1.84 ms +/- 1.58 s.d.). The changes in FISI and FSL were positively correlated (Fig. 2.6B; r^2=0.212, F(1,70) = 18.885, p < 0.001).

Mean FSL increased in units that were suppressed by Sp5 stimulation but did not respond to unimodal Sp5 stimulation

Even units that did not overtly respond to unimodal Sp5 stimulation had significantly longer latencies to sound when preceded by Sp5 stimulation (NR, Fig. 2.6C; ANOVA adjusted for unequal variances with post-hoc Tukey's test, d.f.=5, F=60.949, p<0.01). When the responses to BF tones were suppressed by Sp5 stimulation, the latency of the response also increased significantly (Fig. 2.6D; ANOVA with post-hoc Tukey's test, p<0.05).

Tonotopic organization of Sp5 influence on acoustic responses

The precise organization of the somatosensory inputs to the granule cell domains and their targets via the parallel fibers to DCN cells is not known. Our results suggest that the effects of Sp5 stimulation on firing rate and latency of acoustic responses vary along the tonotopic axis of the nucleus. Bimodal rate suppression progressively increases from low to high and is largest in the 10 kHz best frequency region (Fig. 2.7A, Left). On the other hand, the strength of bimodal rate enhancement shows no apparent trend across best frequencies (Fig. 2.7A, Right). The FSL also shows a best-frequency-dependent increase, being largest between 7 and 10 kHz, with no change on average below 5 kHz or above 12 kHz (Fig. 2.7B, Left). In units with a decrease in the response latency, there is no dependence of the decrease on the BF of the unit (Fig. 2.7B, Right). Changes in the transient CV with bimodal stimulation are slightly larger at middle frequencies (7-10 kHz) (Fig. 2.7C, Left and Right). These results suggest that bimodal integration systematically affects processing in middle frequencies (~10 kHz) of the guinea pig hearing range.

Discussion

These experiments show that multisensory integration at the first stages of auditory processing can affect not only average spike rate, but also spike timing and the temporal representation of sounds in DCN principal neurons. First spike latency to tones and the regularity of subsequent firing is altered when Sp5 stimulation precedes sound. These changes can occur even in the absence of overt rate changes, suggesting that auditory-somatosensory integration is represented in the DCN in the timing of spikes, as is seen in visual-auditory integration in sub-cortical regions (Zahar et al., 2009).

The latency of firing of DCN pyramidal cells can be shifted by prior hyperpolarization as shown by *in vitro* experiments (Manis, 1990; Kanold and Manis, 1999, 2001, 2005). The latency shifts can occur for membrane potential changes that precede a depolarization by as much as 100 ms, and depend on rapidly inactivating transient potassium currents that are de-inactivated by the hyperpolarization (Kanold and Manis, 1999, 2001, 2005). In the present

18

experiments, even though the inhibitory effects on spontaneous activity by Sp5 stimulation had mostly faded prior to the acoustic stimulation, the ensuing latency shift would be consistent with transient potassium current involvement, which can hold the memory of prior hyperpolarization (Kanold and Manis, 2001, 2005). On the other hand, in some units, prior Sp5 stimulation increased the response latency with no observable effect of Sp5 stimulation alone. It is unclear whether this is due to weak hyperpolarization, or the presence of a separate source of inhibition from Sp5 that is gated by acoustic stimulation. However, the increased latency of sound-evoked responses after Sp5-induced suppression of spontaneous activity could also be explained by a long-lasting inhibition. One putative source of the inhibition could be cartwheel cells that can hyperpolarize pyramidal cells to -68 mV (Golding and Oertel, 1997) which in turn can generate a latency increase between 2 and > 25 ms in vitro (Kanold and Manis, 2001).

The latency changes described here may be decoded by time sensitive neurons at the next stage of processing in the inferior colliculus (see Kanold and Manis, 2005), as has been also been postulated for latency changes in T-stellate neurons that are inhibited by D-stellate neurons in the ventral cochlear nucleus (Needham and Paolini, 2006). The DCN may be involved in suppression of self-generated vocalizations or more generally by sounds associated with self-generated movement (Bell et al., 1997a). Activation of somatosensory inputs by self-generated movement may "tune" pyramidal cells to transmit a reduced response to coincident sounds by increasing the first spike latency. This increased latency could correspond to a reduction in gain in the spike latency code for intensity, since intensity and latency are often inversely related (Heil, 2004). The DCN is also thought to play a role in sound localization through its sensitivity to spectral notches in the head-related transfer function (Young et al., 1992; Imig et al., 2000; Reiss and Young, 2005). Sound localization cues, including spectral notches, are better represented by first spike times than by average firing rate in neurons in the inferior colliculus targets of the pyramidal cells (Chase and Young, 2006). By shifting the first spike latency, somatosensory input to the CN could emphasize or de-emphasize particular responses

to spectral notches or other acoustic features depending on the position of the head (in guinea pigs) or the position of the pinnae (in cats).

Another measure of temporal information is spike regularity, as measured here by the CV (Young et al., 1988; Parham and Kim, 1992). Higher CV measurements in this preparation as compared to cat (Parham and Kim, 1992) and guinea pig (Stabler et al., 1996b) preparations may be due to differences in anesthetic (ketamine-xylazine versus pentobarbital), recording electrodes (silicon substrate multi-channel electrodes), or stimulus intensity (60 dB SPL). Ketamine is an antagonist to NMDA receptors and may reduce glutamatergic neurotransmission from parallel fibers to cartwheel and pyramidal cells (Sinner and Graf, 2008). There are also indications that ketamine may reduce glycinergic inhibition, which could weaken the inhibition of pyramidal cells by cartwheel cells (Wang et al., 2005). Thus, the effect of anesthesia might diminish both the effects of glutamatergic somatosensory inputs on granule cells as well as glycinergic inhibition of cartwheel cells on pyramidal cell firing. The results presented here thus likely under represent the putative effects of the somatosensory influence on spike timing, which would be predicted to be stronger in awake animals. Future studies will address these issues in awake animals with more natural, direct somatosensory stimulation.

Our results show that Sp5 stimulation can either increase or decrease the regularity of sound-evoked spikes, depending on the unit's regularity in the absence of Sp5 stimulation. If a common set of mechanisms is responsible for the regularity changes as well as the firing rate and latency changes, we might expect the shifts in these measures following Sp5 stimulation to be correlated across the population of units. As discussed above, latency changes following Sp5 stimulation were correlated with changes in firing rate. However, the effects of Sp5 stimulation on regularity and rate integration were independent, suggesting that multiple mechanisms are engaged by Sp5 pathways. Discharge regularity is influenced by relative contributions of synaptic versus intrinsic ionic mechanisms, or

even different intrinsic mechanisms, and can vary with the rate of synaptic inputs and the discharge rate (Street and Manis, 2007).

In the present study, changes in regularity occurred even in units in which there was no measurable response to unimodal Sp5 stimulation. This could be explained by findings that perturbation of the membrane potential (even subthreshold perturbations) prior to acoustic stimulation can engage multiple, long-lasting effects on discharge patterns. For example, in quiescent DCN pyramidal cells, prior activity can affect spike latency and subthreshold oscillations for as long as 800 msec (Manis et al., 2003). In pyramidal cells driven by dynamic stimuli, brief hyperpolarizations affect spike timing for up to 300 ms, while brief depolarizations have weaker and shorter-lasting effects (Street and Manis, 2007). Although the mechanisms for the *in vitro* phenomena have not been fully elucidated, they meet the requirements to underlie the changes in discharge regularity shown here. They are specifically engaged by prior shifts in membrane potential, and their effects persist long after the membrane potential has decayed to the resting level prior to stimulation. This relationship will need to be substantiated using intracellular recordings in the *in vivo* model.

Another set of mechanisms that could modulate the discharge patterns is the activation of metabotropic receptor systems in the DCN, such as $GABA_B$ receptors that are localized to parallel fibers and apical pyramidal cell dendrites (Evans and Zhao, 1993; Juiz et al., 1994; Lujan et al., 2004) and mGluR receptors, which are localized to cartwheel cell dendrites (Wright et al., 1996; Molitor and Manis, 1997; Mugnaini et al., 1997; Rubio and Wenthold, 1997; Petralia et al., 2000; Spatz, 2001). These mechanisms could be driven within the DCN by Sp5 synaptic activity, and could regulate the strength (Fujino and Oertel, 2003) or dynamics of subsequent synaptic transmission within the DCN circuit. They can also be coupled to the regulation of ion channel availability or channel kinetics in postsynaptic cells.

21

The bi-directional effect of Sp5 stimulation on firing rate (41% suppression; 38 % enhancement), latency (75% of units had longer latencies, 25% of units had shorter latencies), and regularity (57% of units had decreased regularity; 43% of units had increased regularity) implies that there is variability in the underlying mechanisms, with a bias towards inhibition. For example, the same Sp5 stimulus resulting in increases and decreases in latency in different units could be due to the heterogeneous distribution of potassium channel subtypes in pyramidal cells (Rusznak et al., 2008). Alternatively, projections from different regions of Sp5 may activate different patterns of excitatory and inhibitory synaptic activity in pyramidal cells and could be responsible for the heterogeneous effects. The tonotopic organization of Sp5 effects shown here supports the idea that the Sp5 stimulation site and the pattern of innervation in the DCN from that stimulation site could contribute to the observed variability in rate and timing effects.

DCN pyramidal cells integrate Sp5 and acoustic inputs with features both in common with and distinct from those shown previously for trigeminal ganglion stimulation (Shore, 2005; Shore et al., 2008). A common feature is the presence of bimodal enhancement or suppression of firing rate in 80% of neurons recorded. However, several differences are also apparent. While trigeminal ganglion stimulation primarily suppressed sound-evoked firing rates, Sp5 stimulation only showed slightly more suppression of acoustic response rates. Furthermore, while unimodal trigeminal ganglion stimulation resulted in approximately equal numbers of excited or inhibited units, unimodal Sp5 responses were primarily excitatory (Shore, 2005; Shore et al., 2008). Despite the predominance of excitation following unimodal Sp5 stimulation, the increased latencies and suppression of acoustic responses by Sp5 stimulation suggests a predominant inhibitory effect of Sp5 on sound-driven responses. Indeed, the known anatomical connections and physiological effects (Young et al., 1995; Davis and Young, 1997; Kanold and Young, 2001) make it likely that additional sub-threshold inhibitory circuits are activated by Sp5 stimulation.

The responses of pyramidal cells to Sp5 stimulation may also depend on the organization of the projections from Sp5 onto the tonotopic axes of the DCN. Sp5 stimulation produced a larger suppression of firing rate and increases in latency within the mid-frequency region (~10 kHz) of the DCN. The peripheral representation of inputs to the DCN via Sp5 appears to be principally from the face areas (see Figure 2.1), but not from the pinnae region, which is principally carried via the cuneate nucleus pathways (Kanold and Young, 2001). This suggests that the Sp5 pathways are more likely involved with suppression of self-generated sound (Haenggeli et al., 2005b; Shore, 2005) than with sound localization in the vertical plane that depends on pinnae cues (Masterton et al., 1994; Huang and May, 1996). However, guinea pig vocalizations cover a wide frequency range (Wallace and Palmer, 2008), so it is not clear why the Sp5 inputs should show a frequency-specific modulation of DCN activity.

Significance of Findings

The modulation of DCN spike timing by somatosensory inputs as demonstrated here suggests that this circuitry could significantly alter the representation of the acoustic environment by pyramidal cells. For example, changing the temporal response pattern from a chopper to a buildup pattern could result in a code that reports aspects of stimulus duration, whereas changing from a buildup to a pauser pattern might result in a code that signifies the stimulus onset. Similarly, changes in regularity could lead to increased (or decreased) synchronous firing of populations of pyramidal cells, and thus alter their synaptic influence onto inferior colliculus neurons.

Under conditions of sensory deprivation induced by cochlear damage, somatosensory influences on the CN are enhanced (Shore et al., 2008; Zeng et al., 2009b). Similar cochlear insults give rise to phantom perceptions of sound, or tinnitus (Kaltenbach et al., 2005). Thus, we might expect that the spike- timing alterations observed here would be further enhanced under conditions that cause tinnitus. These spike-timing alterations may explain the ability of patients to modulate the pitch and loudness of their tinnitus by manipulations of their face and neck (Levine, 1999; Levine et al., 2003; Biesinger et al., 2008), regions that are innervated by the trigeminal nerve.

Figures
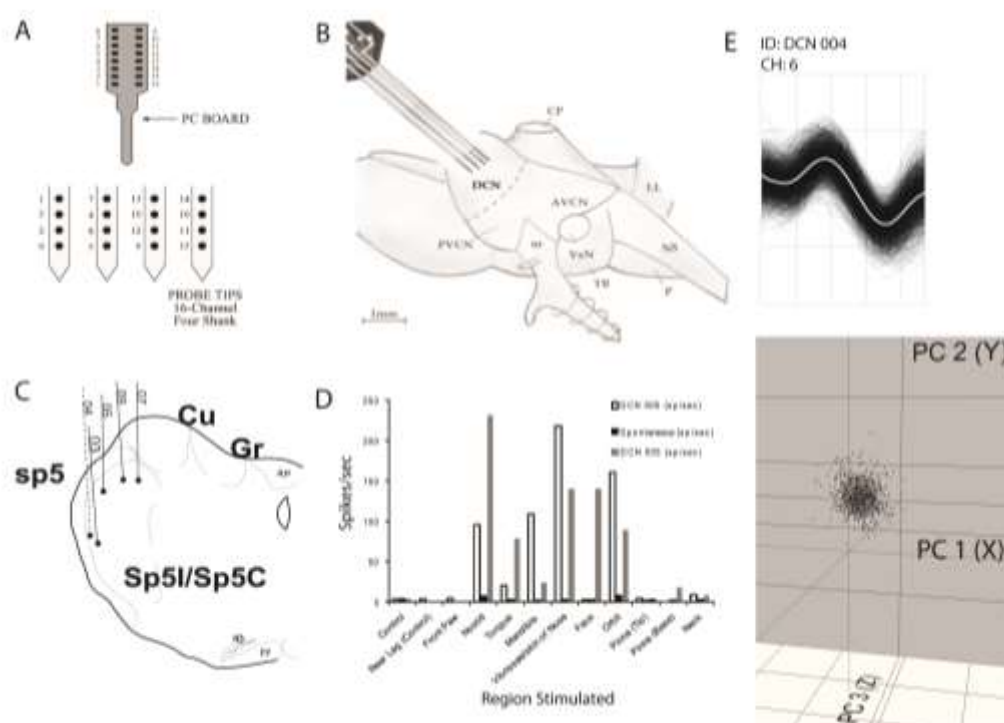
Figure 2.1 – **Single units were recorded in response to Sp5 stimulation.** A. Responses were recorded using a sixteen channel silicon substrate electrode array. Channels are arranged on four shanks in a 4x4 grid. B. The electrode array was visually placed into the DCN in a rostral-caudal/dorsal-ventral plane from the surface of the DCN. C. Schematic of histological reconstruction of the stimulating electrode tracks for 5/7 guinea pigs. D. A receptive field is constructed by plotting spike activity recorded from the Sp5 stimulating electrode in response to mechanical stimulation of various sites in the head and neck region. Black bars indicate spontaneous activity. White (05), see Figure 2C for Sp5 electrode position) and grey (06, see Figure 2C for Sp5 electrode position) bars indicate the level of spike activity in two different guinea pigs elicited by mechanical stimulation of the described region. E. Spike waveforms were sorted and single units identified. Detected spike waveforms were overlaid to aid in verification of consistent waveform shape and size (top). Thick gray line is an average of all spike waveforms. Principal component analysis was used in three dimensions to identify clusters of waveforms (bottom).
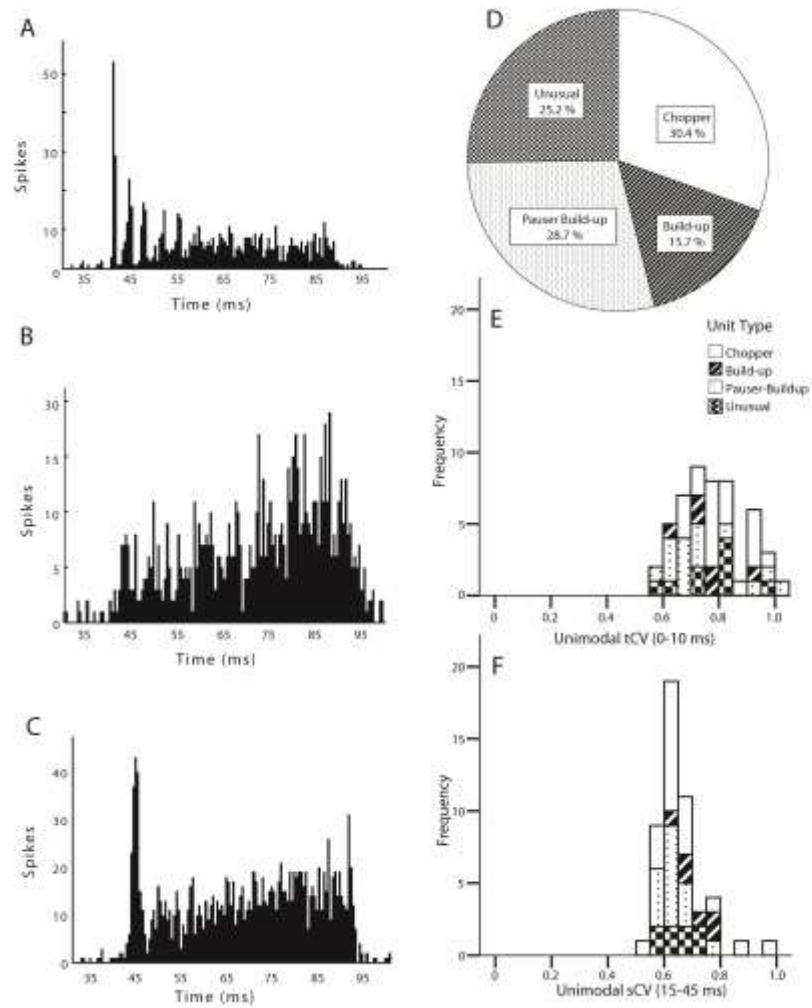
Figure 2.2 - PSTHs of DCN unit responses to BF tones at 20 dB SL. Bin width = 1 ms. 200 Trials. A. Chopper response type. B. Buildup response type. C. Pauser response type. D. Percentage of units that were classified as each type. Some unit responses were unusual. E. Histogram represents the distribution of transient CVs (0-10 ms post stimulus onset) measured from units responding to BF tones at 20 dB SL. F. Histogram represents the distribution of steady-state CVs (15-45 ms post stimulus onset) measured from units responding to BF tones at 20 dB SL.
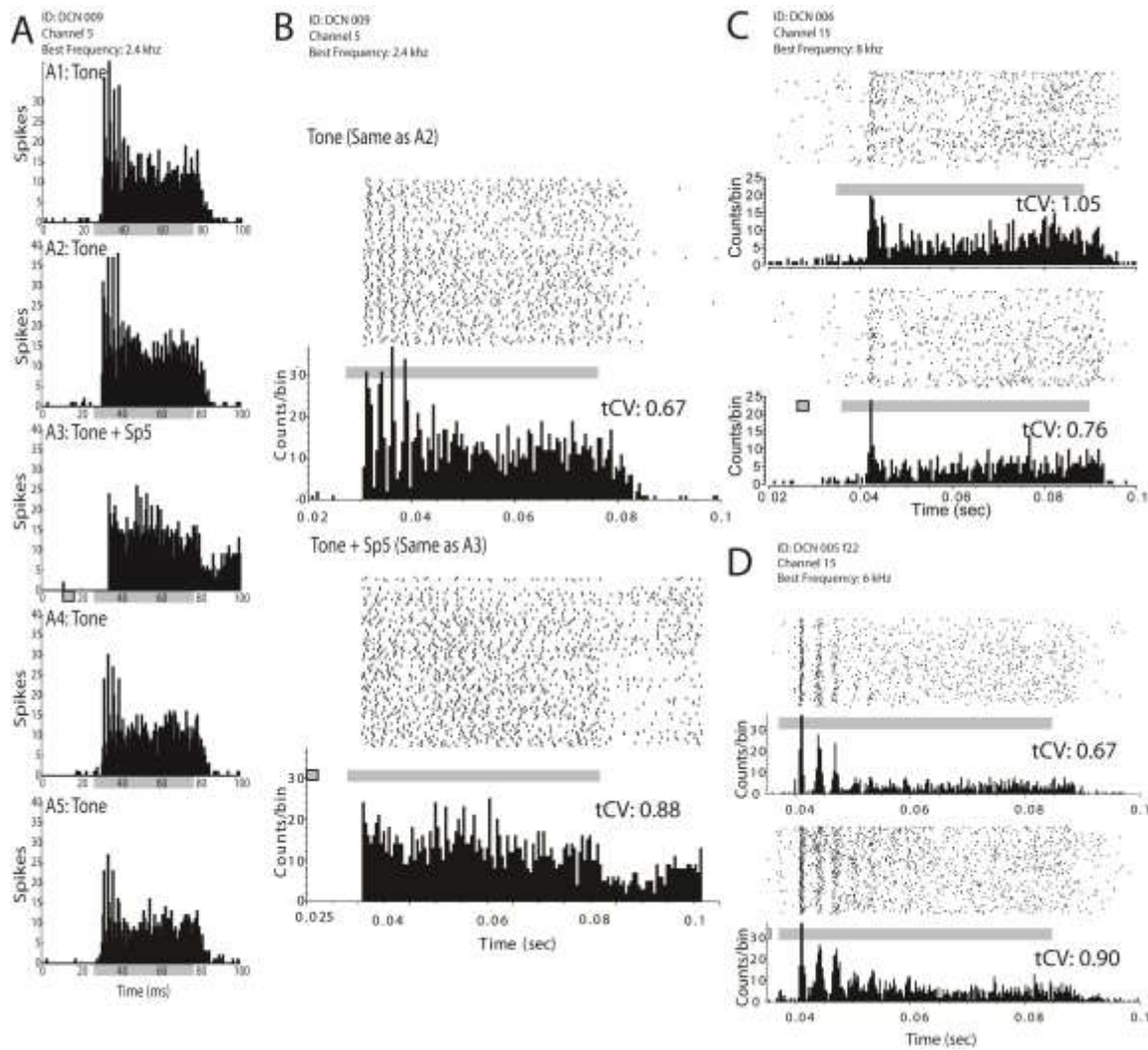
Figure 2.3 - Sp5 stimulation changes firing rate and regularity in DCN pyramidal cells. Firing rate is suppressed and regularity of the acoustic response is decreased when sound is preceded by Sp5 stimulation. A: A1 and A2. Identical responses of a chopper unit response to BF tones are shown prior to bimodal stimulation. A3. Bimodal response showing suppressive integration. A4-A5. Partially recovered acoustic responses at 5 and 10 minutes following the collection of bimodal responses. B. Raster plot and PSTH of a chopper unit response to BF tones (top, same as A2) and BF tones preceded by Sp5 stimulation (bottom, same as A3).C. Raster plot and PSTH of a pauser unit response to BF tones (top) and BF tones preceded by Sp5 stimulation (bottom). D. Raster plot and PSTH of a chopper unit response to BF tones (top) and BF tones preceded by Sp5 stimulation (bottom). Each PSTH is composed of 200 trials. In each raster plot, each point represents a spike and each row represents a single stimulus trial. The bottom row is the first trial. Solid gray bars indicate the duration of the acoustic stimulus. Gray bars with black borders indicate the duration of electrical stimulation of Sp5. The average value of the transient CV (tCV, see methods) is indicated above each response in B, C and D.

26
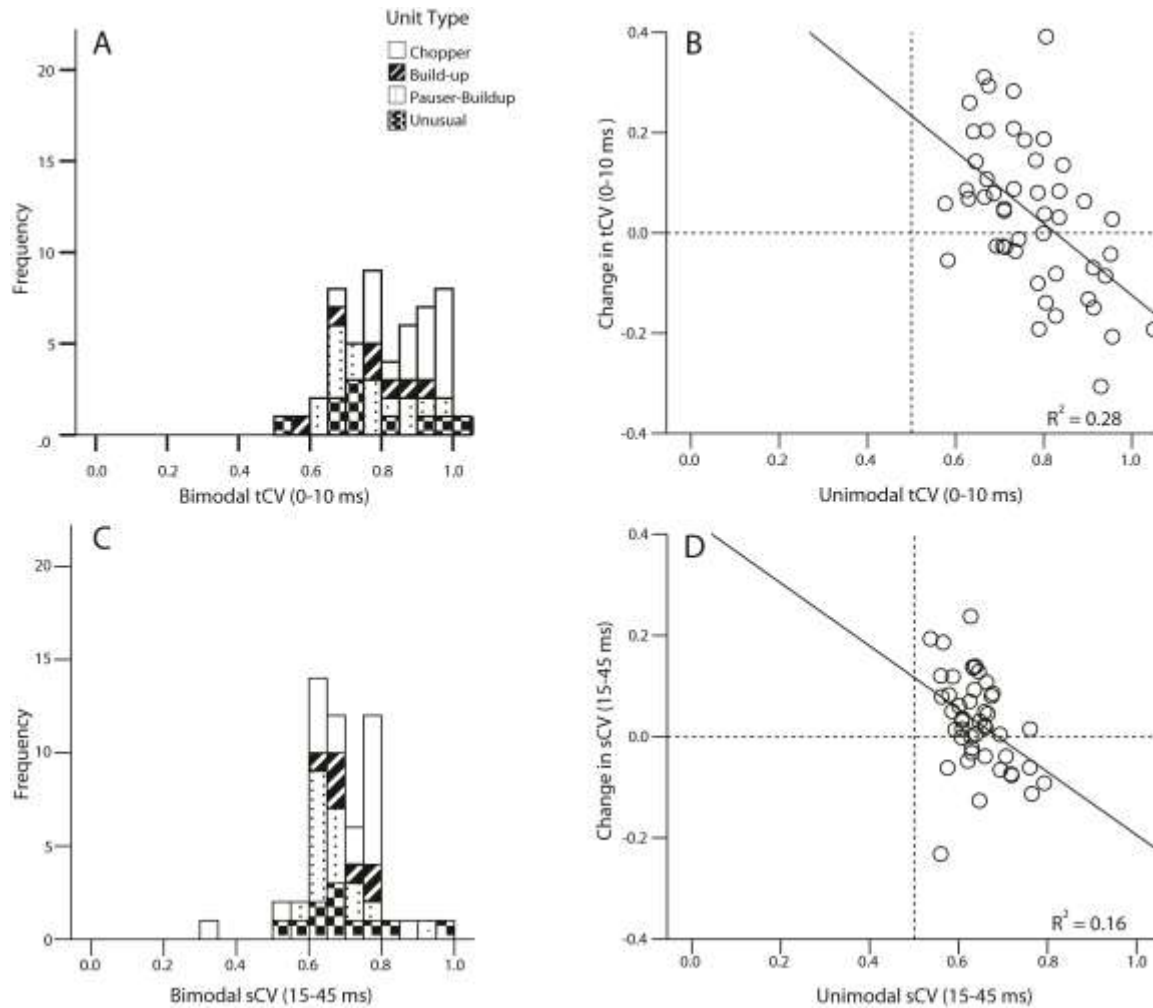
Figure 2.4 - Sp5-induced changes in regularity depend on the regularity of the acoustic response. A. The distribution of transient CVs (0-10 ms post stimulus onset) measured from units responding to bimodal stimulation (BF tones at 20 dB SL preceded by Sp5 stimulation). B. The change in transient CV with bimodal stimulation is plotted against the transient CV in response to sound. C. The distribution of steady-state CVs (15-45 ms post stimulus onset) measured from units responding to bimodal stimulation (BF tones at 20 dB SL preceded by Sp5 stimulation). D. Change in steady-state CV with bimodal stimulation is plotted against the steady-state CV in response to sound. C–D. Dashed vertical line separates regular units (Left, CV<0.5) from irregular units (Right, CV>0.5). Dashed horizontal line separates units that become less regular (Above Line) from units that become more regular (Below Line).

27
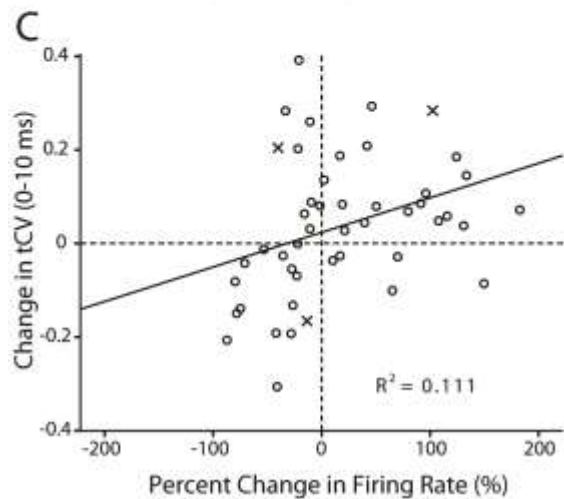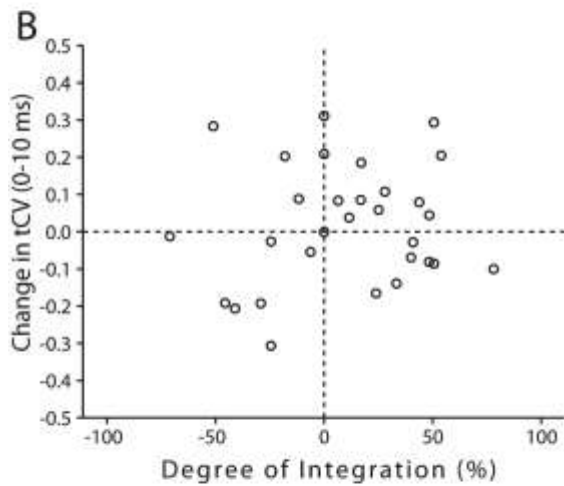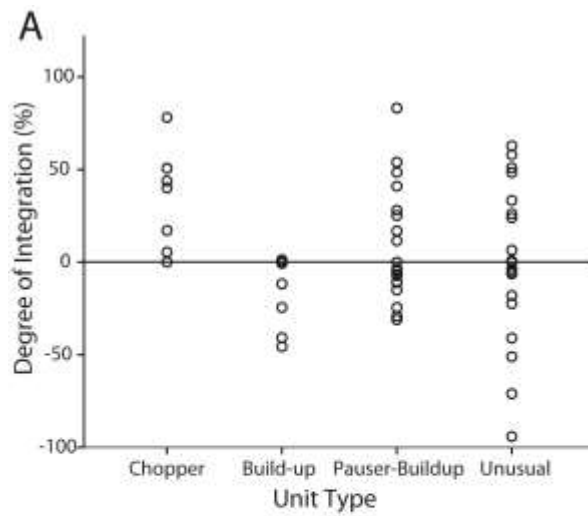
Figure 2.5 - Enhancement and suppression of acoustic responses by Sp5 stimulation. A. The degree of suppression or enhancement in chopper (C), buildup (B), pauser (PB), and unusual units. B. The change in CV is independent of the degree of integration. C. The change in tCV depends in part on the change in firing rate. Units from Figure 2.3B-D are identified with an x. B. and C. Units that become more regular are below the dashed horizontal line while units that become less regular are above it. Units that have increased firing rates are to the right of the dashed vertical line while units that have decreased firing rates are to the left of it.

28
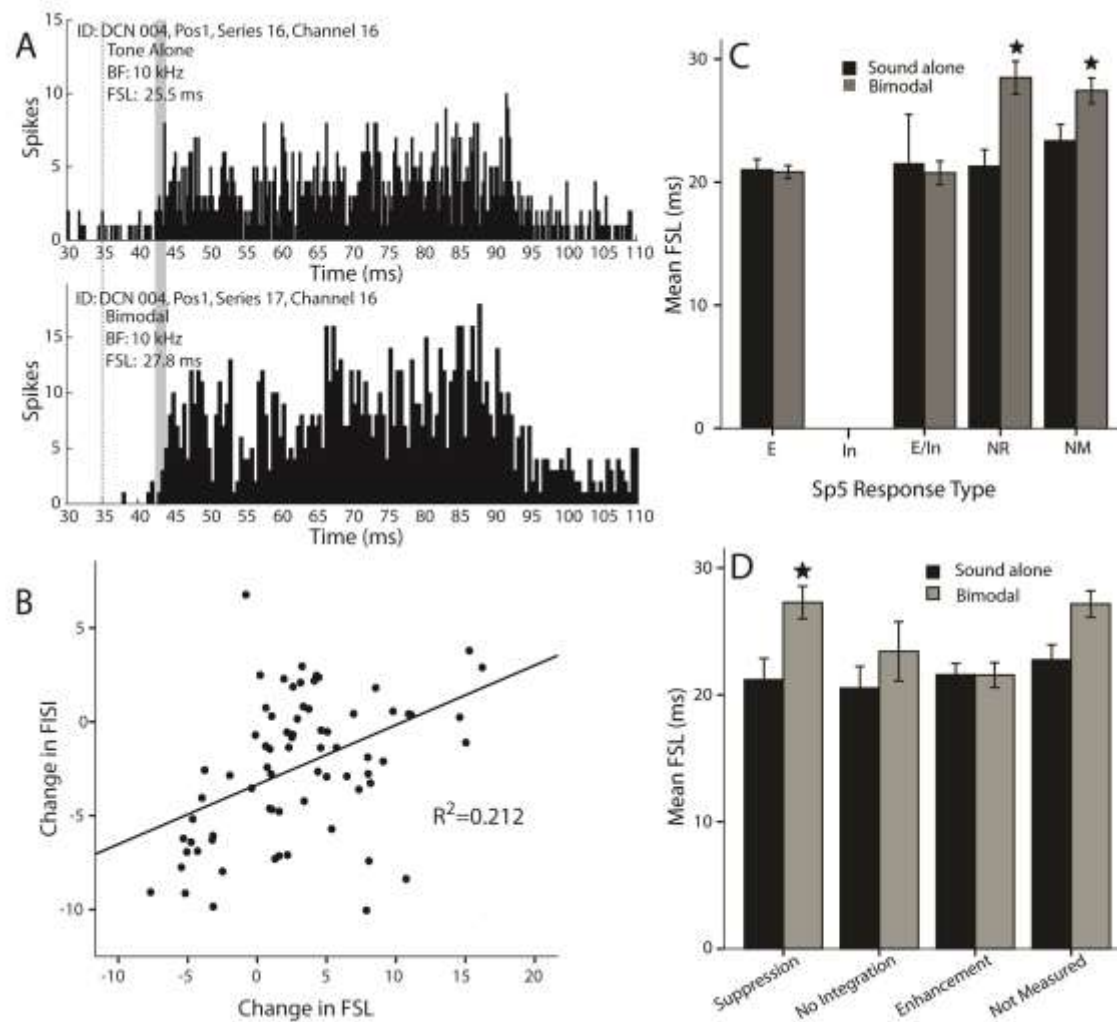
Figure 2.6 - Acoustic response latencies increase with Sp5 stimulation. A. PSTH of unimodal acoustic response (Top) and PSTH of bimodal response to BF tones preceded by Sp5 stimulation (Bottom), 200 Trials. Bin width = 1 ms. Dashed vertical line indicates onset of sound. Shaded vertical line highlights the increase in latency in the bimodal response. B. The change in FISI is correlated with the change in FSL. C. Mean acoustic FSLs are shown for groups of neurons with the same unimodal response to Sp5 stimulation: Bimodal FSLs (dark) are longer than unimodal acoustic FSLs (light) for NR and NM groups. E=excitation; In=inhibition; E/In=mixed; NR=no response to Sp5 stimulation; NM=Response to Sp5 stimulation not measured; Star indicates p< 0.01. D. Average FSLs within groups of neurons with the same type of rate integration (Suppression, Enhancement, or No Integration) are shown. FSL is significantly longer in units with bimodal suppression. Bimodal FSLs (dark); sound alone FSLs (light).
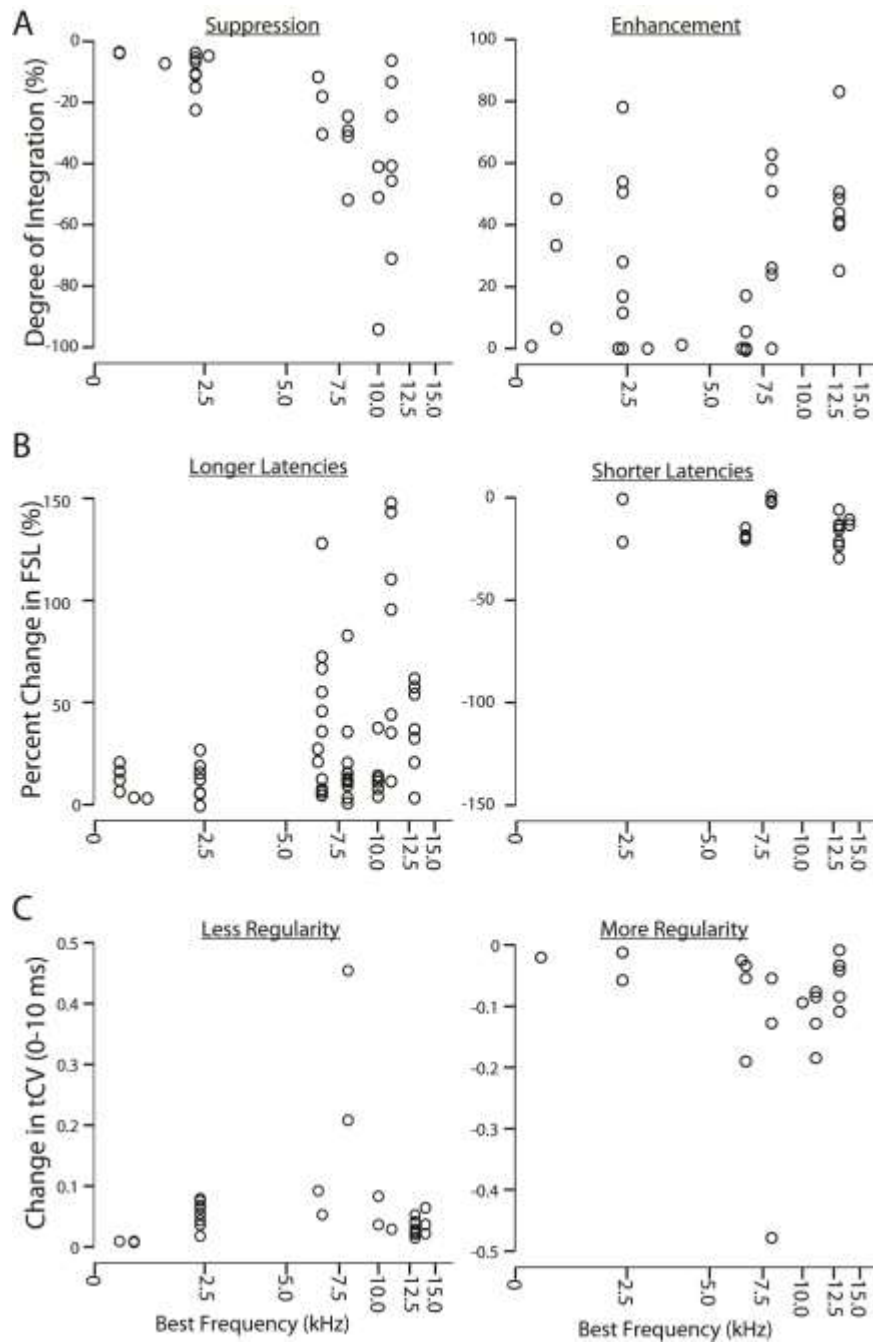
Figure 2.7 - Sp5-induced changes in acoustic responses are tonotopically organized. A. For each unit, the degree of suppression (left) or enhancement (right) is plotted against the best frequency of the unit. B. For each unit, the percent increase (left) or decrease (right) in latency is plotted against the best frequency of the unit. C. For each unit, the increase (left), or decrease (right) in transient CV is plotted against the best frequency of the unit.

Chapter 3: Stimulus-timing dependent bimodal plasticity in DCN

The study presented in Chapter 3 has been accepted for publication in the PLOS One (Koehler and Shore, 2013).

Fusiform cells in the dorsal cochlear nucleus (DCN) integrate auditory and somatosensory information (Shore, 2005; Kanold et al., 2011; Koehler et al., 2011). Responses to sound in these multisensory neurons, the principal output neurons of the DCN, remain enhanced or suppressed for up to two hours following bimodal somatosensory and auditory stimulation (Dehmel et al., 2012c). The mechanisms underlying this long-lasting effect have not been elucidated, but the duration of the effect is consistent with synaptic plasticity.

Specialized spike-timing dependent plasticity (STDP) has been demonstrated *in vitro* at parallel fiber synapses with DCN neurons (Tzounopoulos et al., 2004) and might underlie *in vivo* long-lasting bimodal plasticity (Dehmel et al., 2012c). Parallel-fiber axons from cochlear nucleus granule cells, which receive somatosensory inputs (Zhou and Shore, 2004; Haenggeli et al., 2005a), synapse on the apical dendrites of both fusiform cells and their inhibitory interneurons, cartwheel cells (Fig. 3.1A). Parallel fiber synapses on fusiform and cartwheel cells exhibit Hebbian and anti-Hebbian STDP, respectively, which is induced by the close temporal association of fusiform cell action potentials with excitatory post-synaptic potentials elicited by pre-synaptic action potentials in parallel fibers (Tzounopoulos et al., 2004; Tzounopoulos et al., 2007). Hebbian STDP is induced when synaptic activity preceding a post-synaptic spike potentiates the synapse while synaptic activity following a post-synaptic spike depresses the synapse. In contrast, anti-Hebbian STDP is induced when synaptic activity preceding a post-synaptic spike depresses the synapse while synaptic activity following a post-synaptic spike potentiates the synapse (Markram et al., 2011).

31

DCN models (Roberts et al., 2006) and studies of cerebellar-like structures in electrosensory fish (Bell et al., 1997b; Roberts and Leen, 2010) suggest that STDP may be a generalized learning mechanism for adaptive filtering in early sensory processing centers. DCN neural responses may adapt over time to emphasize or de-emphasize features of auditory signal representation that are temporally associated with non-auditory afferent (Young et al., 1995; Shore, 2005) or top-down feedback (Weedman and Ryugo, 1996; Shore and Moore, 1998) signals supplied through the granule cell network. In this study, we supplied sub-threshold synaptic activity to DCN neurons via the granule cell network by stimulating spinal trigeminal nucleus (Sp5) neurons. The excitatory terminals of these somatosensory neurons, which process vocal feedback signals and other facial somatosenations, end in the granule cell domain (Zhou and Shore, 2004; Haenggeli et al., 2005a; Zhou et al., 2007). We have previously shown that pairing somatosensory stimuli with sound has a long-lasting influence on DCN responses to sound (Dehmel et al., 2012). Here, we examined STDP as an underlying mechanism for multisensory plasticity by varying the relative timing and order of the auditory (equivalent to post-synaptic) and somatosensory (equivalent to pre-synaptic) components of bimodal stimuli following standard stimulus-timing dependent protocols (Caporale and Dan, 2008). Our results show for the first time *in vivo* that long-lasting bimodal plasticity in the DCN is stimulus-timing dependent and thus likely to be driven by STDP at parallel fiber synapses.

Results

Bimodal plasticity induction in the DCN was assessed *in vivo* by measuring sound-evoked and spontaneous firing rates before and after bimodal stimulation. Bimodal stimulation consisted of electrical pulses delivered to Sp5 to activate parallel fiber-fusiform and -cartwheel cell synapses, paired with a 50-ms tone burst to elicit spiking activity in fusiform and cartwheel cells (Fig. 3.1A). Dorsal cochlear nucleus unit responses to unimodal tones and spontaneous activity following bimodal stimulation were recorded with a multi-channel electrode placed into the DCN using a standard protocol (Fig. 3.1B). Bimodal stimulation could either suppress or enhance responses to sound. In the

representative unit shown in Figure 3.1C, spontaneous activity and responses to tones were suppressed 5, 15, and 25 minutes after bimodal stimulation. Bimodal enhancement and suppression in this study refer to unimodal (auditory) response magnitudes at different times after bimodal stimulation compared to unimodal response magnitudes before bimodal stimulation. These are equivalent to the "late" or long-lasting changes previously described (Dehmel et al., 2012) that reflect plasticity. This "bimodal plasticity" contrasts with bimodal integration in which bimodal enhancement and suppression were measured by comparing responses during bimodal stimulation with unimodal (auditory) responses (Shore, 2005; Stein et al., 2009; Kanold et al., 2011).

Bimodal plasticity is stimulus-timing dependent

In vivo stimulus timing dependent plasticity has been shown to reflect underlying Hebbian and anti-Hebbian STDP (Caporale and Dan, 2008). To assess stimulus-timing dependence in the present study, the bimodal stimulation protocol (Fig. 3.1B) was repeated with varying bimodal intervals: i.e., Sp5 stimulation onset minus sound onset. In a representative unit (Fig. 3.2A) the auditory response was suppressed after bimodal stimulation when somatosensory (Sp5) preceded auditory stimulation but was enhanced if auditory preceded somatosensory stimulation. Negative bimodal intervals indicate somatosensory preceding auditory while positive bimodal intervals indicate auditory preceding somatosensory stimulation. Bimodal plasticity was considered stimulus-timing dependent when the sound-evoked firing rates increased or decreased following bimodal stimulation at some, but not all, of the bimodal intervals tested. All units in which responses to sound were modulated by the bimodal pairing protocol showed stimulus-timing dependence (i.e. the firing rate increased or decreased by at least 20% following at least one bimodal interval tested; 16/16 single-unit and 98/110 multi–unit clusters).

For each unit demonstrating stimulus-timing-dependent plasticity, a timing rule was constructed from the percent change in firing rate as a function of bimodal interval (Fig. 3.2B-E). Timing rules were classified into Hebbian-like (Fig. 3.2B), anti-Hebbian-like (Fig. 3.2C), enhanced (Fig. 3.2D), or suppressed (Fig. 3.2E). Mean single unit timing

rules for each group are shown in Figures 3.2F - 2I. Hebbian-like units were maximally enhanced when somatosensory preceded auditory stimulation and maximally suppressed when auditory preceded somatosensory stimulation, likely reflecting Hebbian STDP at the parallel-fusiform cell synapse (n=5; Fig. 3.2 B,F). Anti-Hebbian-like units were maximally suppressed when somatosensory preceded auditory stimulation and maximally enhanced when auditory preceded somatosensory stimulation (n=7; Fig. 3.2C,G). Other units were either enhanced (n=2;Fig. 3.2D, H) or suppressed (n=2; Fig. 3.2E,I) by all bimodal pairing protocols. Comparison of single and multi unit clusters indicated that the same Hebbian-like (n=25), anti-Hebbian-like (n=18), enhanced (n=18), suppressed (n=12) timing rules were observed in multi-unit clusters. Thirty three multi units showed a complex dependence of suppression and enhancement on the bimodal interval (not shown).

Bimodal enhancement and suppression stabilize after 15 minutes and begins to recover by 30 minutes

Synaptic plasticity at parallel fiber synapses in the DCN develops over the course of several minutes (Zhang and Oertel 2004, Tzounopolous 2004). To compare the bimodal plasticity time course to synaptic plasticity time courses, bimodal plasticity was measured 5, 15, and 25 minutes after bimodal stimulation (Fig. 3.1B) for both single and multi units. The maximal enhancement and suppression and the bimodal interval that induced maximal enhancement and suppression were used to estimate the effect of bimodal stimulation on the DCN neural population. The change in firing rate following bimodal stimulation was often greater at 15 or 25 minutes than at 5 minutes after bimodal stimulation (Fig. 3.2B-E). Maximal bimodal enhancement plateaued 15 minutes following bimodal pairing and started to recover at 25 minutes (Fig. 3.3A top). In contrast, maximal bimodal suppression continued to develop over 25 minutes (Fig. 3.3A bottom). Median maximal suppression was -28% (n=126) after 25 minutes while median maximal enhancement was 40% (n=126) by 25 minutes after bimodal pairing. These data indicate that tone responses began to recover towards baseline 25 minutes after bimodal pairing. In some units, responses to tones recovered to baseline levels within 90 minutes after the bimodal pairing (Fig. 3.3B).

The DCN neural population is dominated by anti-Hebbian-like stimulus-timing dependent plasticity

Identifying the maximum bimodal enhancement and suppression with corresponding bimodal intervals

allowed a population estimate of the stimulus-timing dependence of bimodal plasticity in the DCN (Fig 3.4). When the

most effective bimodal pairing protocol consisted of Sp5 following tone stimulation by 20 or 40 ms, Sp5 synchronous

with tone stimulation, or Sp5 preceding tone stimulation by 10 ms, bimodal stimulation was most likely to produce

enhancement. In contrast, when the most effective bimodal stimulation protocol was Sp5 preceding tone stimulation

by 20 or 40 ms or following tones by 10 ms, it primarily induced bimodal suppression.

Bimodal stimulation induced stronger persistent effects than unimodal stimulation

Our proposed hypothesis that STDP underlies long-lasting bimodal plasticity requires that paired auditory and

somatosensory stimulation induce long-lasting suppression or enhancement of tone-evoked responses. To test this,

changes in unimodal tone-evoked responses were measured during protocols in which the bimodal stimulus was

replaced by a unimodal stimulus (either sound or Sp5 stimulation alone). Maximal bimodal enhancement (1-tailed

paired Student's t-test; n=10; p=0.025) and suppression (1-tailed paired Student's t-test; n=17; p=0.00023) were

significantly stronger than enhancement or suppression of the tone-evoked response following unimodal tone

stimulation (Fig. 3.5A). However, only maximal suppression (1-tailed paired Student's t-test; n=20; p=0.017), but not

enhancement (1-tailed paired Student's t-test; n=7; p=0.24), following bimodal stimulation was stronger than that

following unimodal Sp5 stimulation (Fig. 3.5B). Thus, activation of both somatosensory and auditory inputs have a

greater long-lasting affect on DCN unit responses than either activation of auditory or somatosensory inputs aone.

Units excited by Sp5 stimulation exhibited Hebbian timing rules while units inhibited by Sp5 stimulation exhibited

anti-Hebbian timing rules

Activation of somatosensory neurons has previously been shown to elicit excitation, inhibition, or complex

responses in DCN neurons (Young et al., 1995; Shore, 2005). Somatosensory stimulation elicits either excitatory or

inhibitory responses in a particular fusiform cell depending on whether input is conveyed to that fusiform cell directly from parallel fiber inputs or via inhibitory interneurons (cartwheel cells). Although Sp5 stimulation amplitude was selected to activate subthreshold somatosensory inputs, eleven units had measurable excitatory or inhibitory responses to unimodal Sp5 stimulation and clearly defined Hebbian or anti-Hebbian timing rules. Five out of 6 units that responded to Sp5 stimulation with excitatory responses exhibited Hebbian timing rules, suggesting that Hebbian timing rules were driven by parallel fiber-to-fusiform cell synapses (Fig. 3.6A,B). In contrast, four out of 5 units that responded to Sp5 stimulation with inhibition exhibited anti-Hebbian timing rules, suggesting anti-Hebbian dependence on parallel fiber-to-cartwheel cell synapses (Fig. 3.6C,D). Units that did not show clear stimulus-timing dependency were just as likely to be excited or inhibited by Sp5 stimulation alone (not shown).

Stimulus timing rules correlate with inhibitory inputs

Units were classified according to traditional physiological response schemes for guinea pig (Stabler et al., 1996a) by their frequency response maps (n=63 units; types I, II, III, I-III, IV, and IV-T) and their temporal responses properties at best frequency (n=66 units; buildup, pause-buildup, chopper, onset, and primary-like). These physiological response properties are linked to intrinsic, morphological, and network properties of DCN neurons, including their somatosensory innervation. In the present study, the proportion of units with Hebbian and anti-Hebbian-like timing rules correlated with the degree of inhibition reflected in their response areas. Figure 3.7A shows the proportion of Hebbian and anti-Hebbian-like units for types I, I-III, III, and IV, response map classifications usually associated with fusiform or giant cells (Ding et al., 1999). Hebbian-like timing rules were more likely to be found in units with Type I response areas with no inhibition than in units with Type III or IV response areas with significant inhibition away from best frequency or at high intensities.

Timing rules and the strength of bimodal plasticity were also compared for groups of units with each combination of temporal and receptive field response types. Two classes of neurons had consistent bimodal timing

36

rules. Buildup or pauser-buildup units with type I or type II response areas exhibited clear Hebbian-like timing rules (Fig. 3.7B). In contrast, onset units with type IV or IV-T response maps exhibited only anti-Hebbian timing rules (Fig. 3.7C).

Spontaneous rate changes correlate with changes in sound-evoked firing rate

After bimodal stimulation the changes in sound-driven and spontaneous firing rates were significantly correlated for all bimodal intervals except for -20 ms ($0.21 < R^2 < 0.48$). The highest correlation in sound-driven and spontaneous firing rates was observed following the +10 ms bimodal interval (Fig. 3.8A, linear regression analysis, DF=82; R^2=0.48; p=$2.62e^{-13}$). However, changes in sound-evoked and spontaneous firing rates were not significantly correlated following bimodal stimulation at an interval of -20 ms.

Discussion

Evidence for STDP-driven bimodal plasticity in DCN

Bimodal stimulation of auditory and somatosensory inputs to the DCN modulates spontaneous and sound-driven activity in a manner consistent with STDP at parallel fiber synapses with fusiform cells. This stimulus-timing dependent bimodal plasticity in the DCN exhibits timing rules that reflect those found *in vitro* at parallel fiber-fusiform and parallel fiber-cartwheel cell synapses (Tzounopoulos et al., 2004). The time course of bimodal enhancement, which plateaus 15 minutes post-pairing, and bimodal suppression, which continues to develop 25 minutes post-pairing, are also consistent with the time course of STDP. *In vitro* STDP recordings at parallel fiber synapses revealed maximum LTP 2-to-20 minutes after STDP induction and maximum LTD 5-to-15 minutes after STDP induction (Tzounopoulos et al., 2007). Stimulus-timing dependence in the auditory (Dahmen et al., 2008) and visual (Yao and Dan, 2001) cortices develops over 3-5 minutes while STDP in the electrosensory lobe of the mormyrid takes 5 – 10 minutes to develop (Bell et al., 1997b). Adaptive filtering theories suggest that, after plasticity induction, responses should recover to baseline with repeated unimodal tone stimulation (Sawtell, 2010). Enhanced, but not suppressed,

37

firing rates in the present study began to recover towards baseline within 30 minutes but only a few units (Fig. 3.3B)

showed complete recovery within 90 minutes of bimodal stimulation. This recovery duration is consistent with STDP

given the duration of both potentiating and depressing DCN STDP observed *in vitro* (Tzounopoulos et al., 2004;

Tzounopoulos et al., 2007). The kinetics and requirements for recovery from bimodal plasticity deserve careful study

to identify whether responses recover spontaneously to baseline with time or whether sound stimulation is necessary

for recovery.

The equivalent enhancement in DCN induced by bimodal stimulation and Sp5 stimulation alone (Fig. 3.5B)

suggests that synaptic or intrinsic mechanisms, independent of STDP, are partially involved in the long-lasting

somatosensory influence on fusiform cell responses to sound. At parallel fiber synapses in the DCN, high frequency

synaptic stimulation also induces LTP while low frequency synaptic stimulation induces LTD (Fujino and Oertel, 2003).

In addition, spiking activity in cartwheel cells induces retrograde endocannabinoid release, which suppresses parallel

fiber input to cartwheel cells and could potentially enhance the fusiform cell sound-driven response through release

from cartwheel cell inhibition (Sedlacek et al., 2011). Parallel fiber (Manis, 1989, 1990) and bimodal stimulation

(Kanold et al., 2011; Koehler et al., 2011) have also been shown to induce changes in intrinsic firing properties of

fusiform cells through de-inactivation of K^+ channels, although these mechanisms have only been shown to be

effective on the timescale of seconds.

If STDP at parallel fiber synapses is the underlying mechanism for bimodal plasticity, then there must be a

mechanism by which synaptic plasticity at parallel fiber synapses on fusiform cell apical dendrites influences fusiform

cell responses to auditory nerve input on their basal dendrites. One possibility, heterosynaptic plasticity, is unlikely

given that STDP at parallel fiber synapses on fusiform cells is homosynaptic and does not affect remote synapses on

either apical or basal dendrites (Fujino and Oertel, 2003; Tzounopoulos et al., 2004). A more likely possibility is that

synaptic plasticity at parallel fiber synapses broadens the window for temporal summation in fusiform cells by shifting

the resting membrane potential, leading to a decrease in the spike generation threshold at auditory nerve synapses, as demonstrated by modeling and in vitro experiments in fusiform cells (Doiron et al., 2011). Stimulus-timing dependent plasticity in other cell types in the DCN, such as giant cells or vertical cells, which receive few or no parallel fiber inputs may depend in a similar manner on as yet undescribed STDP mechanisms. Fusiform cell stimulus-timing dependent properties may also be conveyed to other DCN cell types via axon collaterals (Rhode et al., 1983). Although the targets of these collaterals have not been well-described, fusiform cell axon collaterals have been shown to synapse on giant cell dendrites (Smith and Rhode, 1985) and correlation analysis suggests the existence of excitatory intra-DCN connectivity in guinea pigs (Kipke et al., 1991).

Network and intrinsic properties influence bimodal plasticity

The timing rule continuum, from Hebbian-like to anti-Hebbian-like to complex, shown in the present study is not surprising given the variety of DCN neural types and suggests that intrinsic or network mechanisms act alongside STDP to control bimodal plasticity. Bimodal plasticity timing rules *in vivo* may also be influenced by cholinergic input from the superior olivary complex or the tegmental nuclei (Shore et al., 1991; Sherriff and Henderson, 1994; Mellott et al., 2011), which modulate STDP in the DCN, converting Hebbian LTP to anti-Hebbian LTD at parallel fiber-fusiform cell synapses (Zhao and Tzounopoulos, 2011).

The finding that physiological classes of DCN neurons exhibit differing stimulus-timing dependencies implies that physiological (and likely morphological) subtypes of DCN neurons perform different functions with their multimodal inputs. The present data indicate that DCN neurons with less inhibitory influence (Type I receptive fields) are more likely to display Hebbian-like stimulus timing dependence while those with significant inhibitory influence (Type III and IV receptive fields) are more likely to display anti-Hebbian-like stimulus timing dependence. This may reflect inhibitory influences from vertical cell or cartwheel cells on post-synaptic spiking patterns which, in fusiform cells, are likely determined by long-lasting or pre-hyperpolarizing inhibition (Kanold and Manis, 1999). The timing

rules for STDP induction in other systems depend not only on the relative timing of pre-synaptic activity and post-synaptic spikes, but also on the number and pattern of post-synaptic spikes (Dan and Poo, 2006).

Alternatively, the source of sound-driven inhibition to DCN principal cells may also exhibit predominantly Hebbian-like stimulus-timing dependent plasticity, resulting in anti-Hebbian-like timing rules in recipient neurons. One source could be type II neurons, putative vertical cells. Type II neurons supply inhibition to fusiform and giant cells (Rhode, 1999), are inhibited by somatosensory and parallel fiber input (Young et al., 1995), and in our data exhibit Hebbian-like stimulus-timing dependent plasticity. Future studies should thus consider the functional connectivity of non-auditory inputs via granule or other cells to different classes of principal cells and how they might shape the spectral selectivity of DCN neurons.

The role of STDP in adaptive processing

Hebbian and anti-Hebbian STDP are important mechanisms for adaptive processing in cerebellar-like circuits. Neural responses to predictable stimuli in these circuits exhibit long-lasting adaptation induced by correlations between primary sensory input and error signals supplied by motor control or secondary sensory inputs (Bell et al., 1997a; Markram et al., 2011; Requarth and Sawtell, 2011). The present study describes the first *in vivo* experiments evaluating mechanisms for multisensory adaptive processing in the DCN. Adaptive processing in the DCN has been proposed as a mechanism to suppress responses to sound predicted by non-auditory signals (Roberts et al., 2006; Roberts and Portfors, 2008), such as self-generated sound preceded by somatosensory input (Oertel and Young, 2004; Shore, 2005). It also may adapt sound localization signals in the DCN (May, 2000) to pinna or head position (Kanold and Young, 2001; Oertel and Young, 2004; Kanold et al., 2011). A high proportion of DCN neurons exhibited anti-Hebbian-like timing rules, with responses to tones suppressed when Sp5 stimulation preceded the tone and enhanced when the tone preceded Sp5 stimulation. This observation is consistent with the hypothesis that DCN neurons cancel self-generated sounds predicted by preceding somatosensory activation. Future studies addressing adaptive

processing should use natural stimuli that would likely activate a smaller group of fibers with less synchronous input to the DCN.

Implications for tinnitus

Reports of elevated spontaneous firing rates in the DCN after tinnitus-inducing noise, implicates this structure as a site of phantom sound, or "tinnitus", generation in animal models of tinnitus (Brozoski et al., 2002; Kaltenbach et al., 2004; Dehmel et al., 2012c). Because DCN neurons are more responsive to somatosensory stimulation following hearing damage (Shore et al., 2008), bimodal plasticity in DCN may play a role in somatic tinnitus, the modulation of the pitch and loudness of a phantom sound perception by pressure or manipulation of the head and neck (Levine, 1999; Sanchez et al., 2007; Levine et al., 2008). In fact, the effect of bimodal stimulation, with Sp5 preceding tone stimulation, shifts from suppression in normal animals to enhancement in guinea pigs with behavioral evidence of tinnitus (Dehmel et al., 2012c), suggests that bimodal plasticity may contribute to DCN hyperactivity in tinnitus. Although auditory nerve inputs to fusiform cells provide weaker drive after noise over-exposure, granule cell input to fusiform cells does not weaken, despite decreases in the input resistance of granule cells (Pilati et al., 2012), perhaps due to cross-modal compensation (Zeng et al., 2009a; Zeng et al., 2012).

Experimental Procedures

Animals

Male pigmented guinea pigs (n=5) from the University of Michigan colony (300-400 g; Ann Arbor, MI) were used in this study. All procedures were performed in accordance with the National Institutes of Health (NIH) *Guidelines for the Use and Care of Laboratory Animals* (NIH publication No. 80–23) and were approved by the University Committee on Use and Care of Animals at the University of Michigan.

Surgical approach and electrode placement

Guinea pigs were anesthetized (subcutaneous injection of ketamine and xylazine, 40 mg/kg, 10 mg/kg; at the incision site a subcutaneous injection of lidocaine, 4 mg/kg) and ophthalmic ointment applied to their eyes. Their heads were fixed in a stereotaxic frame using a bite bar and hollow ear bars were placed into the ear canals. Core temperature was maintained at 38 °C. A left craniotomy was performed and a small amount of cerebellum was aspirated (leaving paraflocculus intact) to allow for visual placement of the recording electrode. Supplemental doses of ketamine and xylazine (I.M.) were administered at least hourly when indicated by response to a toe pinch. The guinea pig's condition was monitored by assessment of body temperature, respiration and heart rates, and unit thresholds. After the completion of neural recording, the guinea pig was sacrificed by intra-peritoneal injection of sodium pentobarbitol followed by decapitation.

A concentric bipolar stimulating electrode (FHC, Bowdoin, ME) was dipped in fluorogold and placed stereotaxically into Sp5; -10 degrees below horizontal, 0.28 +/- 0.03 cm lateral from midline; 0.25 +/- 0.02 cm caudal from transverse sinus; 0.9 +/- 0.1 cm below surface of cerebellum. The location of the electrode was reconstructed post-mortem. A four-shank, thirty two-channel silicon-substrate electrode (site spacing = 100 um, shank pitch = 250 um, site area = 177 um^2, impedance = 1–3 mOhms, NeuroNexus, Ann Arbor, MI) was placed at the DCN surface with each medial-to-lateral shank positioned within a different iso-frequency layer. The electrode was then lowered 0.8 – 1.0 um into DCN until the uppermost site on each shank responded to sound. In one guinea pig, after completing the recording protocol the DCN electrode was moved to a more medial location and a new frequency was selected for stimulation while the Sp5 stimulating electrode remained in place.

Auditory and somatosensory stimulation

Neural activity in response to ***unimodal tones*** was recorded before and at 5, 15, and 25 minutes after the ***bimodal stimulation protocol*** (Fig. 3.1B). ***Tone*** signals (50 ms duration) gated with a cosine window (2 ms rise/fall

time) were generated using Open Ex and an RX8 DSP (TDT, Alachula, FL) with 12 bit precision and sampling frequency set at 100 kHz. Sound was delivered to the left ear through the hollow ear bar by a shielded speaker (DT770, Beyer) driven by an HB7 amplifier (TDT, Alachula, FL). The system response was measured using a condenser microphone attached to the hollow earbar by a ¼" long tube approximating the ear canal. Sound levels were adjusted to account for the system response using a programmable attenuator (PA5, TDT, Alachula, FL) to deliver calibrated levels (dB SPL) at frequencies from 200 Hz to 24 kHz.

The **bimodal stimulation protocol** consisted of 500 trials of the 50 ms tones combined with electrical activation of Sp5 locations known to project to DCN (Shore et al., 2008). Five biphasic (100 us/phase) current pulses at 1000 Hz were delivered to Sp5 through a concentric bipolar electrode using a custom isolated constant current source. The current amplitude was set to the highest level (range: 50-70 µA) that did not elicit movement artifact. The tone level (60-65 dB SPL) and frequency were fixed for the duration of the recording and were selected to reliably elicit responses to sound from most recording sites. The *bimodal interval* was defined as the onset of the Sp5 stimulus minus the onset of the tone, with negative values indicating Sp5-leading tone stimulation and positive values indicating tone-leading Sp5 stimulation. Varied bimodal intervals were used to assess stimulus-timing dependence of bimodal plasticity. During each recording session, the bimodal interval was randomly selected from the following intervals until all conditions were tested: -40, -20, -10, 0, +10, +20, +40, or +60 ms. For the unimodal control protocols, either the current amplitude was set to 0 uA or the sound level was set to 0 dB SPL.

Spike detection and sorting

Voltages recorded from the multi-channel recording electrode were digitized by a PZ2 preamp (Fs=12 kHz, TDT, Alachua, Fl, USA) and band-pass filtered (300 Hz – 3 kHz) before online spike detection using a fixed voltage threshold set at 2.5 standard deviations above background noise (RZ2, TDT, Alachua, Fl, USA). Spike waveform snippets and timestamps were saved to a PC using Open Explorer (TDT, Alachua, Fl, USA). Waveform snippets were

sorted using principal components of the waveform shape and K-means cluster analysis with fixed variance (95%) and 5 clusters (OpenSorter, TDT, Alachua, FL, USA). Clusters with a J2 value (Dehmel et al., 2012c) above 1e-5 were not considered well isolated and were combined. Single units were identified by consistency of waveform shape and amplitude. Spikes up to 15 ms after the onset of the current stimulation were contaminated by electrical artifacts and ringing and excluded from all analyses. While multi-unit clusters could not be identified as isolated single units, the waveform shapes, amplitudes, and response properties were consistent over the duration of the recording.

Experimental design

To characterize unit responses to sound according to standard classification schemes (Stabler et al., 1996a), tone stimuli were presented before any Sp5 stimulation. Tone levels (0 – 85 dB SPL; 5 dB steps) and frequencies were varied (200 Hz – 23 kHz; 0.1 octave steps) between trials (200 ms trial; 50 ms tone) with each condition repeated 10-20 times. The current amplitude for Sp5 stimulation was set at the highest amplitude that did not elicit ipsilateral facial twitches (60-80 µA). At the current amplitude presented, few units showed supra-threshold responses to somatosensory stimulation, but clearly subthreshold responses were elicited, as evidenced by the bimodal effects.

Unimodal trials were recorded at four time points: before, and 5, 15, and 25 minutes after the bimodal stimulation protocol (Fig. 3.1B). Responses were recorded to **unimodal tones** presented at the same level (60 – 65 dB SPL) as in the bimodal stimulation protocol (200 trials, 5 trials per second). Two minutes of **spontaneous activity** was also recorded at each time point before and after the bimodal stimulation protocol. All unimodal tones and rate level functions were at the same frequency used for bimodal stimulation. The entire recording block in Figure 3.1B lasted for 30-35 minutes with unimodal recordings at each time point lasting for 5-7 minutes and the bimodal stimulation protocol lasting for 4-5 minutes.

The recording block in Figure 3.1B was repeated randomly for each bimodal interval tested (-40, -20, -10, 0, 10, 20, 40, or 60 ms). In one guinea pig, control recording blocks were repeated in which unimodal tone or Sp5 stimuli

44

replaced the bimodal stimuli. After the final recording block, the responses to unimodal tones were measured every 15-30 minutes for as long as possible to assess recovery after bimodal stimulation.

Unit characterization

All units were characterized by best frequency, threshold, frequency response map and temporal response patterns at best frequency (Stabler et al., 1996a). Response maps were constructed by computing the sound-evoked firing rate during the 50 ms tone minus spontaneous firing rate measured during the last 50 ms of each trial. Excitation or inhibition was considered significant when the firing rate was greater than 2.5 standard deviations above or below the mean spike rate of all trials with no sound. Post-stimulus time histograms were constructed for each unit from 50-200 trials with the tone level 10-30 dB above threshold and frequency within 0.1 octave of the identified best frequency. Unit classification by receptive field and post-stimulus time histogram provide indirect evidence for the synaptic drive and intrinsic processing, respectively, of individual neurons in DCN.

Statistical Analysis

A paired 1-tailed Student's t-test was used to test the hypothesis that bimodal stimulation had a greater enhancing or suppressing influence than either unimodal tone or unimodal Sp5 stimulation. Linear regression analysis was used to fit changes in sound-evoked firing rates to a least-squares fit model of changes in spontaneous firing rates.

Figures
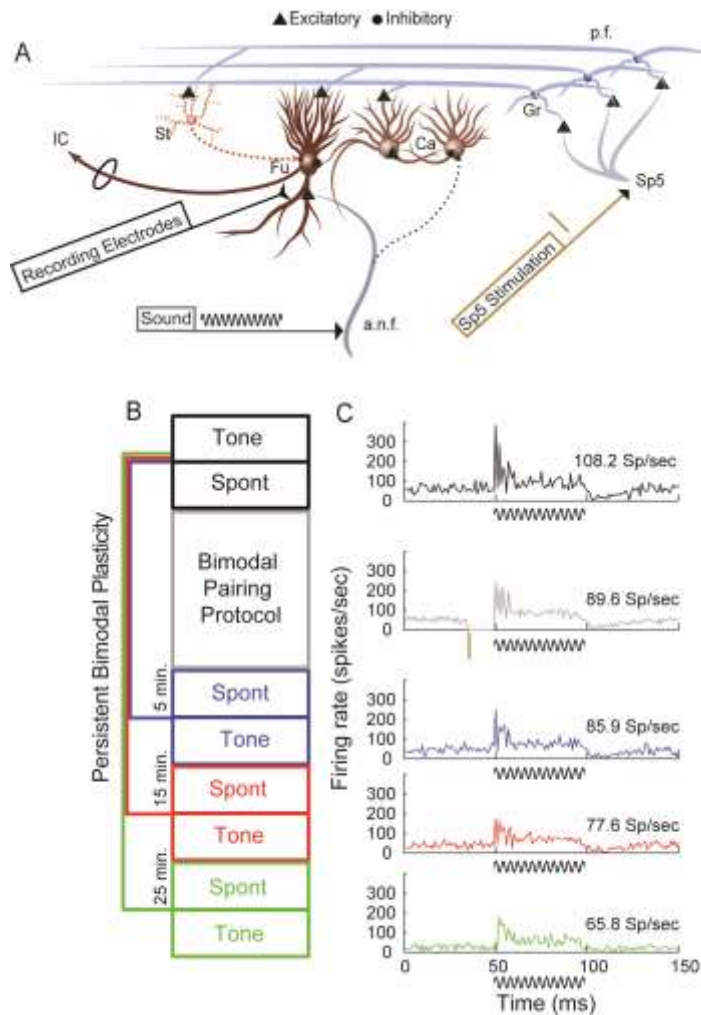
Figure 3.1 - **Bimodal plasticity recorded in vivo from DCN.** A. Schematic of stimulation and recording locations in Sp5 and DCN. Thirty two-channel recording electrodes (black) spanned all layers across the tonotopic axis of the DCN. Short current pulses delivered via a bipolar stimulating electrode (brown) placed into Sp5 activated parallel fiber inputs to DCN. Tones were delivered through calibrated, hollow ear bars. B. The bimodal plasticity recording protocol consisted of tones presented immediately before (black), 5 minutes after (blue), 15 minutes after (red), and 25 minutes after (green) the bimodal pairing protocol (gray). C. Post stimulus time histograms and mean firing rate over the duration of the 50 ms tone stimulus showing responses to sound in one DCN unit before (black), during (grey), 5 minutes after (blue), 15 minutes after (red) and 25 minutes after (green) bimodal stimulation. The stimulus cartoons

46

below each PSTH demonstrate the tone (black sinusoid) presented alone or preceded by electrical pulses in Sp5 (brown tick). Due to artifact contamination, spikes immediately following Sp5 stimulation were removed (second histogram from top). Bin width = 1ms. Ca - cartwheel cell; Fu - fusiform cell; Gr - granule cell; St – Stellate cell; IC - inferior colliculus; Sp5 - spinal trigeminal nucleus; a.n.f - auditory nerve fiber; p.f - parallel fiber.
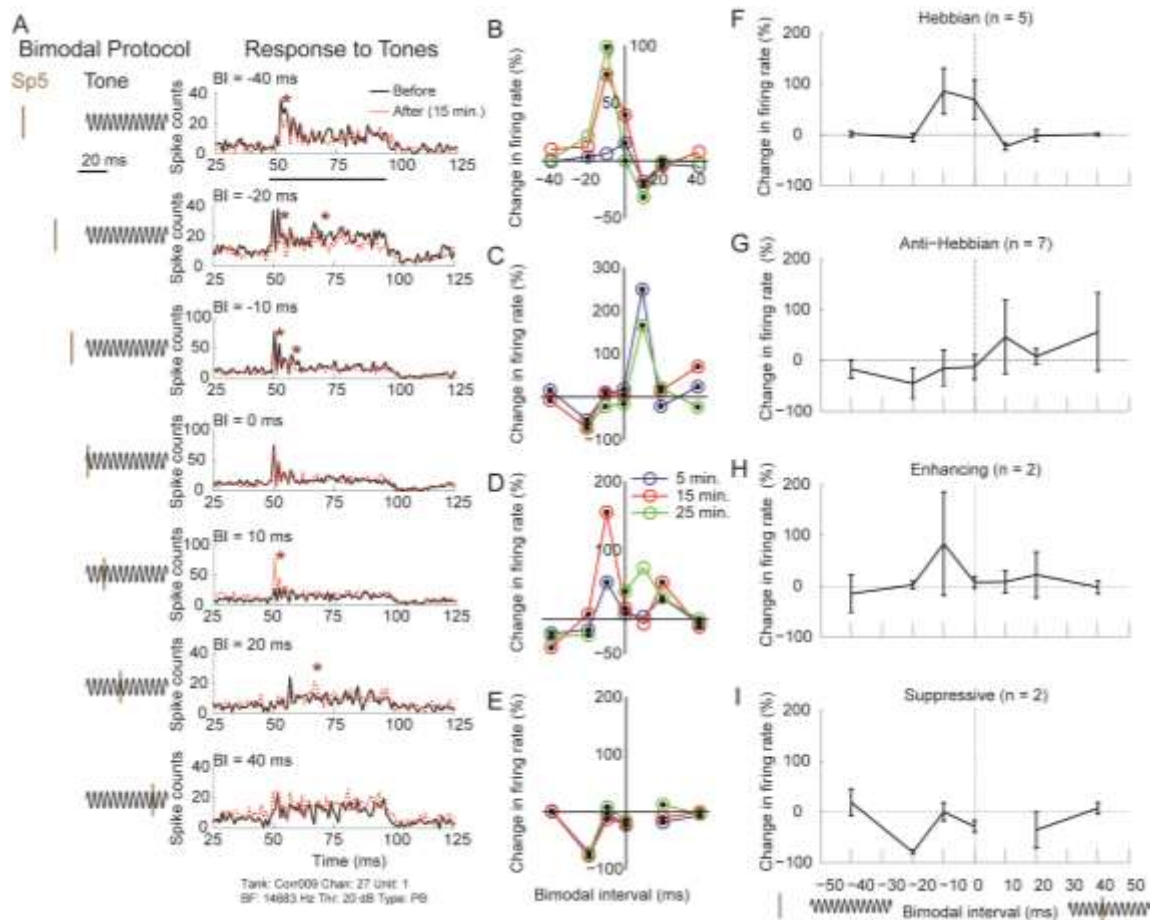
Figure 3.2 - Bimodal plasticity in DCN is stimulus-timing dependent. A. PSTHs of sound-evoked responses for

one single unit 15 minutes after (red dashed line) bimodal stimulation differ from PSTHs of responses to the same

sound before (black solid line) bimodal stimulation. The stimulus cartoons to the left of each PSTH identify the

bimodal interval between the electrical pulses in Sp5 (brown) and the tone (black) for each bimodal pairing protocol.

The bimodal interval (BI) was randomly varied from somatosensory (Sp5) preceding sound by 40 ms (top) to

somatosensory following the onset of sound by 40 ms (bottom). Stars highlight regions of enhancement or

suppression. The horizontal bar below the top PSTH indicates the sound stimulus duration. B. Hebbian-like stimulus-

timing dependence shown in one DCN single unit. C. Anti-Hebbian-like stimulus-timing dependence shown in one

DCN single unit. D. Enhancement-only stimulus-timing dependence shown in a DCN single unit. E. Suppression-only

stimulus-timing dependence shown in a DCN single unit. B-E. Blue, red, and green lines indicate the change in firing

rate 5, 15, and 25 minutes after bimodal stimulation, respectively. F-I. Mean single-unit timing rules at 15 minutes

after bimodal stimulation are grouped by timing rule: Hebbian, anti-Hebbian, enhancing, and suppressing units are

shown from top to bottom. Number of single units shown in parentheses above each panel. Error bars represent

mean +/- 95% confidence interval.
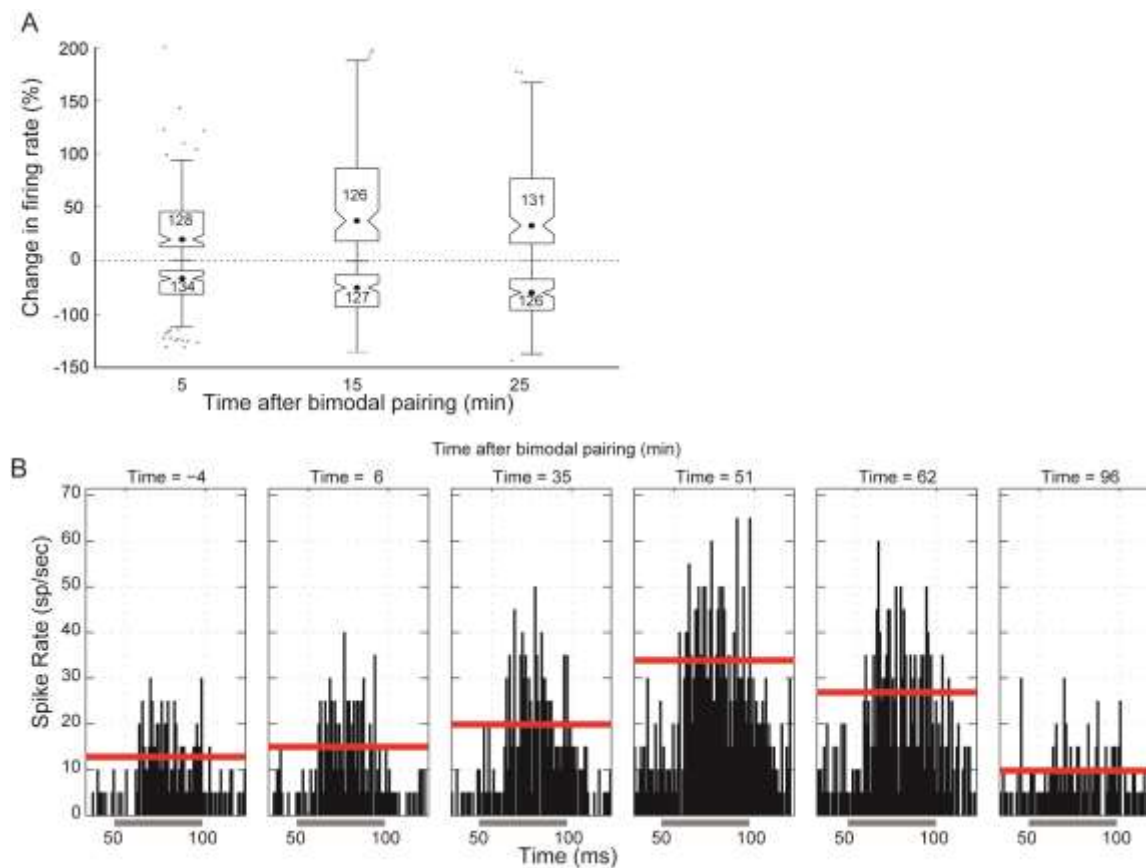
Figure 3.3 - Maximal plasticity continues to develop for 15 minutes and begins to recover by 30 minutes. A. The median and interquartile range for enhancement (top half) and suppression (bottom half). Only the maximum bimodal-induced enhancement and suppression are included. Inward indentations on the bars indicate 95% confidence intervals. Each box is labeled with the number of units. B. PSTHs of responses from an example unit showing maximal bimodal plasticity at 50 minutes post-pairing followed by recovery at 91 minutes post pairing. The time in minutes relative to the bimodal pairing trials is listed above each panel. The solid red line indicates the mean firing rate measured over the duration of the tone (50 – 100 ms). Gray bar below the x-axis indicates the duration of the tone stimulus.
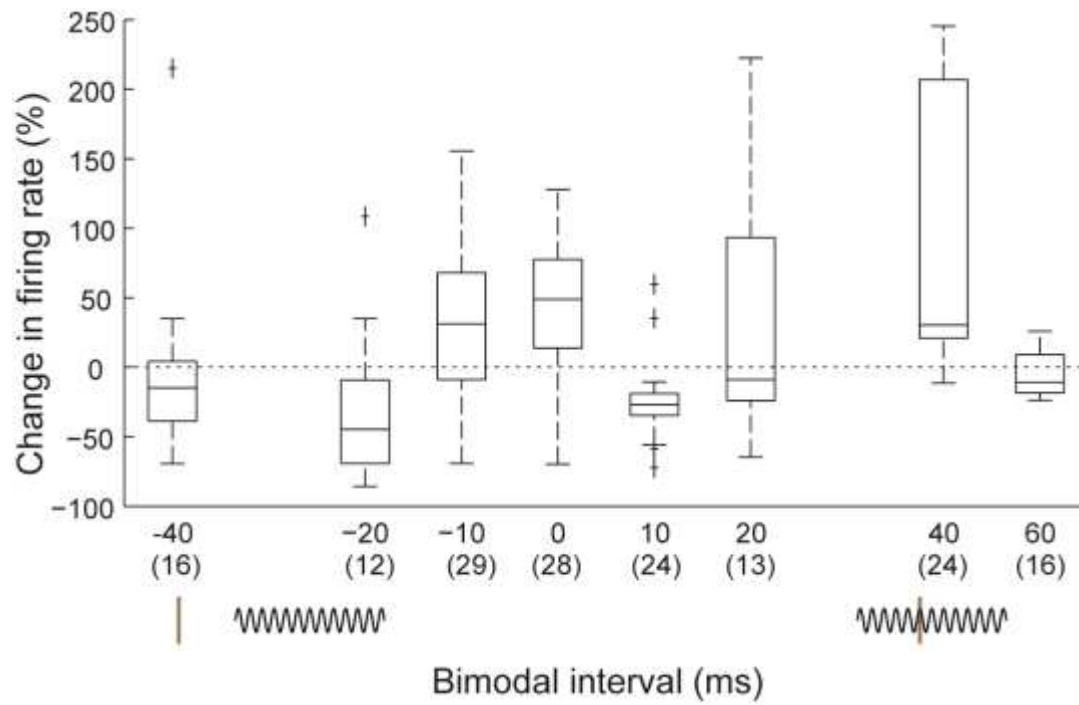
Figure 3.4 - Distribution of preferred bimodal intervals. At 15 minutes, bimodal intervals of 0 and 40 ms

induce maximal enhancement while bimodal intervals of -20 and +10 ms induce maximal suppression. Box and

whisker plots indicate median and interquartile ranges of the maximum change in sound-evoked firing rates. Number

of units shown in parentheses below the x-axis.
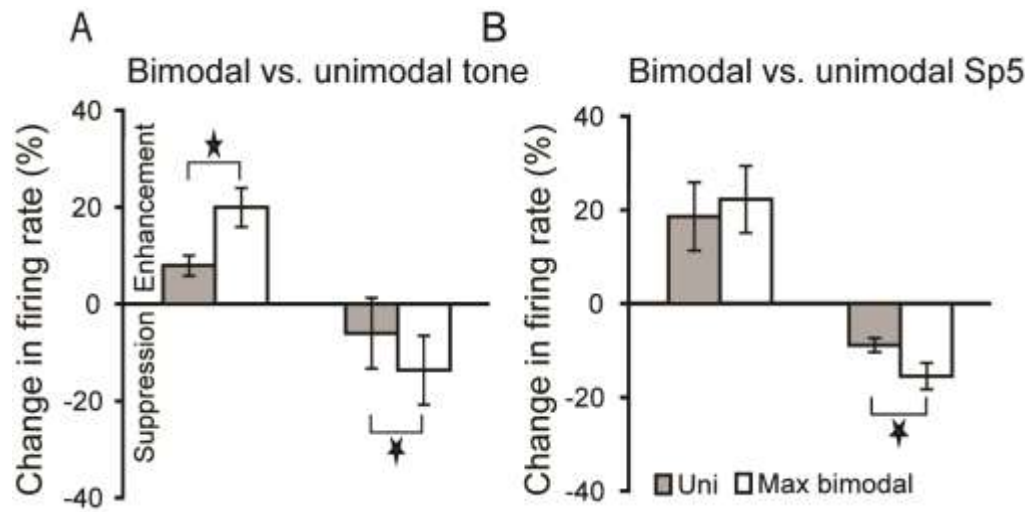
Figure 3.5 - Bimodal stimulation has a greater long-lasting effect than unimodal stimulation. A. Unimodal

sound stimulation (grey bars) induced significantly less enhancement and suppression than maximally effective

bimodal stimulation (white bars). B. Unimodal somatosensory stimulation (grey bars) induced significantly less

suppression, but not significantly less enhancement, than maximally effective bimodal stimulation (white bars). Sp5 –

spinal trigeminal nucleus. Stars indicate significance by paired t-test (p < 0.05).
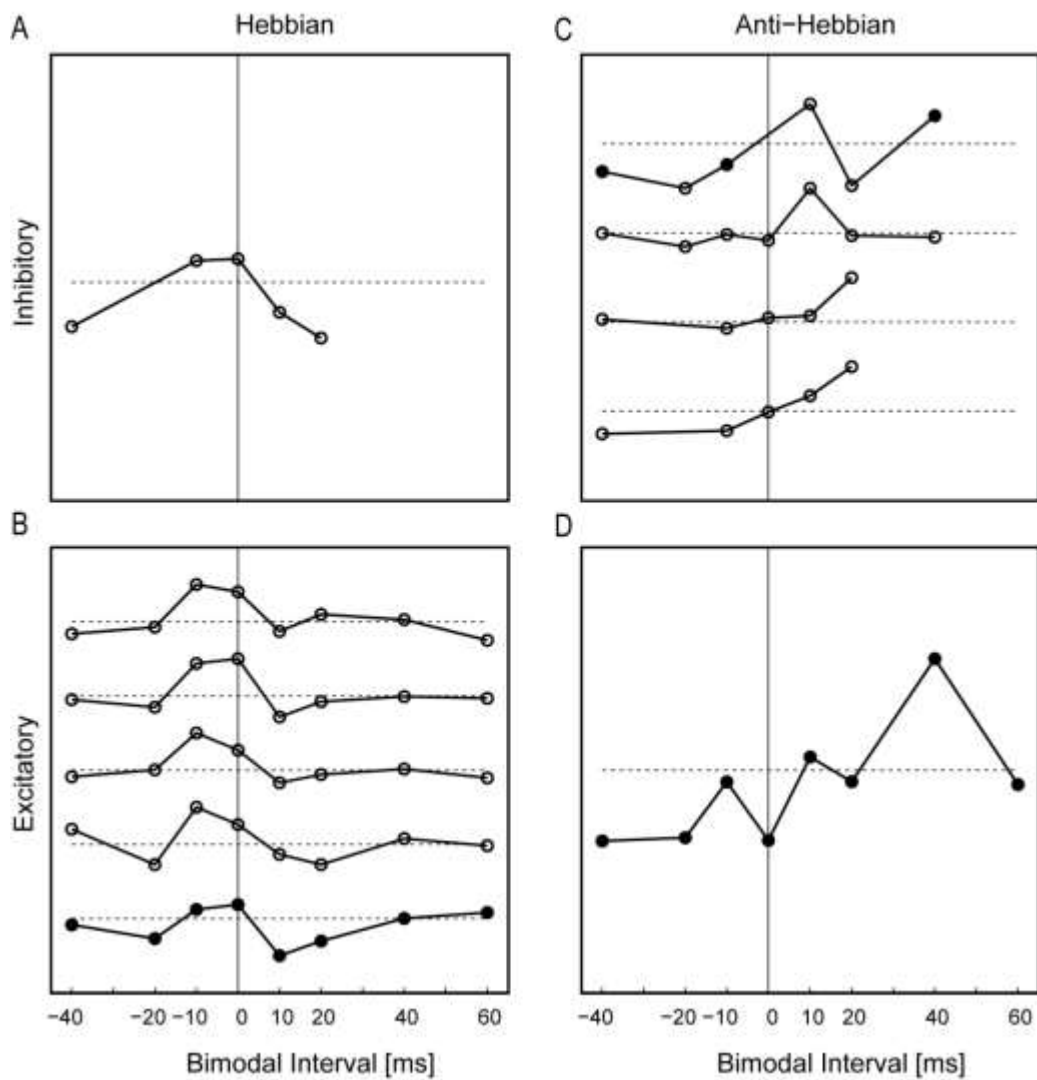
Figure 3.6 - Bimodal timing rules depend on the unimodal somatosensory response. Each plot contains the timing rule from one or more unit, normalized to the maximum change, shifted vertically and centered on the horizontal dashed lines. Empty circles represent mult-unit activity while filled circuits represent single-unit activity. A-B. Units with Hebbian like timing rules with A. inhibitory or B. excitatory responses to Sp5 stimulation. C-D. Units with anti-Hebbian-like timing rules with C. inhibitory or D. excitatory response to Sp5 stimulation.
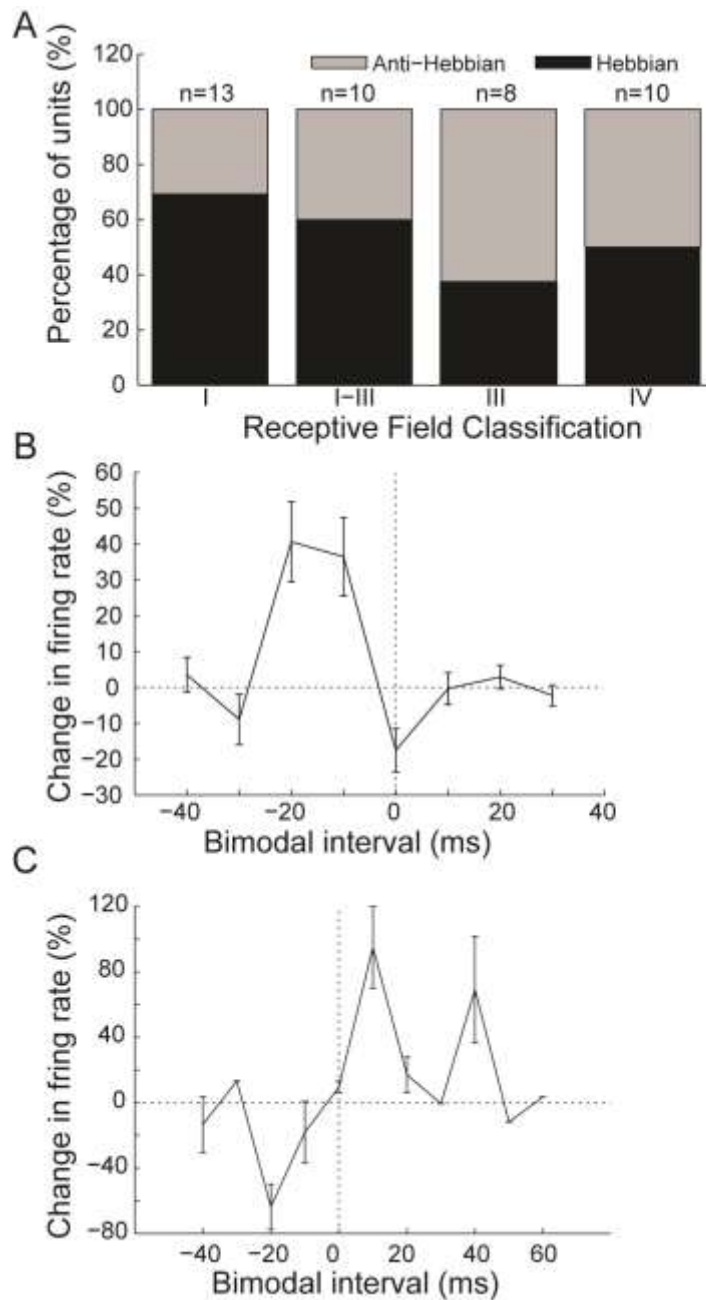
Figure 3.7 - Sound-driven timing rules across unit response types. A. The proportion of Hebbian-like (black) and anti-Hebbian-like (gray) timing rules observed in units with principal (fusiform or giant) cellresponse areas. The number of units included in each group is shown at the top of each bar. B. Mean timing rules from 16 units with either B or PB and Type I or II physiological classifications. All 16 units had Hebbian-like timing rules. C. Mean timing

rules from 4 units with onset and Type IV or IV-T physiological classifications. All 4 units had anti-Hebbian-like timing

rules. B-C. Error bars indicate +/- S.E.M.
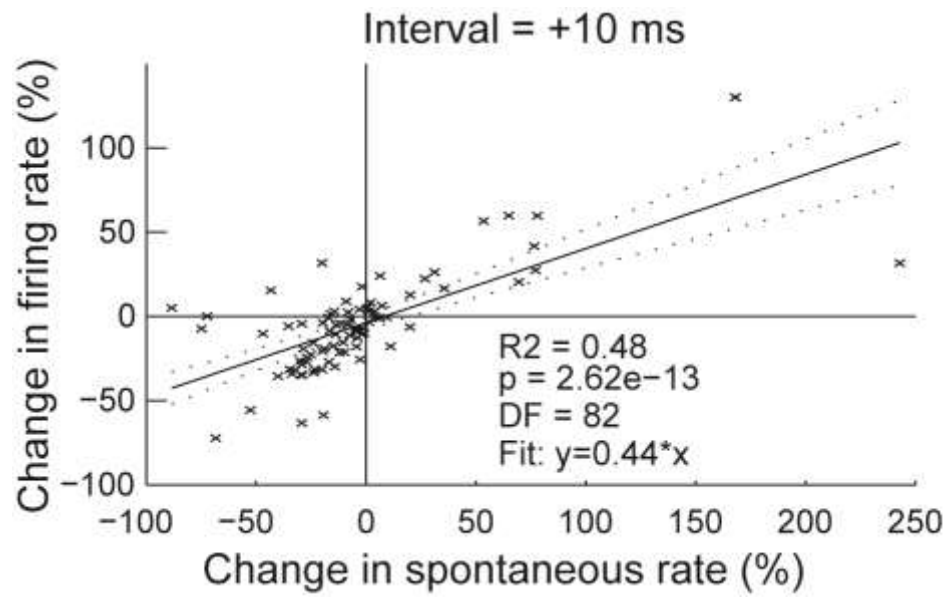
Figure 3.8 - Spontaneous activity timing rules across unit response types. Linear regression analysis of the change in firing rate and the change in spontaneous rate fifteen minutes following bimodal stimulation with a bimodal interval of +10 ms. The solid line represents the best fit model with parameters designated on the figure. Dashed lines represent confidence intervals.

Chapter 4: Shifts in Bimodal Stimulus-Timing Dependent Plasticity Are Associated with Noise-

Exposure Induced Tinnitus

Tinnitus, the phantom perception of sound, has been linked to somatosensory innervation of the auditory system. Both tinnitus patients and normal subjects report that somatosensory stimuli such as pressure on the face or movement of the jaw or neck can elicit or modulate the tinnitus percept (Pinchoff et al., 1998; Levine, 1999; Sanchez et al., 2007) . Converging somatosensory and auditory inputs are integrated in the dorsal cochlear nucleus (DCN), an auditory brainstem nucleus receiving afferent input from the auditory nerve (Kanold and Young, 2001; Haenggeli et al., 2005a; Shore, 2005; Zhou et al., 2007; Kanold et al., 2011; Koehler et al., 2011). Somatosensory input to the DCN plays a role in the induction of tonotopically-restricted hyperactivity in the DCN (Dehmel et al., 2012c) that has been correlated with tinnitus (Kaltenbach et al., 2004).

DCN principal neurons (fusiform cells) respond to mechanical stimulation on the body or electrical stimulation of somatosensory brain regions with both excitatory and inhibitory responses that last up to tens of milliseconds (Young et al., 1995; Davis et al., 1996; Kanold and Young, 2001; Shore, 2005) or minutes (Zhang and Guan, 2008). Fusiform cells "integrate" auditory and somatosensory stimuli when they are presented in close temporal proximity producing sound-evoked responses that are enhanced or suppressed with the addition of the somatosensory stimulus up to 100 ms before the sound (Shore, 2005; Kanold et al., 2011; Koehler et al., 2011). Paired sound and electrical stimulation of somatosensory brainstem nuclei can also suppress or enhance subsequent sound-evoked and spontaneous neural activity for up to 1.5 hours (Dehmel et al., 2012c; Koehler and Shore, 2013) . This long-lasting effect is termed "bimodal plasticity".

Recently, we showed that bimodal plasticity is stimulus-timing dependent with the direction and strength of induced plasticity depending on the order and relative timing of bimodal stimulation: Hebbian-like unit responses were enhanced when somatosensory preceded auditory stimuliation and suppressed when somatosensory followed auditory stimulation while anti-Hebbian-like unit responses were suppressed when somatosensory preceded auditory stimulation and enhanced when somatosensory followed auditory stimulation (Koehler and Shore, 2013). This stimulus-timing dependence of bimodal plasticity implicates spike-timing dependent synaptic plasticity at parallel fiber synapses as a mechanism for adaptive processing of auditory signals in DCN (Roberts and Portfors, 2008; Sawtell and Bell, 2008).

Significant changes in bimodal integration and plasticity and their underlying neural circuitry occur following cochlear damage, a leading cause of tinnitus. Cochlear ablation decreases auditory nerve terminal counts in the DCN leading to a compensatory increase in excitatory somatosensory terminal counts (Zeng et al., 2012). Furthermore, DCN neurons become more sensitive to somatosensory stimulation following permanent threshold shifts caused by broad band noise exposure (Shore et al., 2008). Tinnitus induction after narrowband noise exposure and temporary threshold shifts (TTS) changes bimodal plasticity from suppression to enhancement of tone-evoked responses in the same subset of neurons that show hyperactivity (Dehmel et al., 2012c). To understand the contribution of spike-timing dependent plasticity to tinnitus, it is necessary to evaluate its stimulus-timing dependence in a tinnitus model. To that end, we exposed guinea pigs to a loud narrowband noise known to induce temporary threshold shifts and tinnitus (Dehmel et al., 2012a; Turner et al., 2012),and evaluated gap-detection ability for evidence of tinnitus development. We then recorded DCN neural activity before, 3 and 15 minutes after bimodal stimulation in a stimulus-timing dependent plasticity protocol. Bimodal plasticity, as well as unimodal responses to somatosensory and auditory stimuli, were compared between sham animals and exposed animals with and without tinnitus in order to identify tinnitus correlates. We show that noise exposure and tinnitus related changes in bimodal plasticity, with

58

timing rules shifting from Hebbian-like to anti-Hebbian-like in noise exposed guinea pigs. In guinea pigs with tinnitus, anti-Hebbian-like timing rules were broader in tinnitus than in non-tinnitus animals.

Experimental Procedures

Animals

Female pigmented guinea pigs (n=16) from the Elm Hill colony (300-400 g; Ann Arbor, MI) were used in this study. All procedures were performed in accordance with the National Institutes of Health (NIH) *Guidelines for the Use and Care of Laboratory Animals* (NIH publication No. 80–23) and were approved by the University Committee on Use and Care of Animals at the University of Michigan.

Experimental design

This study was designed to assess the effect of noise-exposure induced tinnitus on stimulus-timing dependent bimodal plasticity of sound-evoked responses and spontaneous activity. Sixteen female guinea pigs (Elm Hill, 10 noise-exposed and 6 sham-exposed) were behaviorally tested semiweekly before and after a two hour noise exposure (Fig. 4.1A; 97 dB noise with ¼ octave band centered at 7 kHz) using an acoustic startle-based gap detection assay for tinnitus (Fig. 4.1B,(Turner et al., 2006; Dehmel et al., 2012b). Ten guinea pigs were first exposed to the narrowband noise 3-6 weeks after baseline gap detection testing. Six to 8 weeks later, each guinea pig was exposed a second time to the same narrowband noise. The remaining 6 guinea pigs were sham-exposed at the same time. Auditory brainstem response (ABR) thresholds were measured before beginning gap detection (B), immediately after the first and second noise exposures to assess threshold shift (E1 & E2), one week after each noise exposure to assess recovery of thresholds (R1 & R2), and immediately before unit recordings (F; Fig. 4.1C). Four to six weeks after the 2nd noise exposure, single and multi-unit spontaneous activity, rate level functions, and bimodal stimulus-timing dependent plasticity were assessed in an acute DCN recording preparation and compared between sham and exposed groups and between tinnitus and no tinnitus groups (Fig. 4.1D).

Gap detection testing for tinnitus

Guinea pigs were behaviorally tested with a startle-based gap detection assay for tinnitus two times per week following the previously described protocol (Dehmel et al., 2012b). In brief, guinea pigs were placed on top of a piezoelectric force measurement plate to measure movement elicited by a loud broad band noise (the startle stimulus; 115 dB, 200-20 kHz). Each trial consisted of a background noise with (Gap trials) or without (No-Gap trials) a 50 ms silent gap embedded 50 ms before the startle stimulus onset. The 60 dB background noise was either broad band noise or bandpass filtered noise with a 2 kHz band and lower cutoff frequencies of 4, 8, 12, 16, or 20 kHz. Intervals between trials randomly varied between 18 and 24 seconds. For each day of testing, an observation of the normalized startle response was computed as the ratio $[A_G / A_{NG}]$ where A_G is the mean amplitude of the startle responses from 10 trials with gap on one day and A_{NG} is the mean amplitude of the startle response from 10 trials with no gap on the same day. To assess the normalized startle responses within each frequency band for evidence of tinnitus, the distribution of normalized startle trials from all observations from all animals was analyzed using Gaussian mixture modeling (Statistics Toolbox, Matlab release 2012b) assuming that the normalized startle observations were drawn from one of two distributions, the normal distribution (Fig. 4.2, top row, black) and the tinnitus distribution (Fig. 4.2, top row, red). The normalized startle observations were placed into the tinnitus group when the posterior probability was greater than 0.55 (Fig. 4.2, second row, red line). For each frequency band, using the threshold established by the Gaussian mixture model, the distributions of normalized startle responses from sham animals after noise exposure (Sham, Fig. 4.2, row 3), all animals before noise exposure (Baseline, Fig. 4.2, row 4), and exposed animals after noise exposure (Exposed, Fig. 4.2, row 5) were partitioned into tinnitus and no tinnitus observations. Animals from the exposed group that demonstrated more tinnitus observations than were found during baseline testing were considered to have tinnitus within the tested frequency band.

Surgical approach for neural recordings

Guinea pigs were anesthetized (subcutaneous injection of ketamine and xylazine, 40 mg/kg, 10 mg/kg; at the incision site a subcutaneous injection of lidocaine, 4 mg/kg) and ophthalmic ointment applied to their eyes. Their heads were fixed in a stereotaxic frame using a bite bar and hollow ear bars were placed into the ear canals. Core temperature was maintained at 38 °C. A left craniotomy was performed and a small amount of cerebellum was aspirated (leaving paraflocculus intact) to allow for visual placement of the recording electrode. Supplemental doses of ketamine and xylazine (I.M.) were administered at least hourly when indicated by response to a toe pinch. The guinea pig's physiological condition was monitored by assessment of body temperature, respiration and heart rates, and unit thresholds. After the completion of neural recording, the guinea pig was sacrificed by I.P. injection of sodium pentobarbitol followed by decapitation.

Electrode placement

A concentric bipolar stimulating electrode (FHC, Bowdoin, ME) was placed stereotaxically into Sp5 after being dipped in fluorogold; -10 degrees below horizontal, 0.28 +/- 0.03 cm lateral from midline; 0.25 +/- 0.02 cm caudal from transverse sinus; 0.9 +/- 0.1 cm below surface of cerebellum. Post-mortem reconstruction confirmed electrode locations. A four-shank, thirty two-channel silicon-substrate electrode (site spacing = 100 um, shank pitch = 250 um, site area = 177 um^2, impedance = 1–3 mOhms, NeuroNexus, Ann Arbor, MI) was placed with the tips 0.8 – 1.0 um below the surface of the DCN with shanks rostral-to-caudal approximately within an iso-frequency layer. If the top site on each shank did not respond to sound, the electrode was lowered until they responded to noise.

Auditory and somatosensory stimulation

Cosine window-gated *Tone* signals (50 ms duration, 2 ms rise/fall time) were generated using Open Ex and an RX8 DSP (TDT, Alachula, FL) with 12 bit precision and sampling frequency set at 100 kHz. A shielded speaker (DT770, Beyer) driven by an HB7 amplifier (TDT, Alachula, FL) delivered sound through a hollow earbar to the left year. The

system response was measured using a condenser microphone attached to the hollow earbar by a ¼" long tube approximating the ear canal. Sound levels were adjusted to account for the system response using a programmable attenuator (PA5, TDT, Alachula, FL) to deliver calibrated levels (dB SPL) at frequencies from 200 Hz to 24 kHz. Neurons in somatosensory brainstem nuclei known to project to DCN were activated by three biphasic (100 us/phase) current pulses at 1000 Hz delivered to Sp5 through a concentric bipolar electrode (Shore et al., 2008). The current amplitude was set to the highest level (range: 50-70 μA) that did not elicit movement artifact.

Assessment of stimulus-timing dependent bimodal plasticity

Stimulus-timing dependent plasticity was assessed in all guinea pigs using an established *in vivo* bimodal plasticity induction protocol (refs: Dehmel et al, 2011; Koehler and Shore 2013). In short, spontaneous activity and responses to unimodal tone stimuli were recorded at three time points: before, and 3 and 15 minutes after the bimodal stimulation protocol. The ***bimodal stimulation protocol*** consisted of 300 trials of the 50 ms tones combined with Sp5 activation. The ***bimodal interval*** was defined as the Sp5 stimulus onset time minus the tone stimulus onset time. Thus, negative bimodal intervals indicate Sp5-leading tone stimulation and positive bimodal intervals indicate tone-leading Sp5 stimulation. Stimulus-timing dependence was assessed by varying the bimodal interval and measuring the change in unimodal tone-evoked firing rates before and after bimodal stimulation. The recording block was repeated with the bimodal interval between tone and somatosensory stimuli randomly selected from the following list: -40, -20, -10, 0, 10, 20, or 40 ms. Control recording blocks were also included in which unimodal tone or Sp5 stimuli replaced the bimodal stimuli. To assess recovery after bimodal stimulation, responses to unimodal tones were measured every 15-30 minutes for as long as possible to assess recovery after bimodal stimulation.

Spike detection and sorting

Voltages from each site were digitized by a PZ2 preamp (Fs=12 kHz, TDT, Alachua, Fl, USA) and band-pass filtered (300 Hz – 3 kHz). Online spike detection used a voltage threshold set 2.5 standard deviations above

background noise (RZ2, TDT, Alachua, Fl, USA). Timestamps and waveform snippets were saved to a PC and sorted

using principal components of the waveform shape and K-means cluster analysis with fixed variance (95%) and 5

clusters (Plexon Offline Sorter). Cluster distinctness was confirmed with pairwise cluster statistics (p>0.05; Plexon

Offline Sorter) and visually by a trained observer. When a spike was present in a 1 ms window across 80% of channels,

any spikes within that window were considered artifact and removed from further analysis. The waveform shapes,

amplitudes, and response properties of multi-unit clusters in this study were consistent over the duration of the

recording.

Results

Narrow-band noise exposure centered at 7 kHz induced temporary threshold shifts between 7 and 16 kHz

Noise exposure induced a TTS as demonstrated by auditory brainstem response (ABR) thresholds. ABR

thresholds in the exposed ear (Fig. 4.3A) but not the unexposed ear (Fig. 4.3B) were elevated immediately after

exposure and recovered to baseline by 1 week after noise exposure. Maximum threshold elevation was 35 dB (mean)

+/- 3.5 dB (s.d.) at 9 kHz after the first exposure and 19 dB (mean) +/- 2.1 dB (s.d.) at 10 kHz after the second

exposure with thresholds elevated in a band from the exposure frequency to 2 octaves above the exposure

frequency. ABR thresholds in sham-exposed guinea pigs were not elevated above baseline in either ear (Fig. 4.3C,D).

Exposure to narrowband noise induced tinnitus in the 12 – 14 kHz band in 60 % of guinea pigs

Gap-induced prepulse inhibition of acoustic startle (GPIAS) was used to assess each guinea pig for evidence of

a frequency specific tinnitus percept (Fig. 4.4A). Impaired gap detection, which was assumed to reflect tinnitus, was

identified by a significantly elevated normalized startle response. The normalized startle response was defined as the

ratio of the startle response amplitude with gap prepulse (A_G) to the startle response amplitude without gap (A_{NG}).

Following the TTS-inducing noise exposure, 60 percent of exposed guinea pigs were identified as having tinnitus in the

12 - 14 kHz band and 30 % in the 8-10 kHz band (Fig. 4.4B, See methods and supplemental material for additional

detail). Guinea pigs with evidence for tinnitus in the 8-10 or 12-14 kHz bands were thus placed into the Exposed with Tinnitus (ET) group. The remaining 40% of exposed guinea pigs were placed into the Exposed with No Tinnitus (ENT) group while the sham animals were considered as a separate group (Sham).

To validate the ET and ENT groupings, gap detection ability was compared between all exposed and sham guinea pigs (Fig 4.4C), and between the ET, ENT and sham guinea pigs (Fig. 4.4D). Normalized startle responses were significantly elevated, indicating impaired gap detection ability, for the 4-6, 8-10, and 12-14 kHz bands in the ET group but not in the ENT group (Fig. 4.4D) or in all exposed guinea pigs (Fig. 4.4C). The normalized startle response was not significantly elevated for the BBN background signal or the 16-18 kHz background signal either for the ET group or the ENT group (Fig. 4.4C), or for all exposed guinea pigs (Fig. 4.4D).

Timing rules were broader and likelier anti-Hebbian in noise-exposed animals

Previously, we measured the stimulus-timing dependence of bimodal plasticity to reveal the contribution of spike-timing dependent synaptic plasticity to bimodal plasticity (Koehler and Shore, 2013). Here, we recorded responses from Sham (n = 100 units), ENT (n = 63 units), and ET (n = 225 units) guinea pigs before, 3 and 15 minutes after bimodal stimulation with varying orders and intervals (Fig 4.5A).

Mean population timing rules from all sham and noise-exposed units 3 and 15 minutes after bimodal stimulation reveal that noise exposure shifts the population timing rule from Hebbian-like to anti-Hebbian-like in noise-exposed animals (Fig. 4.5B). In sham animals, both 3 and 15 minutes after bimodal stimulation, the mean population timing rule was Hebbian-like, with enhancement of sound-evoked firing rates when Sp5 preceded sound stimulation and suppression when Sp5 stimulation followed sound stimulation (Fig. 4.5B, black). In noise-exposed animals, the reverse occurred, with suppression of sound-evoked firing rates for Sp5 precededing sound stimulation and enhancement with Sp5 following sound stimulation (Fig. 4.5B, red).

Timing rules were broadest in noise-exposed animals with tinnitus compared to those without tinnitus

Mean population timing rules for ET, ENT, and sham units revealed that long-lasting bimodal plasticity 15 minutes after bimodal stimulation was converted from Hebbian-like to anti-Hebbian-like timing rules in both the ET and ENT groups, but were broader in only the ET group (Fig. 4.5C). Additionally, in ENT animals, maximal enhancement and suppression were found at bimodal intervals of -20 ms and +20 ms respectively, similar to what was observed in sham guinea pigs with maximal enhancement and suppression observed at 10 ms and -20 ms respectively. However, in ET animals, maximal enhancement and suppression were observed at the broadest bimodal intervals tested (+40 and -40 ms), suggesting that bimodal plasticity timing rules broaden in association with tinnitus.

Anti-Hebbian bimodal plasticity was dominant in animals exhibiting tinnitus, while suppressive bimodal plasticity was dominant in animals without tinnitus

Timing rules were constructed for individual units from responses 15 minutes after bimodal stimulation and were classified following the scheme previously described (Koehler and Shore, 2013) as Hebbian-like (n = 132), anti-Hebbian-like (n = 69), suppressing (n = 143), or enhancing (n = 44) timing rules. Units from sham animals were distributed among the timing rule classes similarly to units from normal animals (Koehler and Shore, 2013) but after noise exposure, anti-Hebbian-like units were most common in ET animals while suppressive units were predominant in ENT animals (Fig. 4.6A). This corresponds with the shift in the population timing rule from Hebbian-like to anti-Hebbian-like (Fig 4.5C).

Mean timing rules are shown for Hebbian, anti-Hebbian, and suppressive units from sham and ET animals in Figures 4.6B-G. Hebbian-like timing rules were similar and highly variable in both sham and ET animals (Fig. 4.6B-C). Additionally, bimodal suppression was weaker in ET animals than in sham animals (Fig. 4.6F-G).

65

Anti-Hebbian, but not Hebbian, timing rules were broader in tinnitus animals

For each unit, the maximal bimodal plasticity (both enhancement and suppression) and the bimodal intervals that elicited maximal bimodal plasticity were identified. The peak effects for both suppression and enhancement were compared in scatter plots for sham (Fig 4.7A) and ET (Fig 4.7B) animals. Hebbian-like unit peaks (black circles) fall in the upper left and lower right quadrant, consistent with Hebbian like timing rules. Peaks were most commonly found at bimodal intervals of -20 ms and +20 ms in sham animals, but at -10 ms and +10 and 40 ms in ET animals. Anti-Hebbian peaks (empty circles) fall in the lower left and upper right quadrants as is expected for anti-Hebbian-like units. However, anti-Hebbian unit peaks from tinnitus animals were spread across all bimodal intervals but were restricted to -20 ms or +40 ms. This is consistent with the broader population timing rules observed in noise-exposed (Fig. 4.5B) and tinnitus (Fig. 4.5C) animals and the broader anti-Hebbian population timing rules observed in ET animals (Fig. 4.6D-E).

Exposed with tinnitus animals had more excitatory responses to Sp5 stimulation

Responses to Sp5 stimulation alone were recorded to identify whether the distribution of excitatory, inhibitory, and complex unimodal Sp5 responses differed with TTS-inducing noise exposure and with tinnitus (Fig 4.8). Unimodal responses were more likely to be excitatory and less likely to be inhibitory in ET animals than in sham animals. In contrast, unimodal responses were more likely to be complex (E/In) in ENT animals.

Discussion

Our previous observation that bimodal plasticity is stimulus-timing dependent (Koehler and Shore, 2013) suggests that in vivo bimodal plasticity reflects in vitro STDP at somatosensory synapses in DCN (Tzounopoulos et al., 2004). Long-lasting bimodal enhancement is stronger in animals that develop tinnitus after noise damage (Dehmel et al., 2012c), possibly reflecting metaplasticity, an activity dependent change in the strength or form of synaptic plasticity (Abraham and Bear, 1996). Here, we used stimulus-timing dependent bimodal plasticity to asses STDP

66

metaplasticity in a guinea pig model of tinnitus. Bimodal plasticity timing rules were broader and more likely to be

anti-Hebbian in guinea pigs with tinnitus than in sham guinea pigs or those without tinnitus after noise damage. This

suggests that tinnitus may be linked to metaplasticity of STDP in the DCN.

Noise exposure causes temporary threshold shifts and tinnitus

Noise exposure is a leading cause of tinnitus in human patients, with the tinnitus frequency usually matched to

the frequency region of greatest hearing loss (Heller, 2003). In the present study, narrow band noise centered at 7

kHz produced a unilateral TTS with maximum threshold shifts at 9-12 kHz. This induced tinnitus in the 12 - 14 kHz

band in 60% of tested guinea pigs, consistent with several studies that have observed tinnitus in frequency bands

above the noise exposure frequency (Turner et al., 2006; Bauer et al., 2008). While tinnitus was previously observed

in the 8-10 kHz band with the same noise exposure(Dehmel et al., 2012b), maximum threshold shifts in those animals

were observed closer to the exposure frequency at 8 kHz instead of 9-12 kHz.

Alterations in bimodal stimulus-timing dependent plasticity associated with noise exposure and tinnitus

To identify changes in stimulus-timing dependence associated with noise-exposure, bimodal plasticity timing

rules were compared between sham and all noise- exposed animals. We observed three significant noise-exposure

associated changes: 1) Timing rules were more likely to be anti-Hebbian than Hebbian, 2) Timing rules were broader,

and 3) timing rules were more likely to be suppressive than enhancing. To identify changes specifically associated with

noise-exposure induced tinnitus, we compared timing rules from noise-exposed animals with tinnitus to timing rules

from noise-exposed animals without tinnitus and sham animals. There were two striking differences in bimodal

plasticity in tinnitus animals: 1) Timing rules were more likely to be governed by Hebbian or anti-Hebbian timing rules

than suppressive or enhancing timing rules, and 2) Anti-Hebbian timing rules were broader. These results likely

represent underlying changes in STDP (Tzounopoulos et al., 2004; Tzounopoulos et al., 2007), suggesting a potential

role for STDP in generating tinnitus.

Bimodal stimulus-timing dependent plasticity as a mechanism for tinnitus

The role of bimodal STDP in the DCN is to identify spatiotemporal patterns in auditory nerve activity that are correlated with somatosensory inputs. In the normal system, narrow STDP timing rules (Masquelier et al., 2008) heighten or suppress the responsivity of DCN neurons to auditory nerve inputs that are tightly correlated with somatosensory events (Sawtell, 2010). The broader timing rules in tinnitus animals would increase the likelihood of a somatosensory event triggering anti-Hebbian or Hebbian plasticity, leading to heightened responsivity to spontaneous, as well as driven, auditory nerve spiking patterns. The resulting hyperactivity could be a neural representation of tinnitus (Kaltenbach and McCaslin, 1996). This mechanism could act cooperatively with the decreases in granule cell resistance observed after noise exposure that further enhance the strength of somatosensory inputs (Pilati et al., 2012). Furthermore, the corresponding decrease in bimodal suppression in tinnitus animals would further enhance the hyperactivity. The tinnitus-associated changes in bimodal stimulus-timing dependent plasticity suggest that somatosensory inputs have a greater influence on DCN neural activity in animals that developed tinnitus than in those that did not. A similar process is found in visual cortex, where broadened STDP timing rules after visual deprivation cause long-term potentiation of spontaneous inputs to visual cortex at lower spontaneous firing rates than in the normal visual cortex (Guo et al., 2012).

Potential mechanisms for noise-exposure induced STDP metaplasticity

We have identified four potential mechanisms that could lead to the observed changes in DCN stimulus-timing dependent plasticity. Because we are indirectly assessing changes in STDP *in vivo* , we must consider the influence of noise exposure-induced DCN circuitry modifications (1 and 2) in addition to metaplastic changes in STDP through cellular plasticity mechanisms (3) and modulatory neurotransmission (4). There are several potential metaplastic mechanisms that could be involved (for review see (Abraham, 2008) but we have identified two below that are supported by specific evidence in DCN.

1) A reduction in glycinergic inhibition that has been observed with noise exposure (Suneja et al., 1998b; Suneja et al., 1998a) and tinnitus (Wang et al., 2009) could lead to a shift in the balance of sound-evoked excitation and inhibition, with relatively weaker inhibition leading to more neurons with excitatory response maps . Changes in sound-driven responses could lead to changes in correlated somatosensory and auditory synaptic inputs. Given that neurons with excitatory response maps are more likely to exhibit Hebbian-like plasticity (Koehler and Shore, 2013) a reduction in sound-driven inhibition would predict a shift towards Hebbian-like plasticity. However, this prediction is counter to the increase in anti-Hebbian-like plasticity in guinea pigs with tinnitus, suggesting that tinnitus-associated changes in bimodal plasticity are not due to changes in the sound-driven netork properties.

2) Somatosensory innervation of the DCN is distributed to produce direct excitatory responses as well as inhibitory responses through interneurons (Young et al., 1995; Shore, 2005) that demonstrate Hebbian and anti-Hebbian STDP, respectively (Tzounopoulos et al., 2004). After cochlear ablation, there is increased somatosensory innervation of the DCN (Zeng et al., 2009a; Zeng et al., 2012) that could, in the noise exposure TTS model, manifest as a restricted increase in somatosensory innervation driven by more subtle deficits in cochlear function. The redistribution of unimodal somatosensory responses to include more excitation (Fig. 4.8) suggests that new somatosensory terminals preferentially innervate fusiform cells directly vs. through cartwheel cells. Along with the reduction in glycinergic inhibition above, the preferential redistribution of somatosensory innervation away from cartwheel cells would also reduce the influence of glycinergic interneurons such as cartwheel cells on bimodal stimulus-timing dependent plasticity. Parallel fiber synapses onto cartwheel cells exhibit endocannabinoid mediated anti-Hebbian STDP that has the inverse Hebbian influence on fusiform cells (Tzounopoulos et al., 2007; Doiron et al., 2011). Thus, a reduction in cartwheel cell influence would lead to a reduction in Hebbian somatosensory influence, as is observed in the present data.

3) Changes in the distribution of post-synaptic N-methyl-D-apartate receptors (NMDARs), specifically the NR2B subunit, can lead to metaplasticity (Lee et al., 2010) and in particular can result in broader STDP timing rules, as shown *in vitro* in visual cortical neurons after sensory deprivation (Guo et al., 2012). In DCN, NMDAR-2B are found in relevant neuronal subpopulations, including fusiform cells, granule cells, and vertical cells (Sato et al., 2000) Changes in NMDAR-2B have not yet been studied in a tinnitus model or after hearing loss. However, synaptic plasticity is often under the control of NMDAR-initiated signaling cascades that are protein kinase C (PKC) dependent. The expression of PKC isoforms is enhanced in DCN neurons after cochlear ablation (Garcia et al., 2000). There is not currently sufficient evidence to suggest that changes in NMDAR activity or signaling cascades are responsible for noise-exposure and tinnitus associated changes in STDP.

4) Cholinergic inputs to DCN modulate STDP at parallel fiber to fusiform cell synapses, converting it from Hebbian to anti-Hebbian timing rules (Zhao and Tzounopoulos, 2011). In the present study, bimodal plasticity timing rules shifted from Hebbian-like to anti-Hebbian-like after noise exposure. If cholinergic modulation of STDP were involved in tinnitus-associated metaplastic changes, we would predict increased cholinergic activity in tinnitus models. Although cholinergic activity has not been tested in a tinnitus model, there increased choline acetyltransferase activity and stronger carbachol-induced suppression of neural activity in the DCN (Zhang and Kaltenbach, 2000; Jin et al., 2006), suggesting that increased cholinergic activity after noise exposure may contribute to the Hebbian to anti-Hebbian shift observed in tinnitus animals in the present study.

We conclude that noise-exposure and tinnitus are associated with STDP metaplasticity that is likely driven by a combination of redistribution of somatosensory innervation and reduced influence of glycinergic cartwheel cells, cholinergic neuromodulation, and potentially changes in NMDAR and PKC-mediated signaling cacades.

STDP metaplasticity as a neural correlate for tinnitus

Our results show that metaplasticity of STDP in the DCN is a new neural correlate of tinnitus. The specific combination of STDP changes in DCN after noise exposure may drive spontaneous neural activity toward spiking patterns that represent tinnitus in DCN and higher auditory structures in the auditory system. The influence of metaplasticity in higher centers could further drive spontaneous activity towards perceptual awareness.

Bimodal plasticity similar to that observed in DCN has been demonstrated in auditory cortex (Basura et al., 2012) where STDP has also been implicated as a mechanism underlying stimulus-timing dependent shifts in frequency tuning (Dahmen et al., 2008). Stimulus-timing dependent frequency tuning suggests that STDP may be important for tonotopic remapping, which has been implicated as a correlate for tinnitus (Muhlnickel et al., 1998; Komiya and Eggermont, 2000). In other sensory systems, STDP has been implicated in cortical remapping following sensory deprivation and deafferentation in visual (Guo et al., 2012) and somatosensory (Gambino and Holtmaat, 2012) cortices, respectively.

Our identification of tinnitus-associated changes in STDP opens up avenues for new tinnitus treatments. Already, manipulation of cortical map plasticity through vagal nerve stimulation has been proposed as a tinnitus treatment (Engineer et al., 2013). Our results suggest potential approaches to tinnitus management including non-invasive paired stimulation of the auditory and somatosensory modalities and pharmacological targeting of STDP mechanisms.

Figures
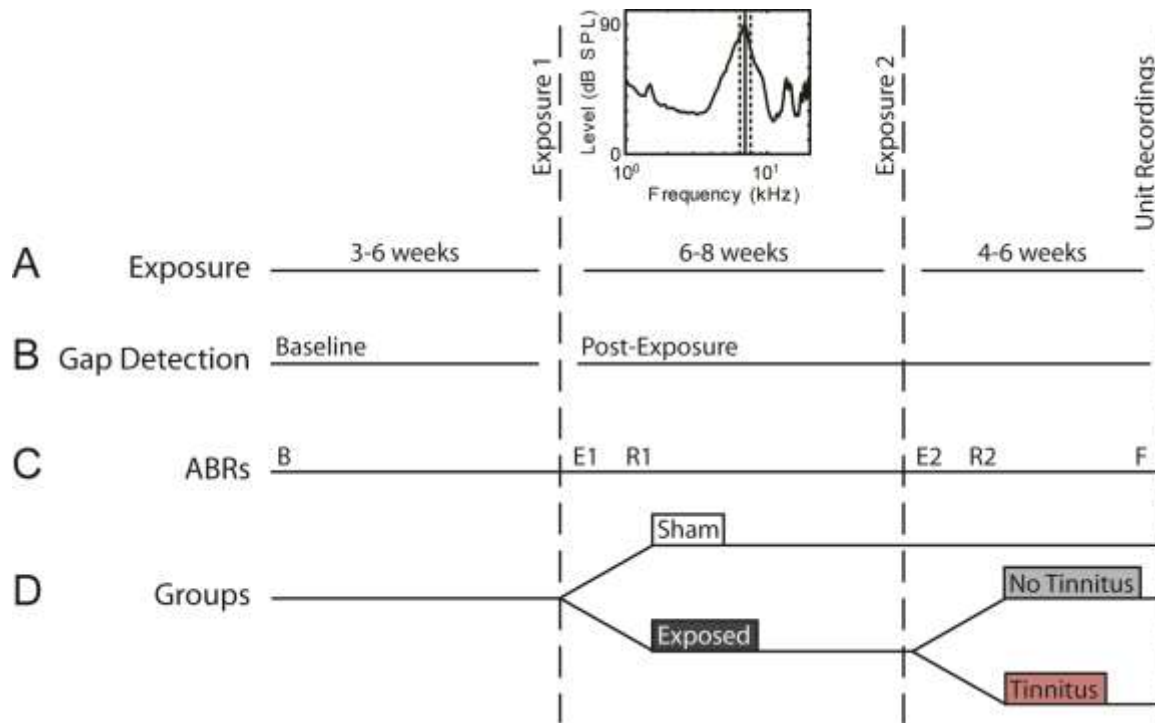
Figure 4.1 – Timeline describing the experimental protocol and schedule. (A) noise exposure (including noise exposure spectrum), (B) gap detection testing for tinnitus, (C) auditory brainstem response threshold measurements, and (D) the partition of guinea pigs into sham, exposure, and tinnitus groups. B – Baseline ABRs. E1 and E2 – ABRs measured immediately after exposure. R1 and R2 – ABRs measured 1 week after noise exposure. F – Final ABR measurements just before single unit recordings.
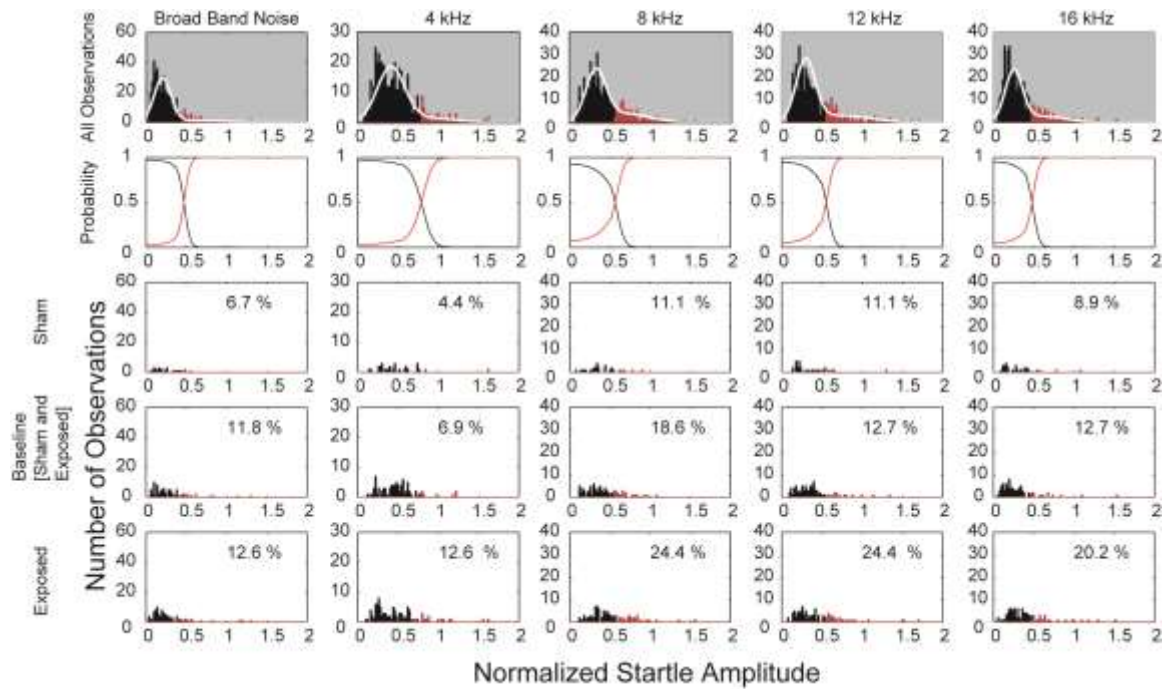
Figure 4.2 – Gaussian-mixture model analysis of normalized startle observations. Each column shows the Gaussian-mixture model analysis for normalized startle observations from the noise band listed above the column (from left to right: broad band noise, 4-6 kHz, 8-10 kHz, 12-14 kHz, and 16-18 kHz). Row 1 shows a histogram of the normalized startle observation distribution partitioned into two distributions, lack of evidence for tinnitus (black bars) and evidence for tinnitus (red bars) using the posterior probabilities shown in row two. Histograms of the partitioned distribution of normalized startle observations for sham animals (Row 3), baseline observations from sham and exposed animals (Row 4), and observations from exposed animals (Row 5) are shown. The percentage of observations placed into the tinnitus group is shown on each panel.

73
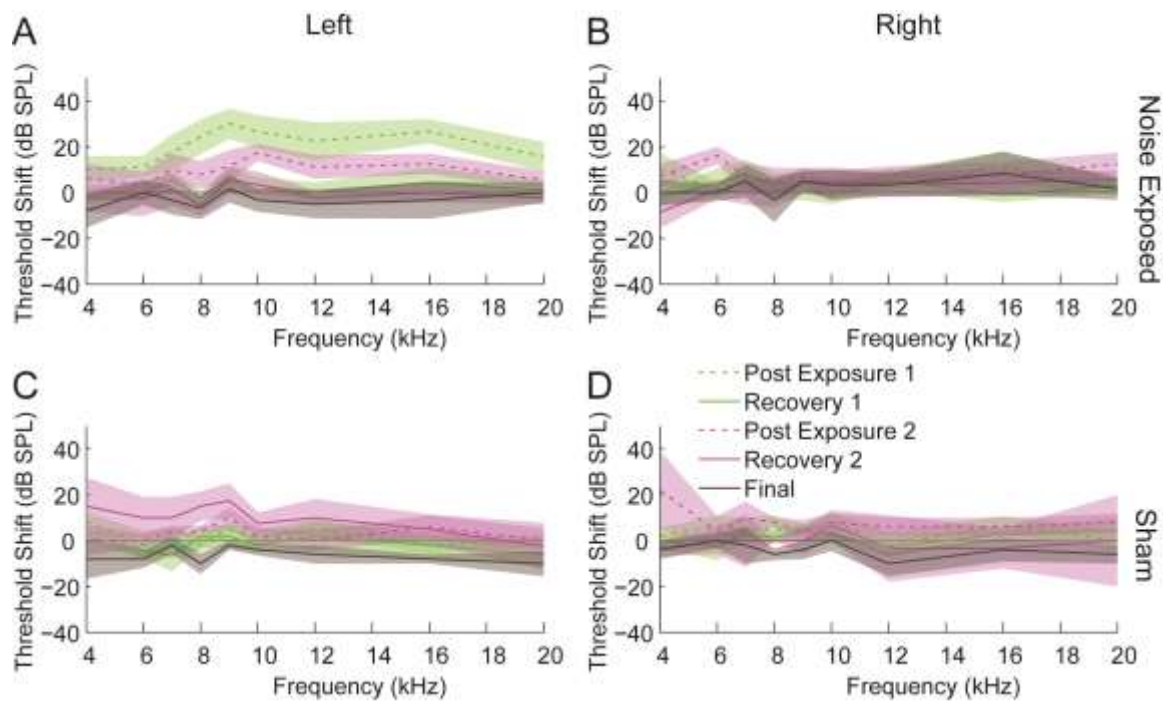
Figure 4.3 – ABR thresholds were temporarily elevated after noise exposure. ABR threshold shifts for noise-exposed guinea pigs in the exposed (A) and un-exposed (B) ear and sham guinea pigs in both ears (C, D). Thresholds were measured after the first exposure (green), the second exposure (pink), and before the acute unit recordings (black). Dashed lines indicate thresholds measured immediately after the noise exposure while solid lines indicate threshold shifts measured after recovering 1 or more weeks after noise exposure. Shaded bands represent 95% confidence intervals.
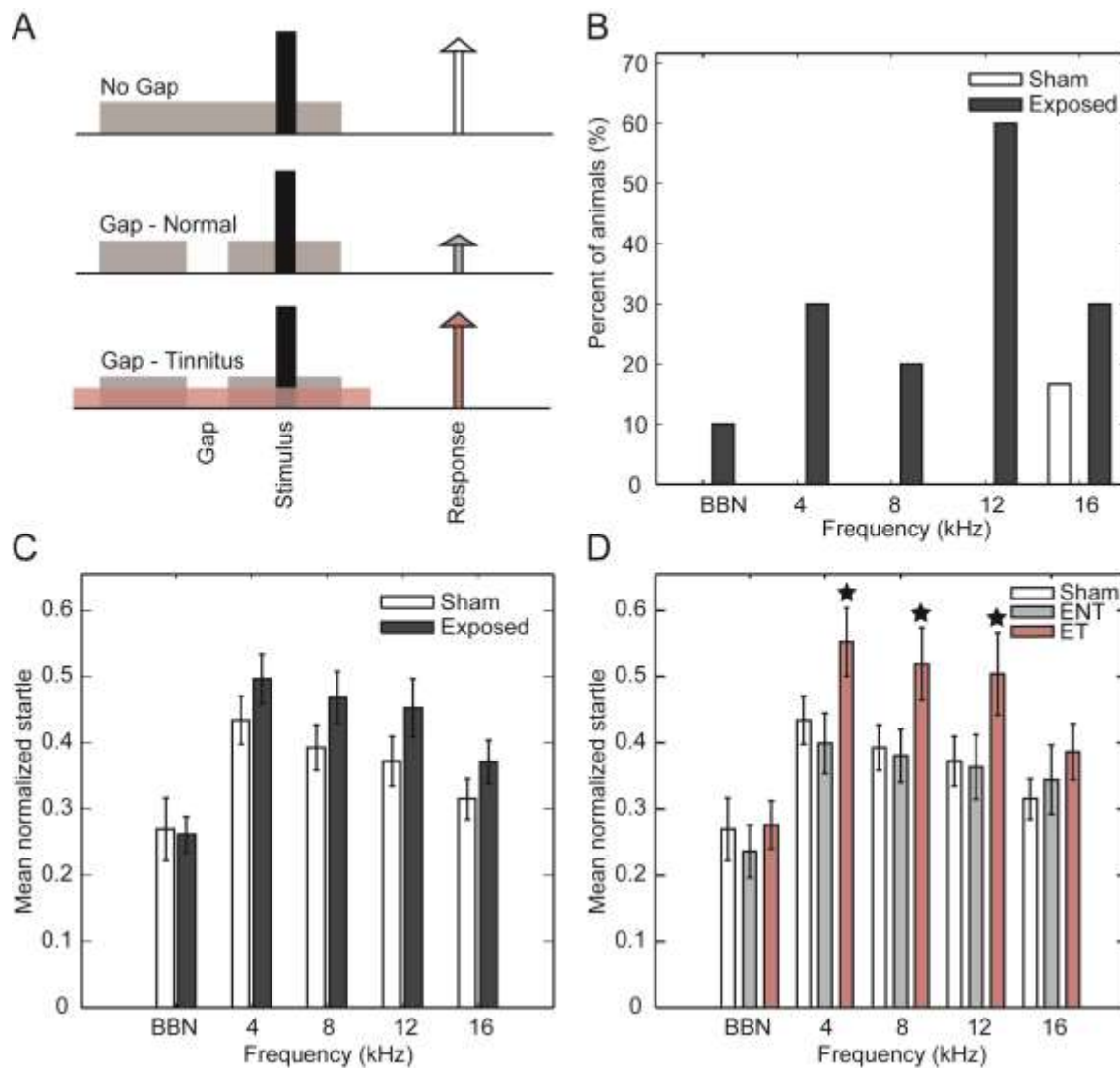
Figure 4.4 Elevated normalized startle responses demonstrate tinnitus in the 4 to 12 kHz bands. A. Schematic describing the startle based gap-detection assay for tinnitus. No gap (top row) and gap trials (50 ms gap, 50 ms before the startle sound; bottom two rows) are presented to the animal. Each trial consists of a long 60 dB background sound (tan bar) with an 10 ms, 115 dB startle pulse embedded (black bar). The guinea pig jumps in response to the startle stimulus, with the amplitude of the response shown by the height of each arrow. In animals without tinnitus, the gap introduces a suppression of the startle response (middle row). In animals with tinnitus, the gap is filled by the tinnitus (red) and the startle response is reduced less relative to the no gap startle response (white arrow). B. Percent of sham (white bars) and exposed (black bars) guinea pigs that show evidence for tinnitus in different frequency bands. C. Normalized startle response amplitudes in each frequency band for tinnitus animals (ET, red bars) as compared to animals without tinnitus (ENT, gray bars) and sham animals (white bars). D. Normalized startle response amplitudes in each frequency band for exposed animals (black bars) as compared to sham animals (white bars). C-D. Stars indicate bars significantly different from other bars within the same frequency band.
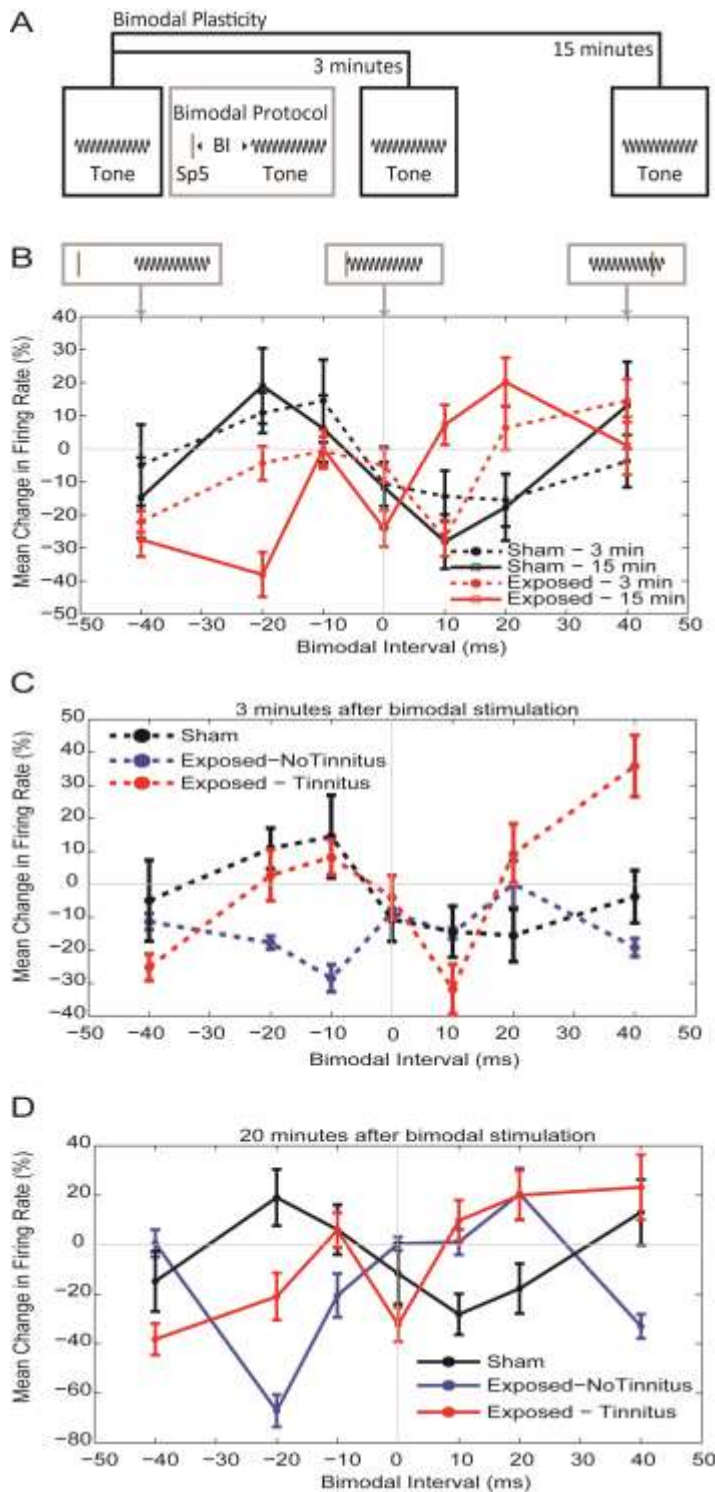
Figure 4.5 – Bimodal plasticity population timing rules differ between exposed guinea pigs with tinnitus, exposed guinea pigs with no tinnitus, and sham guinea pigs. A. Schematic of the bimodal stimulus-timing dependent plasticity protocol. B-D are constructed from the difference between the response to the tone stimulus at each time point and the response to the tone stimulus before the bimodal pairing protocol. For three of seven bimodal intervals, a cartoon sketch of the timing of the bimodal stimuli is presented. The brown vertical line represents the Sp5 stimulation and

76

the sinusoid represents the tone stimulus. B. Mean population timing rules for all units at 3 (dashed lines) and 15 (solid lines) minutes after bimodal stimulation from sham (black lines) and exposed (red lines) guinea pigs. C. Population timing rules 3 minutes after bimodal stimulation from ET (red), ENT (blue), and sham (black) guinea pigs. D. Population timing rules 15 minutes after bimodal stimulation from ET (red), ENT (blue), and sham (black) guinea pigs. Bars indicate s.e.m. BI – Bimodal Interval in ms.
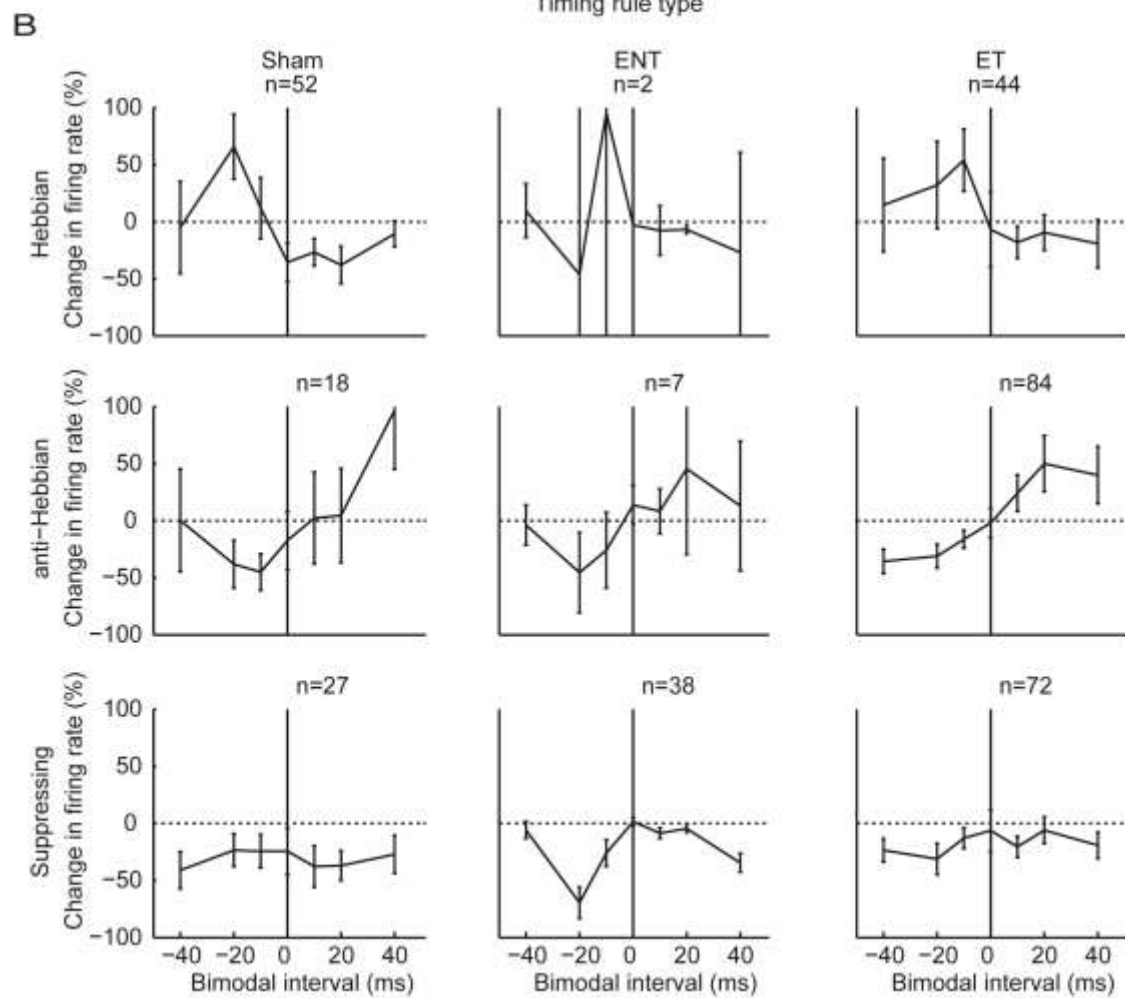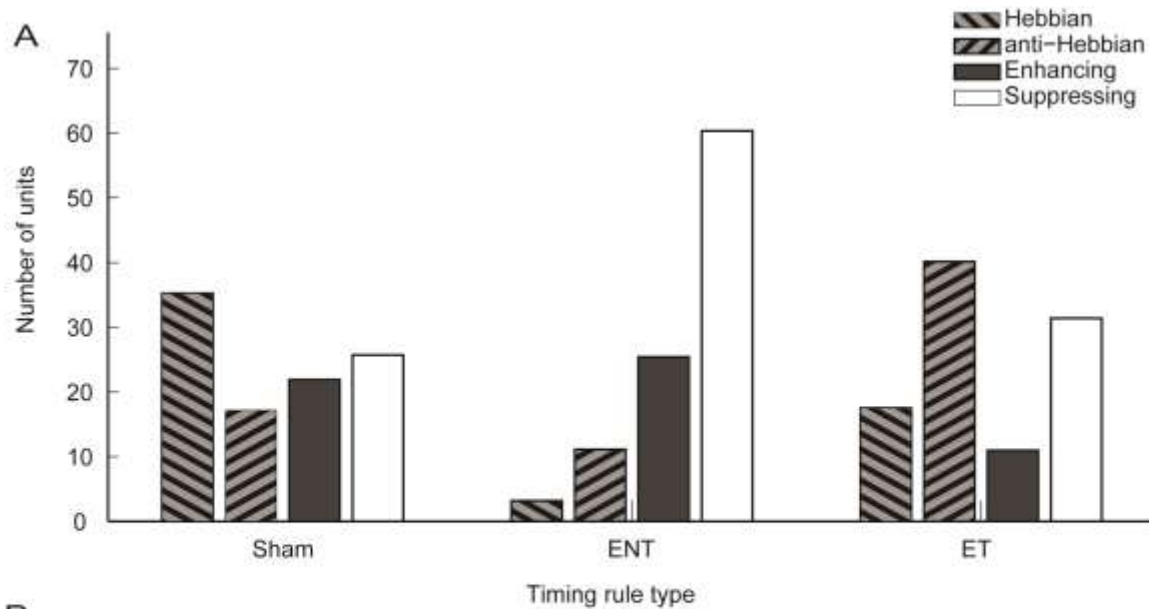
Figure 4.6 – Bimodal plasticity shifts from predominantly Hebbian to suppressive in guinea pigs without tinnitus and anti-Hebbian in guinea pigs with tinnitus. A. The percent of units that showed Hebbian-like (diagonal down), anti-Hebbian-like (diagonal up), enhancing (black) and suppressing (empty) timing rules within each group of animals. B. Mean population timing rules for Hebbian (top row), anti-Hebbian (middle row), and suppressing (bottom row) units grouped by sham (left column), ENT (middle column), and ET guinea pigs (right column). Error bars indicate +/- 1 sem.
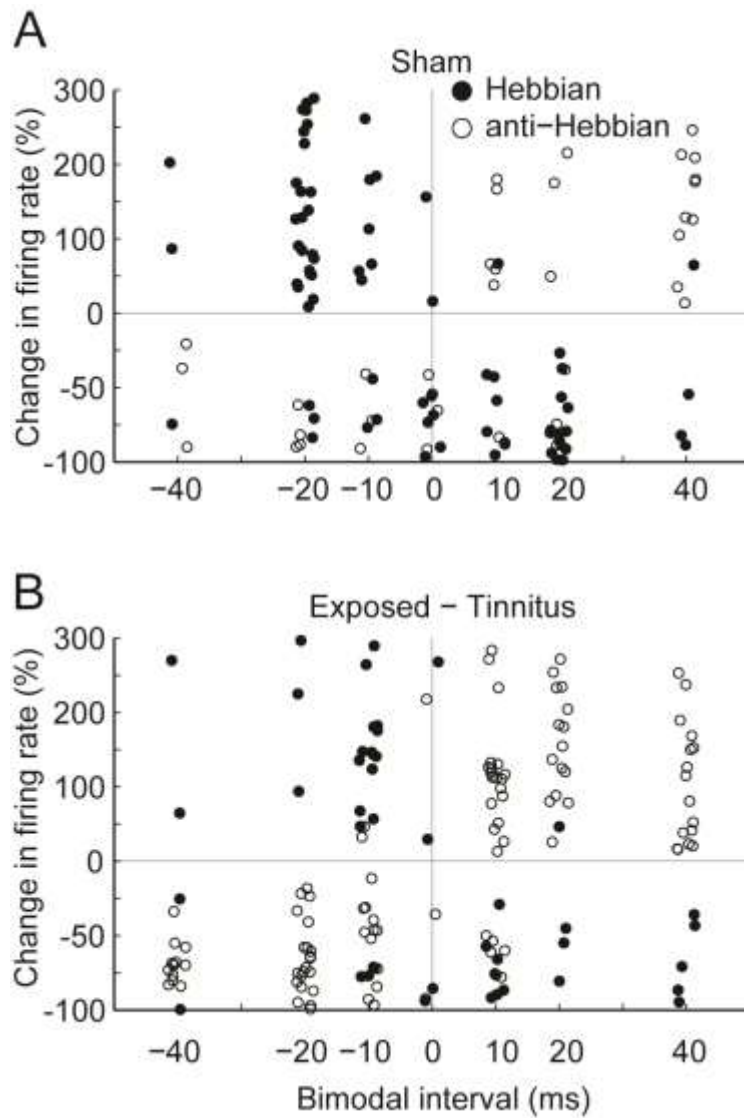
Figure 4.7 – Peak enhancement and suppression reflect broader timing rules with tinnitus. A. Peak enhancement (black) and suppression (hollow) are plotted here vs. bimodal interval for all units from sham animals. B. Peak enhancement (black) and suppression (hollow) are plotted here vs. bimodal interval for all units from the exposed-tinnitus group.
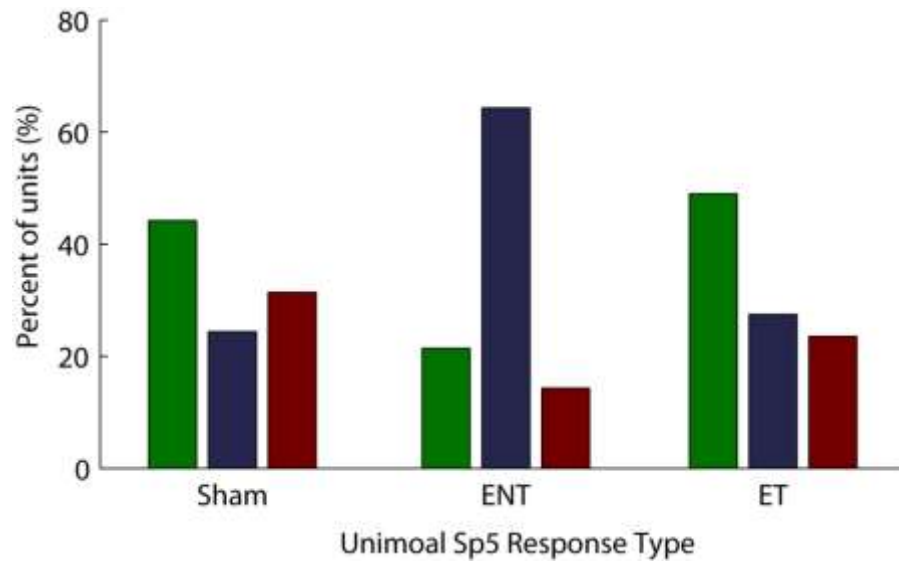
Figure 4.8 – Tinnitus-associated shifts in the distribution of unimodal response types after noise exposure. The percent of units showing excitatory (green), complex (blue), and inhibitory (red) responses to unimodal Sp5 stimulation in Sham, ENT, and ET groups. ET – Exposed with tinnitus. ENT – Exposed with no tinnitus.

Chapter 5: Significance and Conclusions

The DCN is a fascinating cerebellar-like structure with well-described circuitry (Young and Davis, 2002; Shore and Zhou, 2006) and cellular mechanisms, including intrinsic ion channel conductances (Kanold and Manis, 1999), and synaptic plasticity (Fujino and Oertel, 2003; Tzounopoulos et al., 2004; Tzounopoulos et al., 2007; Sedlacek et al., 2011). It provides an ideal mammalian model system for exploring mechanisms underlying integration of information from multiple sensory systems. The studies presented here are the first to elucidate the contributions of two mechanisms to *in vivo* neural encoding of acoustic and multisensory information in the normal and noise-exposure damaged auditory system.

In chapter 2, bimodal integration resulted in changes in sound-evoked response *regularity*, possibly representing pitch coding (Wiegrebe and Meddis, 2004), and *latency*, possibly representing loudness coding (Heil, 2004). Responses to multisensory stimuli are historically represented by the average neural firing rates of multisensory neurons. Multisensory integration is often defined as the difference between firing rates elicited by the multimodal stimulus and firing rates elicited by the component unimodal stimuli (Stein and Stanford, 2008). However, the nature of the auditory environment requires that the auditory system detect and process sounds in tens of milliseconds, which suggests that spike-timing coding may be important (Heil, 2004; VanRullen et al., 2005).

Fusiform cells in the DCN possess history-dependent spike timing precision (Kanold and Manis, 1999, 2001; Street and Manis, 2007), distinct sources of auditory and non-auditory synaptic drive (Ryugo et al., 2003; Zhou and Shore, 2004), and observable multisensory enhancement and suppression of firing rate (Shore, 2005). Thus, they present an ideal model for exploring spike timing representations of multisensory integration. Increased latencies and altered regularity of sound-evoked responses were observed with multimodal stimulation, suggesting that spike timing is an important consideration for multisensory integration in the cochlear nucleus. This work raises questions about what sensory information is being encoded by precise spike times and regularity in DCN neurons. To fully understand DCN

function, further work is needed to understand how pitch, loudness, and other properties of the acoustic environment are differently encoded by average firing rates and precise spike-timing.

In chapter 3, DCN neurons showed stimulus-timing dependent bimodal plasticity of sound-evoked responses in normal guinea pigs. Firing rates in response to sound were enhanced or suppressed for up to two hours after bimodal stimulation (Dehmel et al., 2012c). The amount of enhancement or suppression was dependent on the stimulus-timing interval between the bimodal stimuli. The observed bimodal timing rules and temporal kinetics for bimodal plasticity reflected those observed for Hebbian and anti-Hebbian STDP at multisensory synapses in the DCN (Tzounopoulos et al., 2004; Tzounopoulos et al., 2007). The STDP at multisensory parallel fiber synapses has been shown to influence responses to unimodal synaptic input from the auditory nerve (Doiron et al., 2011). Thus, synaptic plasticity induced by correlated input from auditory and non-auditory sources likely provides a direct and long-lasting influence on DCN responses to sound, potentially changing the way DCN neurons encode the intensity and spectral content and of sound signals.

Because of its cerebellar-like circuitry and distinct, excitatory auditory nerve and somatosensory inputs (Oertel and Young, 2004), the DCN is proposed to adaptively filter auditory signals using statistical correlations between auditory and multisensory signals that drive STDP (Roberts et al., 2006; Roberts and Portfors, 2008; Roberts and Leen, 2010). Cerebellar circuits in electrosensory fish use multisensory signals to develop learned predictions about electrosensory signals (Montgomery and Bodznick, 1994; Bell et al., 1997a). The DCN may perform similar functions, such as suppression of responses to self-generated sounds, which would be correlated with premotor, somatosensory, or vestibular signals. Additionally, STDP could aid in the encoding of head or pinnae positions that correlate with spectral information used by the DCN for sound localization in the vertical plane (May, 2000). These two different functions may be accomplished by different subpopulations of DCN neurons. For both functions, DCN

responses to sensory stimuli would be expected to adapt to multisensory experiences through STDP driven by correlated auditory and multisensory signals, as described in this dissertation.

The *in vivo* demonstation of stimulus timing dependent bimodal plasticity in DCN raises several interesting questions. First, it is not yet clear how bimodal plasticity influences DCN neural encoding of sound spectrum and intensity. Future assessment of receptive fields, tuning curves, and rate level functions after bimodal stimulation will provide evidence for how bimodal inputs influence functional auditory processing. Second, while *in vitro* recordings suggest that NMDAR and endocannabinoid receptor mediated signaling are necessary for STDP (ref: Tzounopolous), it has not been definitively established that these neurotransmitter systems mediate bimodal stimulus-timing dependent plasticity. Assessment of bimodal plasticity while pharmacologically manipulating candidate receptors can help elucidate relevant neurotransmitter systems. Third, we have inferred that bimodal plasticity depends on the changing strength of parallel fiber synapses. Direct assessment of long-lasting changes in somatosensory responses after bimodal stimulation through unit or local field potential recordings would clarify the influence of bimodal stimulation on parallel fiber-driven responses.

In chapter 4, bimodal timing rules noise-exposed guinea pigs were more likely to be Hebbian or anti-Hebbian than suppressive in those exhibiting tinnitus and more likely to be suppressive in those without tinnitus. Furthermore, Hebbian and anti-Hebbian timing rules were broader in animals with tinnitus. Taken together, the results in Chapters 3 and 4 show that specific changes in STDP are directly associated with noise-exposure induced tinnitus. It is important to understand the mechanisms that produce anti-Hebbian timing rules that are broader and more prominent in animals that develop tinnitus but suppressive timing rules in animals that don't develop tinnitus. In spite of similar exposure, differences in hearing damage or predisposing factors may lead to different effects on plasticity and different tinnitus outcomes. Understanding the mechanisms that produce different plasticity in animals with and without tinnitus may help understand why hearing damage only leads to chronic tinnitus in some cases.

These results suggest a novel mechanism for developing DCN spontaneous hyperactivity that may lead to tinnitus. In the normal DCN, bimodal plasticity timing rules result in modulation of DCN neural responses for enhanced detection of correlated auditory and non-auditory input. In the noise-damaged system, broader timing rules mean that multisensory signals do not require close temporal correlations with auditory signals to induce bimodal plasticity. As a result, uncorrelated auditory and somatosensory synaptic input could drive bimodal plasticity, leading to enhanced detection of those uncorrelated inputs. These uncorrelated auditory and somatosensory synaptic inputs could include spontaneous inputs from auditory nerve or parallel fibers. In this way, DCN neurons could adaptively respond to spontaneous synaptic input as if it were stimulus-driven activity, thus leading to elevated spontaneous activity in DCN. Elevated spontaneous activity that mimics stimulus-driven activity would be conveyed to higher auditory centers leading to tinnitus. Furthermore, increases in bimodal suppression in exposed animals without tinnitus may reflect a homeostatic mechanism to counteract increased central gain(Schaette and Kempter, 2006) that is absent in animals with tinnitus. Whether or not changes in bimodal plasticity and STDP are the driving mechanism underlying spontaneous hyperactivity and tinnitus, these results suggest the possibility of utilizing timed multisensory stimuli to reduce spontaneous activity and thus suppress tinnitus.

References

Abraham WC (2008) Metaplasticity: tuning synapses and networks for plasticity. Nat Rev Neurosci 9:387.

Abraham WC, Bear MF (1996) Metaplasticity: the plasticity of synaptic plasticity. Trends in neurosciences 19:126-130.

Basura GJ, Koehler SD, Shore SE (2012) Multi-sensory integration in brainstem and auditory cortex. Brain research 1485:95-107.

Bauer CA, Turner JG, Caspary DM, Myers KS, Brozoski TJ (2008) Tinnitus and inferior colliculus activity in chinchillas related to three distinct patterns of cochlear trauma. J Neurosci Res 86:2564-2578.

Bell C, Bodznick D, Montgomery J, Bastian J (1997a) The generation and subtraction of sensory expectations within cerebellum-like structures. Brain Behav Evol 50 Suppl 1:17-31.

Bell CC, Han VZ, Sugawara Y, Grant K (1997b) Synaptic plasticity in a cerebellum-like structure depends on temporal order. Nature 387:278-281.

Biesinger E, Reisshauer A, Mazurek B (2008) [The role of the cervical spine and the craniomandibular system in the pathogenesis of tinnitus. Somatosensory tinnitus]. HNO 56:673-677.

Brozoski TJ, Bauer CA, Caspary DM (2002) Elevated fusiform cell activity in the dorsal cochlear nucleus of chinchillas with psychophysical evidence of tinnitus. J Neurosci 22:2383-2390.

Calvert GA, Thesen T (2004) Multisensory integration: methodological approaches and emerging principles in the human brain. Journal of physiology, Paris 98:191-205.

Caporale N, Dan Y (2008) Spike timing-dependent plasticity: a Hebbian learning rule. Annual review of neuroscience 31:25-46.

Chase SM, Young ED (2006) Spike-timing codes enhance the representation of multiple simultaneous sound-localization cues in the inferior colliculus. J Neurosci 26:3889-3898.

Dahmen JC, Hartley DE, King AJ (2008) Stimulus-timing-dependent plasticity of cortical frequency representation. The Journal of neuroscience : the official journal of the Society for Neuroscience 28:13629-13639.

Dan Y, Poo MM (2006) Spike timing-dependent plasticity: from synapse to perception. Physiol Rev 86:1033-1048.

Davis KA, Young ED (1997) Granule cell activation of complex-spiking neurons in dorsal cochlear nucleus. J Neurosci 17:6798-6806.

Davis KA, Miller RL, Young ED (1996) Effects of somatosensory and parallel-fiber stimulation on neurons in dorsal cochlear nucleus. J Neurophysiol 76:3012-3024.

Dehmel S, Eisinger D, Shore SE (2012a) Gap prepulse inhibition and auditory brainstem-evoked potentials as objective measures for tinnitus in guinea pigs. Front Syst Neurosci 6:42.

Dehmel S, Eisinger D, Shore SE (2012b) Gap prepulse inhibition and auditory brainstem-evoked potentials as objective measures for tinnitus in guinea pigs. Front Syst Neurosci 6:42.

Dehmel S, Pradhan S, Koehler S, Bledsoe S, Shore S (2012c) Noise overexposure alters long-term somatosensory-auditory processing in the dorsal cochlear nucleus--possible basis for tinnitus-related hyperactivity? The Journal of neuroscience : the official journal of the Society for Neuroscience 32:1660-1671.

Ding J, Benson TE, Voigt HF (1999) Acoustic and current-pulse responses of identified neurons in the dorsal cochlear nucleus of unanesthetized, decerebrate gerbils. Journal of neurophysiology 82:3434-3457.

Doiron B, Zhao Y, Tzounopoulos T (2011) Combined LTP and LTD of modulatory inputs controls neuronal processing of primary sensory inputs. J Neurosci 31:10579-10592.

Ebert U (1996) Noradrenalin enhances the activity of cochlear nucleus neurons in the rat. The European journal of neuroscience 8:1306-1314.

Engineer ND, Moller AR, Kilgard MP (2013) Directing neural plasticity to understand and treat tinnitus. Hearing research 295:58-66.

Evans EF, Zhao W (1993) Varieties of inhibition in the processing and control of processing in the mammalian cochlear nucleus. Prog Brain Res 97:117-126.

Fujino K, Oertel D (2003) Bidirectional synaptic plasticity in the cerebellum-like mammalian dorsal cochlear nucleus. Proc Natl Acad Sci U S A 100:265-270.

Gambino F, Holtmaat A (2012) Spike-timing-dependent potentiation of sensory surround in the somatosensory cortex is facilitated by deprivation-mediated disinhibition. Neuron 75:490-502.

Garcia MM, Edwards R, Brennan GB, Harlan RE (2000) Deafferentation-induced changes in protein kinase C expression in the rat cochlear nucleus. Hearing research 147:113-124.

Golding NL, Oertel D (1997) Physiological identification of the targets of cartwheel cells in the dorsal cochlear nucleus. J Neurophysiol 78:248-260.

Guo Y, Huang S, de Pasquale R, McGehrin K, Lee HK, Zhao K, Kirkwood A (2012) Dark exposure extends the integration window for spike-timing-dependent plasticity. The Journal of neuroscience : the official journal of the Society for Neuroscience 32:15027-15035.

Hackney CM (1990) Anatomy of the cochlear nuclear complex of guinea pig. Anatomy and embryology 182:123.

Haenggeli CA, Pongstaporn T, Doucet JR, Ryugo DK (2005a) Projections from the spinal trigeminal nucleus to the cochlear nucleus in the rat. J Comp Neurol 484:191-205.

Haenggeli CA, Pongstaporn T, Doucet JR, Ryugo DK (2005b) Projections from the spinal trigeminal nucleus to the cochlear nucleus in the rat. J Comp Neurol 484:191-205.

Hebb DO (2002) The organization of behavior: A neuropsychological theory: Lawrence Erlbaum.

Heil P (2004) First-spike latency of auditory neurons revisited. Curr Opin Neurobiol 14:461-467.

Heller AJ (2003) Classification and epidemiology of tinnitus. Otolaryngol Clin North Am 36:239-248.

Hewitt MJ, Meddis R (1993) Regularity of cochlear nucleus stellate cells: a computational modeling study. J Acoust Soc Am 93:3390-3399.

Huang AY, May BJ (1996) Sound orientation behavior in cats. II. Mid-frequency spectral cues for sound localization. J Acoust Soc Am 100:1070-1080.

Imig TJ, Bibikov NG, Poirier P, Samson FK (2000) Directionality derived from pinna-cue spectral notches in cat dorsal cochlear nucleus. J Neurophysiol 83:907-925.

Jin Y-M, Godfrey DA, Wang J, Kaltenbach JA (2006) Effects of intense tone exposure on choline acetyltransferase activity in the hamster cochlear nucleus. Hearing research 216:168-175.

Juiz JM, Albin RL, Helfert RH, Altschuler RA (1994) Distribution of GABAA and GABAB binding sites in the cochlear nucleus of the guinea pig. Brain Res 639:193-201.

Kaltenbach JA, McCaslin DL (1996) Increases in spontaneous activity in the dorsal cochlear nucleus following exposure to high intensity sound: A possible neural correlate of tinnitus. Auditory Neuroscience 3:57-78.

Kaltenbach JA, Afman CE (2000) Hyperactivity in the dorsal cochlear nucleus after intense sound exposure and its resemblance to tone-evoked activity: a physiological model for tinnitus. Hear Res 140:165-172.

Kaltenbach JA, Zhang J, Finlayson P (2005) Tinnitus as a plastic phenomenon and its possible neural underpinnings in the dorsal cochlear nucleus. Hear Res 206:200-226.

Kaltenbach JA, Zacharek MA, Zhang J, Frederick S (2004) Activity in the dorsal cochlear nucleus of hamsters previously tested for tinnitus following intense tone exposure. Neurosci Lett 355:121-125.

Kanold PO, Manis PB (1999) Transient potassium currents regulate the discharge patterns of dorsal cochlear nucleus pyramidal cells. J Neurosci 19:2195-2208.

Kanold PO, Young ED (2001) Proprioceptive information from the pinna provides somatosensory input to cat dorsal cochlear nucleus. J Neurosci 21:7848-7858.

Kanold PO, Manis PB (2001) A physiologically based model of discharge pattern regulation by transient K+ currents in cochlear nucleus pyramidal cells. J Neurophysiol 85:523-538.

Kanold PO, Manis PB (2005) Encoding the timing of inhibitory inputs. J Neurophysiol 93:2887-2897.

Kanold PO, Davis KA, Young ED (2011) Somatosensory context alters auditory responses in the cochlear nucleus. Journal of neurophysiology 105:1063-1070.

Kipke DR, Clopton BM, Anderson DJ (1991) Shared-stimulus driving and connectivity in groups of neurons in the dorsal cochlear nucleus. Hearing research 55:24-38.

Kirzinger A, Jurgens U (1991) Vocalization-correlated single-unit activity in the brain stem of the squirrel monkey. Exp Brain Res 84:545-560.

Koehler SD, Shore S (2013) Stimulus-timing dependent multisensory plasticity in the guinea pig dorsal cochlear nucleus PLoS One.

Koehler SD, Pradhan S, Manis PB, Shore SE (2011) Somatosensory inputs modify auditory spike timing in dorsal cochlear nucleus principal cells. Eur J Neurosci 33:409-420.

Komiya H, Eggermont JJ (2000) Spontaneous firing activity of cortical neurons in adult cats with reorganized tonotopic map following pure-tone trauma. Acta Otolaryngol 120:750-756.

Lee MC, Yasuda R, Ehlers MD (2010) Metaplasticity at single glutamatergic synapses. Neuron 66:859-870.

Levine RA (1999) Somatic (craniocervical) tinnitus and the dorsal cochlear nucleus hypothesis. Am J Otolaryngol 20:351-362.

Levine RA, Abel M, Cheng H (2003) CNS somatosensory-auditory interactions elicit or modulate tinnitus. Exp Brain Res 153:643-648.

Levine RA, Nam EC, Melcher J (2008) Somatosensory pulsatile tinnitus syndrome: somatic testing identifies a pulsatile tinnitus subtype that implicates the somatosensory system. Trends Amplif 12:242-253.

Lujan R, Shigemoto R, Kulik A, Juiz JM (2004) Localization of the GABAB receptor 1a/b subunit relative to glutamatergic synapses in the dorsal cochlear nucleus of the rat. J Comp Neurol 475:36-46.

Luthe L, Hausler U, Jurgens U (2000) Neuronal activity in the medulla oblongata during vocalization. A single-unit recording study in the squirrel monkey. Behav Brain Res 116:197-210.

Manis PB (1989) Responses to parallel fiber stimulation in the guinea pig dorsal cochlear nucleus in vitro. J Neurophysiol 61:149-161.

Manis PB (1990) Membrane properties and discharge characteristics of guinea pig dorsal cochlear nucleus neurons studied in vitro. J Neurosci 10:2338-2351.

Manis PB, Brownell WE (1983) Synaptic organization of eighth nerve afferents to cat dorsal cochlear nucleus. J Neurophysiol 50:1156-1181.

Manis PB, Molitor SC, Wu H (2003) Subthreshold oscillations generated by TTX-sensitive sodium currents in dorsal cochlear nucleus pyramidal cells. Exp Brain Res 153:443-451.

Markram H, Gerstner W, Sjostrom PJ (2011) A history of spike-timing-dependent plasticity. Front Synaptic Neurosci 3:4.

Markram H, Gerstner W, Sjostrom PJ (2012) Spike-timing-dependent plasticity: a comprehensive overview. Front Synaptic Neurosci 4:2.

Masquelier T, Guyonneau R, Thorpe SJ (2008) Spike timing dependent plasticity finds the start of repeating patterns in continuous spike trains. PLoS One 3:e1377.

Masterton RB, Granger EM, Glendenning KK (1994) Role of acoustic striae in hearing: mechanism for enhancement of sound detection in cats. Hear Res 73:209-222.

May BJ (2000) Role of the dorsal cochlear nucleus in the sound localization behavior of cats. Hear Res 148:74-87.

Mellott JG, Motts SD, Schofield BR (2011) Multiple origins of cholinergic innervation of the cochlear nucleus. Neuroscience 180:138-147.

Meredith MA (2002) On the neuronal basis for multisensory convergence: a brief overview. Cognitive Brain Research 14:31-40.

Meredith MA, Keniston LR, Dehner LR, Clemo HR (2006) Crossmodal projections from somatosensory area SIV to the auditory field of the anterior ectosylvian sulcus (FAES) in Cat: further evidence for subthreshold forms of multisensory processing. Exp Brain Res 172:472-484.

Molitor SC, Manis PB (1997) Evidence for functional metabotropic glutamate receptors in the dorsal cochlear nucleus. J Neurophysiol 77:1889-1905.

Montgomery JC, Bodznick D (1994) An adaptive filter that cancels self-induced noise in the electrosensory and lateral line mechanosensory systems of fish. Neuroscience letters 174:145-148.

Mugnaini E, Dino MR, Jaarsma D (1997) The unipolar brush cells of the mammalian cerebellum and cochlear nucleus: cytology and microcircuitry. Prog Brain Res 114:131-150.

Muhlnickel W, Elbert T, Taub E, Flor H (1998) Reorganization of auditory cortex in tinnitus. Proceedings of the National Academy of Sciences of the United States of America 95:10340-10343.

Needham K, Paolini AG (2006) Neural timing, inhibition and the nature of stellate cell interaction in the ventral cochlear nucleus. Hear Res 216-217:31-42.

Oertel D, Young ED (2004) What's a cerebellar circuit doing in the auditory system? Trends Neurosci 27:104-110.

Parham K, Kim DO (1992) Analysis of temporal discharge characteristics of dorsal cochlear nucleus neurons of unanesthetized decerebrate cats. J Neurophysiol 67:1247-1263.

Petralia RS, Rubio ME, Wang YX, Wenthold RJ (2000) Differential distribution of glutamate receptors in the cochlear nuclei. Hear Res 147:59-69.

Pilati N, Ison MJ, Barker M, Mulheran M, Large CH, Forsythe ID, Matthias J, Hamann M (2012) Mechanisms contributing to central excitability changes during hearing loss. Proceedings of the National Academy of Sciences of the United States of America 109:8292-8297.

Pinchoff RJ, Burkard RF, Salvi RJ, Coad ML, Lockwood AH (1998) Modulation of tinnitus by voluntary jaw movements. Am J Otol 19:785-789.

Populin L, Yin T (2002) Bimodal interactions in the superior colliculus of the behaving cat. Journal of Neuroscience 22:2826.

Reiss LA, Young ED (2005) Spectral edge sensitivity in neural circuits of the dorsal cochlear nucleus. J Neurosci 25:3680-3691.

Requarth T, Sawtell NB (2011) Neural mechanisms for filtering self-generated sensory signals in cerebellum-like circuits. Current opinion in neurobiology 21:602-608.

Rhode WS (1999) Vertical cell responses to sound in cat dorsal cochlear nucleus. Journal of neurophysiology 82:1019-1032.

Rhode WS, Smith PH, Oertel D (1983) Physiological response properties of cells labeled intracellularly with horseradish peroxidase in cat dorsal cochlear nucleus. The Journal of comparative neurology 213:426-447.

Roberts PD, Portfors CV (2008) Design principles of sensory processing in cerebellum-like structures. Early stage processing of electrosensory and auditory objects. Biol Cybern 98:491-507.

Roberts PD, Leen TK (2010) Anti-hebbian spike-timing-dependent plasticity and adaptive sensory processing. Front Comput Neurosci 4:156.

Roberts PD, Portfors CV, Sawtell N, Felix Ii R (2006) Model of auditory prediction in the dorsal cochlear nucleus via spike-timing dependent plasticity. Neurocomputing 69:1191-1194.

Rubinstein B, Axelsson A, Carlsson GE (1990) Prevalence of signs and symptoms of craniomandibular disorders in tinnitus patients. J Craniomandib Disord 4:186-192.

Rubio ME, Wenthold RJ (1997) Glutamate receptors are selectively targeted to postsynaptic sites in neurons. Neuron 18:939-950.

Rusznak Z, Bakondi G, Pocsai K, Por A, Kosztka L, Pal B, Nagy D, Szucs G (2008) Voltage-gated potassium channel (Kv) subunits expressed in the rat cochlear nucleus. J Histochem Cytochem 56:443-465.

Ryugo DK, Haenggeli CA, Doucet JR (2003) Multimodal inputs to the granule cell domain of the cochlear nucleus. Experimental brain research Experimentelle Hirnforschung Experimentation cerebrale 153:477-485.

Saade NE, Frangieh AS, Atweh SF, Jabbur SJ (1989) Dorsal column input to cochlear neurons in decerebrate-decerebellate cats. Brain Res 486:399-402.

Sanchez TG, da Silva Lima A, Brandao AL, Lorenzi MC, Bento RF (2007) Somatic modulation of tinnitus: test reliability and results after repetitive muscle contraction training. Ann Otol Rhinol Laryngol 116:30-35.

Sato K, Shiraishi S, Nakagawa H, Kuriyama H, Altschuler RA (2000) Diversity and plasticity in amino acid receptor subunits in the rat auditory brain stem. Hearing research 147:137-144.

Sawtell NB (2010) Multimodal integration in granule cells as a basis for associative plasticity and sensory prediction in a cerebellum-like circuit. Neuron 66:573-584.

Sawtell NB, Bell CC (2008) Adaptive processing in electrosensory systems: links to cerebellar plasticity and learning. J Physiol Paris 102:223-232.

Schaette R, Kempter R (2006) Development of tinnitus-related neuronal hyperactivity through homeostatic plasticity after hearing loss: a computational model. The European journal of neuroscience 23:3124-3138.

Schofield BR, Coomes DL (2006) Pathways from auditory cortex to the cochlear nucleus in guinea pigs. Hearing research 216-217:81-89.

Sedlacek M, Tipton PW, Brenowitz SD (2011) Sustained firing of cartwheel cells in the dorsal cochlear nucleus evokes endocannabinoid release and retrograde suppression of parallel fiber synapses. J Neurosci 31:15807-15817.

Sherriff FE, Henderson Z (1994) Cholinergic neurons in the ventral trapezoid nucleus project to the cochlear nuclei in the rat. Neuroscience 58:627-633.

Shore SE (2005) Multisensory integration in the dorsal cochlear nucleus: unit responses to acoustic and trigeminal ganglion stimulation. Eur J Neurosci 21:3334-3348.

Shore SE, Moore JK (1998) Sources of input to the cochlear granule cell region in the guinea pig. Hearing research 116:33-42.

Shore SE, Zhou J (2006) Somatosensory influence on the cochlear nucleus and beyond. Hear Res 216-217:90-99.

Shore SE, El Kashlan H, Lu J (2003) Effects of trigeminal ganglion stimulation on unit activity of ventral cochlear nucleus neurons. Neuroscience 119:1085-1101.

Shore SE, Vass Z, Wys NL, Altschuler RA (2000) Trigeminal ganglion innervates the auditory brainstem. The Journal of comparative neurology 419:271-285.

Shore SE, Helfert RH, Bledsoe SC, Jr., Altschuler RA, Godfrey DA (1991) Descending projections to the dorsal and ventral divisions of the cochlear nucleus in guinea pig. Hearing research 52:255-268.

Shore SE, Koehler S, Oldakowski M, Hughes LF, Syed S (2008) Dorsal cochlear nucleus responses to somatosensory stimulation are enhanced after noise-induced hearing loss. Eur J Neurosci 27:155-168.

Shulz DE, Jacob V (2010) Spike-timing-dependent plasticity in the intact brain: counteracting spurious spike coincidences. Front Synaptic Neurosci 2:137.

Sinner B, Graf BM (2008) Ketamine. Handb Exp Pharmacol:313-333.

Smith PH, Rhode WS (1985) Electron microscopic features of physiologically characterized, HRP-labeled fusiform cells in the cat dorsal cochlear nucleus. The Journal of comparative neurology 237:127-143.

Spatz WB (2001) Unipolar brush cells in the human cochlear nuclei identified by their expression of a metabotropic glutamate receptor (mGluR2/3). Neurosci Lett 316:161-164.

Stabler SE, Palmer AR, Winter IM (1996a) Temporal and mean rate discharge patterns of single units in the dorsal cochlear nucleus of the anesthetized guinea pig. Journal of neurophysiology 76:1667-1688.

Stabler SE, Palmer AR, Winter IM (1996b) Temporal and mean rate discharge patterns of single units in the dorsal cochlear nucleus of the anesthetized guinea pig. J Neurophysiol 76:1667-1688.

Stein B, Meredith M (1993) The Merging of the Senses. . Cambridge, MA. : MIT Press

Stein BE, Meredith MA (1990) Multisensory integration. Neural and behavioral solutions for dealing with stimuli from different sensory modalities. Ann N Y Acad Sci 608:51-65; discussion 65-70.

Stein BE, Stanford TR (2008) Multisensory integration: current issues from the perspective of the single neuron. Nat Rev Neurosci 9:255-266.

Stein BE, Stanford TR, Ramachandran R, Perrault TJ, Jr., Rowland BA (2009) Challenges in quantifying multisensory integration: alternative criteria, models, and inverse effectiveness. Experimental brain research Experimentelle Hirnforschung Experimentation cerebrale 198:113-126.

Street SE, Manis PB (2007) Action potential timing precision in dorsal cochlear nucleus pyramidal cells. J Neurophysiol.

Suneja SK, Potashner SJ, Benson CG (1998a) Plastic changes in glycine and GABA release and uptake in adult brain stem auditory nuclei after unilateral middle ear ossicle removal and cochlear ablation. Exp Neurol 151:273-288.

Suneja SK, Benson CG, Potashner SJ (1998b) Glycine receptors in adult guinea pig brain stem auditory nuclei: regulation after unilateral cochlear ablation. Exp Neurol 154:473-488.

Tajadura-Jimenez A, Kitagawa N, Valjamae A, Zampini M, Murray MM, Spence C (2009) Auditory-somatosensory multisensory interactions are spatially modulated by stimulated body surface and acoustic spectra. Neuropsychologia 47:195-203.

Turner J, Larsen D, Hughes L, Moechars D, Shore S (2012) Time course of tinnitus development following noise exposure in mice. J Neurosci Res 90:1480-1488.

Turner JG, Brozoski TJ, Bauer CA, Parrish JL, Myers K, Hughes LF, Caspary DM (2006) Gap detection deficits in rats with tinnitus: a potential novel screening tool. Behav Neurosci 120:188-195.

Tzounopoulos T, Kim Y, Oertel D, Trussell LO (2004) Cell-specific, spike timing-dependent plasticities in the dorsal cochlear nucleus. Nat Neurosci 7:719-725.

Tzounopoulos T, Rubio ME, Keen JE, Trussell LO (2007) Coactivation of pre- and postsynaptic signaling mechanisms determines cell-specific spike-timing-dependent plasticity. Neuron 54:291-301.

VanRullen R, Guyonneau R, Thorpe SJ (2005) Spike times make sense. Trends Neurosci 28:1-4.

Wallace MN, Palmer AR (2008) Laminar differences in the response properties of cells in the primary auditory cortex. Exp Brain Res 184:179-191.

Wang H, Brozoski TJ, Turner JG, Ling L, Parrish JL, Hughes LF, Caspary DM (2009) Plasticity at glycinergic synapses in dorsal cochlear nucleus of rats with behavioral evidence of tinnitus. Neuroscience 164:747-759.

Wang X, Huang ZG, Dergacheva O, Bouairi E, Gorini C, Stephens C, Andresen MC, Mendelowitz D (2005) Ketamine inhibits inspiratory-evoked gamma-aminobutyric acid and glycine neurotransmission to cardiac vagal neurons in the nucleus ambiguus. Anesthesiology 103:353-359.

Weedman DL, Ryugo DK (1996) Projections from auditory cortex to the cochlear nucleus in rats: synapses on granule cell dendrites. The Journal of comparative neurology 371:311-324.

Wiegrebe L, Meddis R (2004) The representation of periodic sounds in simulated sustained chopper units of the ventral cochlear nucleus. J Acoust Soc Am 115:1207-1218.

Wright DD, Ryugo DK (1996) Mossy fiber projections from the cuneate nucleus to the cochlear nucleus in the rat. J Comp Neurol 365:159-172.

Wright DD, Blackstone CD, Huganir RL, Ryugo DK (1996) Immunocytochemical localization of the mGluR1 alpha metabotropic glutamate receptor in the dorsal cochlear nucleus. J Comp Neurol 364:729-745.

Yao H, Dan Y (2001) Stimulus timing-dependent plasticity in cortical processing of orientation. Neuron 32:315-323.

Young ED, Davis KA (2002) The cochlear nucleus. Integrative Functions in the Mammalian Auditory Pathway 15:160.

Young ED, Robert JM, Shofner WP (1988) Regularity and latency of units in ventral cochlear nucleus: implications for unit classification and generation of response properties. J Neurophysiol 60:1-29.

Young ED, Nelken I, Conley RA (1995) Somatosensory effects on neurons in dorsal cochlear nucleus. J Neurophysiol 73:743-765.

Young ED, Spirou GA, Rice JJ, Voigt HF (1992) Neural organization and responses to complex stimuli in the dorsal cochlear nucleus. Philos Trans R Soc Lond B Biol Sci 336:407-413.

Zahar Y, Reches A, Gutfreund Y (2009) Multisensory enhancement in the optic tectum of the barn owl: spike count and spike timing. J Neurophysiol 101:2380-2394.

Zeng C, Nannapaneni N, Zhou J, Hughes LF, Shore S (2009a) Cochlear damage changes the distribution of vesicular glutamate transporters associated with auditory and nonauditory inputs to the cochlear nucleus. The Journal of neuroscience : the official journal of the Society for Neuroscience 29:4210-4217.

Zeng C, Nannapaneni N, Zhou J, Hughes LF, Shore S (2009b) Cochlear damage changes the distribution of vesicular glutamate transporters associated with auditory and nonauditory inputs to the cochlear nucleus. J Neurosci 29:4210-4217.

Zeng C, Yang Z, Shreve L, Bledsoe S, Shore S (2012) Somatosensory projections to cochlear nucleus are upregulated after unilateral deafness. The Journal of neuroscience : the official journal of the Society for Neuroscience 32:15791-15801.

Zhang J, Kaltenbach J (2000) Modulation of spontaneous activity by acetylcholine receptors in the rat dorsal cochlear nucleus in vivo. Hearing research 140:7-17.

Zhang J, Guan Z (2008) Modulatory effects of somatosensory electrical stimulation on neural activity of the dorsal cochlear nucleus of hamsters. J Neurosci Res 86:1178-1187.

Zhao Y, Tzounopoulos T (2011) Physiological activation of cholinergic inputs controls associative synaptic plasticity via modulation of endocannabinoid signaling. The Journal of neuroscience : the official journal of the Society for Neuroscience 31:3158-3168.

Zhou J, Shore S (2004) Projections from the trigeminal nuclear complex to the cochlear nuclei: a retrograde and anterograde tracing study in the guinea pig. J Neurosci Res 78:901-907.

Zhou J, Shore S (2006) Convergence of spinal trigeminal and cochlear nucleus projections in the inferior colliculus of the guinea pig. J Comp Neurol 495:100-112.

Zhou J, Nannapaneni N, Shore S (2007) Vessicular glutamate transporters 1 and 2 are differentially associated with auditory nerve and spinal trigeminal inputs to the cochlear nucleus. J Comp Neurol 500:777-787.